Selecting Best Compromises among Performance Measures during In-Mold Coating of Sheet Molding Compound Compression Molding Parts

DISSERTATION

Presented in Partial Fulfillment of the Requirements for the Degree Doctor of Philosophy in the Graduate School of The Ohio State University

By

Seunghyun Ko

Graduate Program in Industrial and Systems Engineering

The Ohio State University

2015

Dissertation Committee:

Jose M. Castro - Advisor

L. James Lee

Allen Yi

Abstract

In recent years, the application of thermosetting resins as coatings and in high performance composites have received increasing attention from the automotive and aerospace industries needing light weight, good mechanical properties and good surface quality. Unlike the processing of thermoplastic materials, the processing of thermosetting resins is accompanied by chemical reaction. As the material reacts, it transforms from low viscosity material to a solid, this transformation is referred to as the curing process. The curing behavior of the thermoset resin significantly affects the physical, chemical and mechanical properties of the final product. Therefore, understanding of the rheological changes and the chemical reaction during curing in the mold is critical for better design and control of molding process.

In-mold coating (IMC) has been applied to sheet molding compound (SMC) compression molded parts, as an environmentally friendly approach to improve its surface quality and provide the required conductivity for electrostatic painting. In the IMC process, when the SMC part, has become rigid enough so that the mold can be opened without damaging the part, the mold is slightly opened and the required volume of a liquid heat activated reactive thermosetting mixture is injected onto the surface of the SMC part while still in the mold. The mold is re-closed and the clamping force is re-applied to spread the coating material across the surface of the part. During the curing

stage of IMC, the coating solidifies by chemical reaction. Once the coating is stiff enough, the mold is opened; and the part removed.

Due to the success of IMC for SMC parts, its use on injection molded parts is being explored. Unlike its SMC counterparts, most thermoplastic injection molds have no shear edges. Any opening of the mold caused by injection of the liquid coating will result in coating leakage. Thus the mold needs to be kept close and the coating advances by compressing the thermoplastic substrate. To avoid leakage, the clamping tonnage needs to be greater than the hydraulic force generated by the IMC during flow. Thus, the IMC viscosity needs to be lower than for SMC coating. Another challenge of IMC of thermoplastics is the relatively low processing temperatures compared to SMC compression molding. Thus balancing curing time with coating pot life is a challenge.

Selecting the best compromises among performance measures during in mold coating and how this compromises are affected by the controllable variables is one of the challenges faced by the molder. The goal of this research is to develop a methodology to select the controllable variables that result in the best compromises among the performance measures of the in-mold coating process for compression molded sheet molding compound mostly between time available for flow (flow time), which we want to maximize and mold opening time (cure time), which we want to minimize. As mentioned earlier, in order to identify the best compromises among flow time and cure time, the chemo-rheology of the coating system needs to be studied and related to molding parameters. For the case of IMC of thermoplastic, the balance between injection pressure and conductivity is an added challenge, as briefly discussed in the last part of

iii

this work. The desired conductivity is achieved by adding Carbon Black (CB) to the coating formulation. Increasing CB: increases the conductivity, however, the viscosity is also increased, thus the increase of conductivity needs to be balanced with the increase of viscosity.

In order to select the best compromises among performance measures, models to predict both the flow time and cure time are needed. These models are developed using experimental curing information, which in this research is done using Differential Scanning Calorimetry (DSC). A multivariable optimization method, based on Data Envelopment Analysis (DEA), is used; to identify the region of best compromises or Pareto frontier between flow time and cure time. The method is recursive and uses both design of experiments and metamodels, to increase the number of solutions in or near the Pareto frontier. Examples of how the proposed approach can be used in actual practice are given for commercial coating materials.

Dedication

This document is dedicated to my family, especially my wife Seonhyeong and son

Wonik.

Acknowledgments

I would like to express my deepest appreciation towards my adviser, Dr. Jose M. Castro for his academic guidance, patience, care and continuous support all through my graduate studies and research at The Ohio State University (OSU). I am thankful to him for a great opportunity to work in the field of polymer processing. He is an exemplary adviser, professor, scientist, family man and a role model to me.

I am grateful to Dr. L. James Lee and Dr. Allen Yi for their inspiring guidance, helpful advice, and encouragement during my research work. I would like to thank Dr. Jerald Brevick for serving on my Ph. D. candidacy examination committee. I enjoyed taking Dr. Brevick's classes during the course of my studies at The Ohio State University.

My gratitude is also expressed to Elliott J. Straus for his knowledge and great helpful with experimental work. I am thankful to OMNOVA Solutions, Inc. for the financial support for this work.

I would like to thank my research group, Dr. Matt Mulyana, Dr. Eusebio Duarte Cabrera, Dr. Ziwei Zhao and Dr. Lupita Villareal. I would like to thank Dr, Yi's research group, Dr. Peng He and Dr. Likai Lee for their help. I also would like to thank the ISE lab supervisors, Josh Hassenzahl for his help in cutting samples, in teaching me how to use the different machines, and valuable knowledge on design. I am really proud to know them and thank you for not only being a great research team but also my friends.

Finally, I would like to thank my father and mother for their support, love and prayers. Especially, I specially would like to thank my wife Seonhyeong Kim and son Wonik Aaron Ko for their love, support and encouragement for my entire Ph. D. studies.

Vita

December 12, 1977 ....Born in Daegu, South Korea

February, 2000 ....B.S. Mechanical and Automotive
Engineering, Catholic University of Daegu,
South Korea

August, 2003 ....M.S. Mechanical Engineering,
The Ohio State University, Columbus, OH

September, 2003 – April, 2007 ....Junior Research Engineer,
Sindoricoh Co. Ltd., South Korea

2010 – present ....Graduate Research Associate,
Integrated Systems Engineering,
The Ohio State University, Columbus, OH

Publications

1. Seunghyun Ko and Jose M. Castro, "In Mold Coating: The Environmentally Friendly Alternative to Painting for Injection Molded Parts", Polymer Processing Society Tech Papers, 2012.

2. Seunghyun Ko, Eusebio D. Cabrera, Elliott J. Straus and Jose M. Castro, "In Mold Coating of Thermoplastic Parts: Electrical Conductivity versus Injection Pressure", Proceedings of Annual Technical Conference- Society of Plastic Engineers, 2013.

3. Seunghyun Ko, Elliott J. Straus and Jose M. Castro, "Chemorheology of In-Mold Coating for Compression Molded SMC Applications", Polymer Processing Society Tech Papers, 2014.

4. E.D. Cabrera, S. Ko, X. Ouyang, E. Straus, L.J. Lee and J.M. Castro, "Technical Feasibility of a New Approach to Electromagnetic Interference (EMI) Shielding of Injection Molded Parts Using In-Mold Coated (IMC) Nanopaper", Journal of Polymer Engineering, Vol. 34, 739-746, 2014.

Fields of Study

Major Field: Industrial and Systems Engineering

Table of Contents

List of Tables

List of Figures

xvi

xvii

Chapter 1: Introduction

1.1 Overview

Fiber reinforced polymeric composites (FRPC) and injection molded thermoplastic parts have been used extensively in automotive, marine, construction and a variety of other industries. These applications often require a coating onto the surface of the molded parts to facilitate electrostatic painting, or to satisfy surface property requirements for durability and cosmetic reasons. The coating can be sprayed onto the molded part in which case it will emit volatile organic compounds (VOC) into the workspace and environment [1, 2].

In-mold coating (IMC) process has been applied to sheet molding compound (SMC) compression molded parts, as an environmentally friendly approach to improve its surface quality and provide the required conductivity for electrostatic painting [3]. To date, the use of IMC as a conductive primer for SMC compression molded automotive and truck exterior body panels requiring painting is a standard practice. Examples of commercial applications of IMC can be seen in Figure 1.1. In the IMC process for SMC, a liquid coating material is injected onto the surface of the SMC substrate at the end of the molding process while the part is still in the mold. After the coating material solidifies by chemical reaction, the coated SMC part is removed from the mold. Fully reacted IMC

is 100% solids and, therefore, no volatile chemicals are released during the chemical reaction (curing). Figure 1.2 shows the stages of IMC for SMC process.

Due to the success of IMC in SMC compression molding, the use of IMC during thermoplastic injection molding is being developed. The IMC cycle for thermoplastics is composed of three stages: filling, packing and curing. During the filling stage, the coating flows by compressing the substrate and spreads until it reaches the mold end. In the packing stage, more coating is introduced until the volume for the desired coating thickness is injected. During the curing stage, the coating solidifies by a chemical reaction. The stages of thermoplastic injection molding integrated with IMC process is illustrated in Figure 1.3. Unlike its SMC counterparts, most thermoplastic injection molds have no shear edges. Any opening of the mold caused by injection of the liquid coating will result in coating leakage as shown in Figure 1.4. To avoid this problem, the clamping tonnage needs to be greater than the hydraulic force generated by the injected coating material at any time [4, 5]. Another challenge of IMC of thermoplastics is the relatively low processing temperatures. The typical mold temperature of SMC processing is approximately 150°C or higher [6]. At this temperature, the coating can be cured at an adequate rate. In thermoplastic processing, the mold temperatures are varied and mostly much lower than 150°C, depending on the type of thermoplastics. This lower mold temperature increases the cure time of the coating material as well as the cycle time of the entire process.

The main goal of this research is to develop a methodology to select the controllable variables that result in the best compromises among the performance

measures of the in-mold coating process for compression molded sheet molding compound. Some comments are made in the last part of the thesis related to injection molded parts. As shown schematically in Figure 1.5, there are many controllable process variables and performance measures relevant for the in-mold coating process. In a typical coating process, the resin system is selected based on the compatibility with the substrate to be coated, adhesion to the substrate being the critical issue. The resin system is formulated with several additives to facilitate flow, improve hardness, and carbon black is added to provide electrical conductivity when needed. Initiators, promoters and inhibitors are added to control the chemical reaction. Relevant process variables include the substrate temperature at the time of injection in the case of injection molding or the mold temperature in the case of SMC compression molding, the desired injection time. The surface area of the part coated; as well as the coating volume injected. Among the relevant performance measures we have the time available for flow, the cure time, the pot life, injection pressure, conductivity of the part and the clamping force. We will assume that the coating system is selected for proper adhesion to the substrate and the required surface hardness. Based on the research importance and input from our research partner (Omnova Solutions) we focused on the controllable process variables and performance measure highlighted in red in Figure 1.5.

Since the coating process is an added step to the molding process, it is critical to minimize its impact on the overall molding cycle time. The coating being a thermosetting reactive mixture, solidification occurs due to chemical reaction. Typical rheological changes of the coating during the process are shown schematically in Figure 1.6. The

3

initial coating viscosity is low and remains low while the inhibitor is present. Once the inhibitor is consumed, the reaction starts and the IMC viscosity rise sharply. Coating flow needs to occur during this stage. The mold can be opened once the part is stiff enough [7–10] so that the mold opening does not blemish the part. In order to predict the time available for flow and the needed curing time, we need to understand the chemorheology of the system and relate it to part quality and to extent of reaction or conversion. The cure models needed to investigate the best compromises among flow and cure time are developed using differential scanning calorimeter data. Using the predicted conversion, the viscosity changes as the material changes from liquid to solid, are correlated to conversion.

When the coating is used as a primer, conductivity is needed for electrostatic painting; in this case, Carbon Black (CB) is used to provide the required conductivity. The CB level, not only increases conductivity but greatly increases the viscosity of the coating. In the case of thermoplastic, it is critical to balance the increase of viscosity with the required conductivity. As it was explained before, if the viscosity is too large, coating pressures will be too large and coating leakage cannot be avoided. In the case of SMC compression molded, this is not a major issue as the mold shear edges act as a seal, allowing for mold opining during injection, to facilitate flow.

1.2 Research Objectives

The main purpose of this research is to develop a method to select the best compromises among the relevant performance measures for the IMC process. In the case of SMC as explained later the most relevant performance measures for the molder are time available for flow and cure time. In the case of thermoplastic, predicting the relationship between injection pressure and conductivity is also critical. . In summary, the specific objectives of this thesis are:

- Investigate the chemorheology of IMC that is, to study viscosity changes during the curing process and relate them to actual molding quality, and thus be able to predict flow and mold opening time of in-mold coating.

- Develop the cure model to predict inhibition time and degree of cure of IMC resin and understand the effect of carbon black filler and initiators on curing rate.

- Apply the multivariable optimization iterative method developed by Villarreal [11] to identify the Pareto frontier for relevant performance measures.

- Study the effect of carbon black filler on electrical conductivity for the electrostatic painting process and related it to the required injection pressure of for the coating of thermoplastic parts.

1.3 Contributions

In-mold coating is currently an integral part of the SMC compression molding process for exterior automotive body panels. This success has attracted the interest of thermoplastic manufacturers to use IMC as a primer, or depending of the required surface quality, as a topcoat eliminating painting altogether. In-mold coating is a very attractive method since the coating resin is cured in the mold without opening the mold and releases no chemicals during the molding process.

The main contribution of this research is to develop a method to select the best compromises among the relevant performance measures for the application of in-mold coating process for compression molded SMC parts. The optimization method is applied to find efficient solutions based on cure model and chemorheological studies. This research can attribute to the increased application of thermosetting resins as coating materials. The chemorheology of typical coating material was studied and related to molding quality. The CB level was related to conductivity and required injection pressure for the case of IMC of injection molding thermoplastic parts.

1.4 Thesis Outline

This thesis is organized as follows: Chapter 1 provides an overview of the in-mold coating process for compression molded SMC and injection molded parts and discusses the objectives and contributions of this research. In Chapter 2, a chemorheological study of a typical commercial IMC resins is presented. Chemorheology is correlated to molding quality in order to predict the time available for flow and the required cure time.

Chapter 3 develops the cure IMC model needed for selecting the best compromises among flow time and cure time. In this chapter, Differential Scanning Calorimeter experiments are used to develop a cure model to predict the inhibition and degree of conversion. The effect of initiators and carbon black on curing is discussed. The predictions of the model are verified experimentally.

In Chapter 4, the multiple criteria optimization method is applied to select best compromises among inhibition time and cure time.

Chapter 5 discusses the effect of carbon black on electrical conductivity and IMC injection pressure. Finally, Chapter 6 presents the conclusions of this thesis and suggests future work.
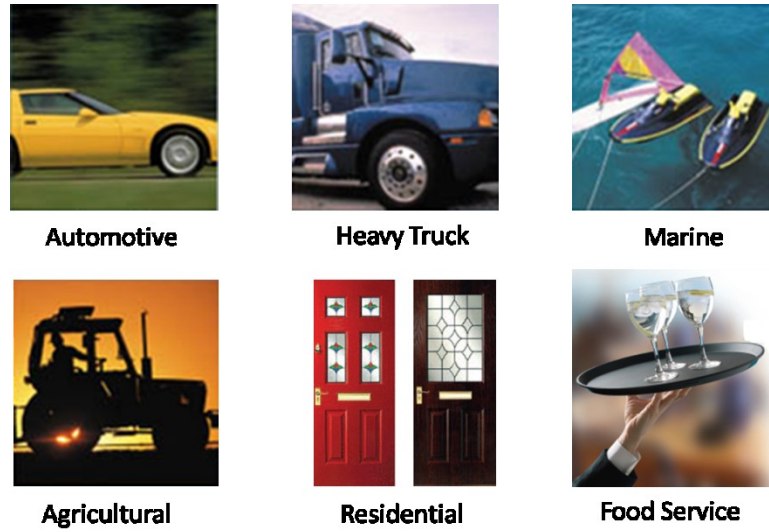
Figure 1. 1 Commercial IMC applications
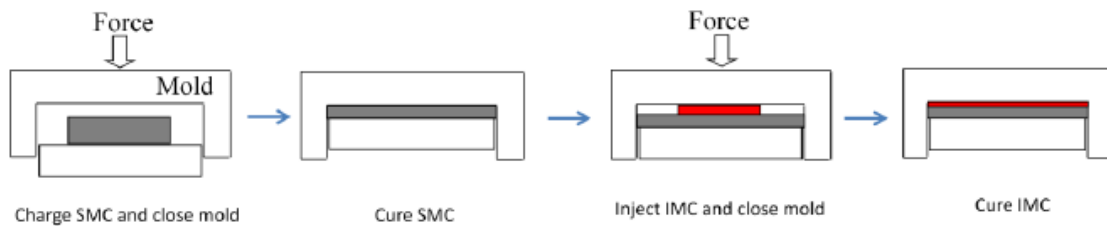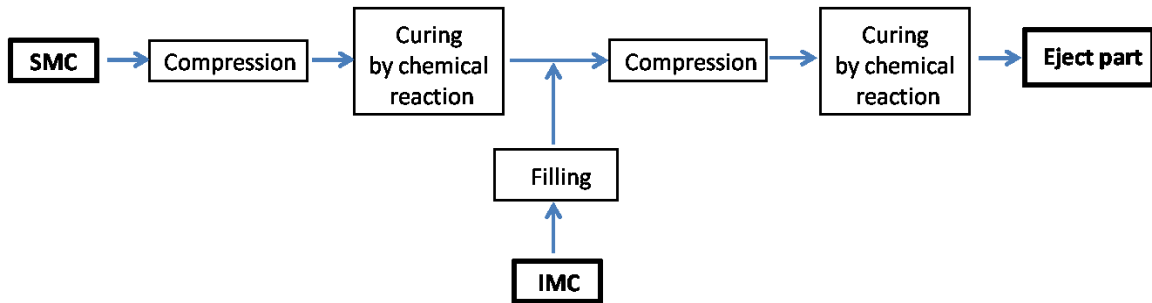
Figure 1. 2 Schematic representation of the stages of IMC during the SMC process

8
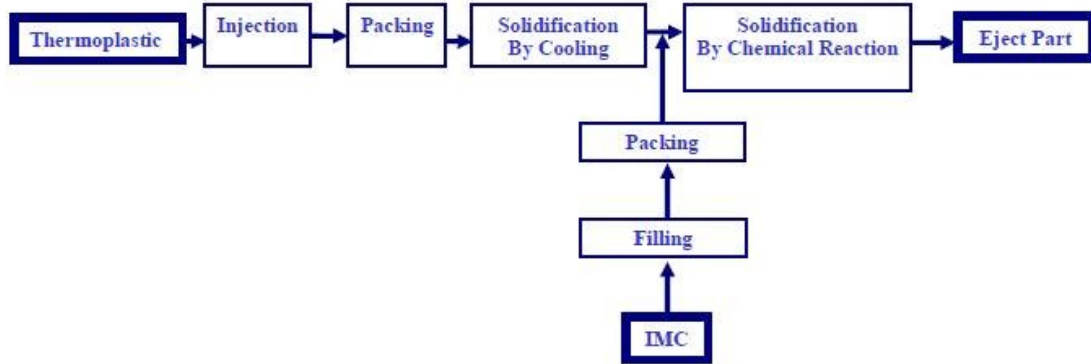
Figure 1. 3 Schematic representation of the stages of IMC during the thermoplastic injection molding process [5]
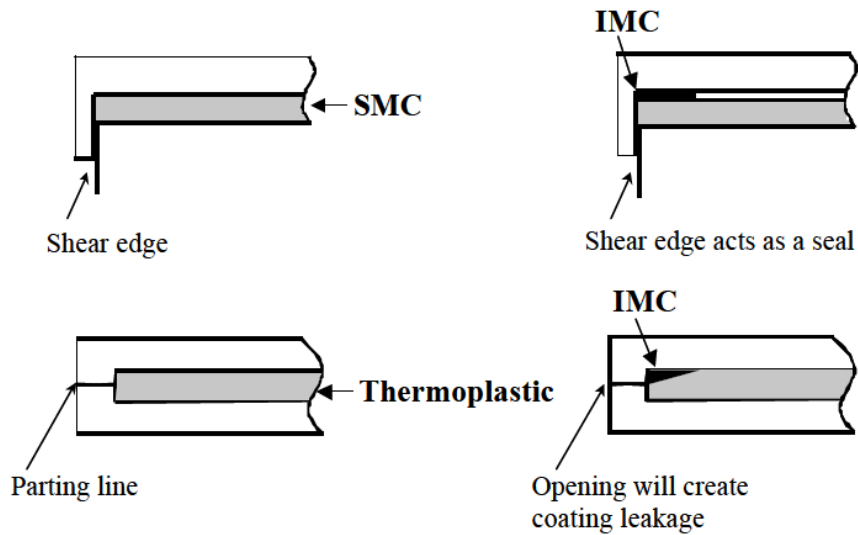
Figure 1. 4 Key differences between SMC and Thermoplastic IMC [6]
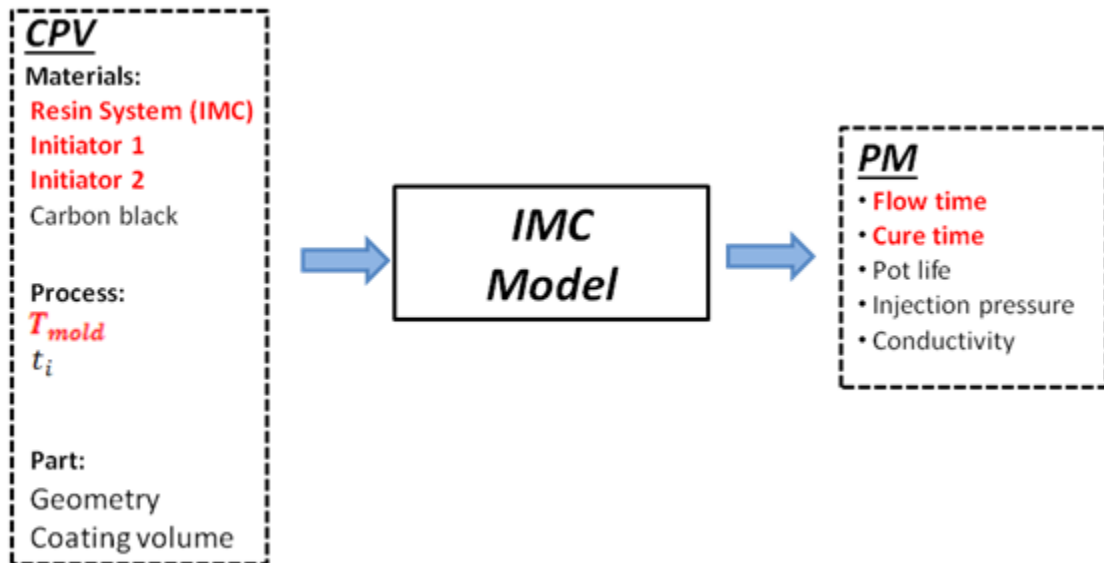
Figure 1. 5 Controllable process variables and performance measures of in-mold coating process studied in this research
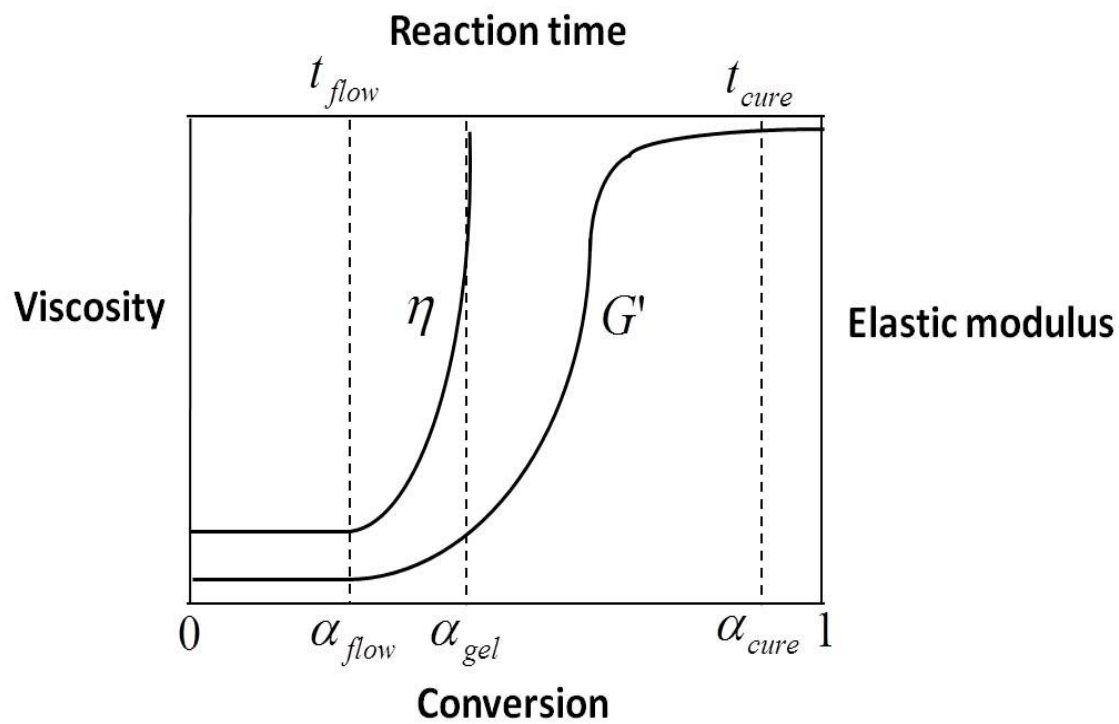
Figure 1. 6 Schematic representation of the change in viscosity and elastic modulus for a typical IMC system, as a function of conversion and reaction time

1.5 References

1. J. M. Castro and R. M. Griffith, "In-Mold Coating," in *Sheet Molding Compound: Science and Technology,* edited by Hamid G. Kia, Munich: Hanser, 1993, pp. 163-180.

2. William Rogers, Christoper Hoppins, Zoltan Gombos and John Summercales, "In-mould gel-coating of polymer composites: a review", Journal of clear production, 70, 282-291, 2014.

3. J. M. Castro and R. M. Griffith, "Mathematical modeling of the in-mold coating process", Polymer engineering and science, 30, 677, 1990.

4. Xu Chen, "Mathematical modeling of the in-mold coating process for injection molded thermoplastic parts", Ph. D. Dissertation, The Ohio State University, 2003.

5. Narayan L. Bhagavatula, "Modeling and experimental verification of pressure prediction in the in-mold coating process for thermoplastic substrates", Ph. D. Dissertation, The Ohio State University, 2006.

6. Konstantin S. Zuyev, "Processing studies in reactive in-mold coating for thermoplastic substrates", Ph. D. Dissertation, The Ohio State University, 2006.

7. Konstantin S. Zuyev, "Applications of chemo-rheology to develop process windows in reactive in-mold coating", Journal of polymer engineering, Vol. 22, No. 4, 2002.

8. Aramphongphun, C, "In-mold coating of thermoplastic and composite parts: microfludics and rheology", Ph. D. Dissertation, The Ohio State University, 2006.

9. Emily Cortright, "Microfludics and DNA suspensions", M.S. Thesis, The Ohio State University, 2009.

10. P. J. Halley and M. E. Mackay, "Chemo-rheology of thermoset: an overview", *Polym. Eng. Sci.* **36**, 593-609 (1996).

11. Maria G. Villareal-Mirroquin, "A metamodel based multiple criteria optimization vis simulation method for polymer processing", Ph.D. Thesis, The Ohio State University, (2012)

Chapter 2: Chemo-rheology of In-mold Coating

To predict both the flow time and the mold opening time, it is critical to study the chemorheology of IMC. In this chapter, we study the chemorheology for a typical commercial IMC system, and show its relevance to both the inhibition and cure time for the IMC.

2.1 Introduction

In recent years, the processing of thermosetting resins has received increased attention from automotive and aerospace industries as excellent choices for lightweight materials. The processing of thermosetting resins requires understanding, the effect of chemical reaction on the rheology of the reacting system.

The IMC resin is a thermosetting liquid that when injected onto the surface of the part cures and bonds to provide a smooth conductive surface. In the IMC process, when the SMC is cured adequately (part stiff enough so that the mold can be opened without surface blemishes), the mold is slightly opened and the required coating volume is injected onto the surface of the SMC while the part is still in the mold. Once the coating solidifies by chemical reaction, the mold is opened; and the part removed. In order to optimize the coating process, an understanding of the chemorheology of the reactive mixture is needed. The time available for flow is limited by the time at which the

viscosity starts to increase. On the other hand, the time when the part can be removed from the mold is given by the time at which the initially liquid resin has undergone the transition to solid and its mechanical strength is large enough so that the part can be removed without surface blemishes. Figure 2.1 shows the typical rheological changes that the IMC undergoes during the in-mold coating process [1, 3]. The changes in viscosity and elastic modulus are shown as a function of conversion and reaction time. During the initial period, the viscosity remains low. After all inhibitor is consumed, viscosity increases nearly vertically (gel point). Before the gel point, the elastic modulus starts to rise until it reaches a value sufficiently high (cure time) where the mold can be opened without damaging the coating. The rheological changes of the reactive systems during curing, are directly related to the change from liquid state to solid state at is fully cured condition [4]. Very limited information is available between the chemorheology of reactive systems and the relation between flow and cure time during actual molding [5-10, 17]. This study investigated the chemorheology of a commercial IMC system, Genglaze EC610 with 2.8 wt. % carbon black content, to determine flow and mold opening time during actual moldings. In-mold coating experiments for SMC compression molding were carried out at varying mold opening times and different molding temperatures and related to the chemo rheological changes for the IMC.

15
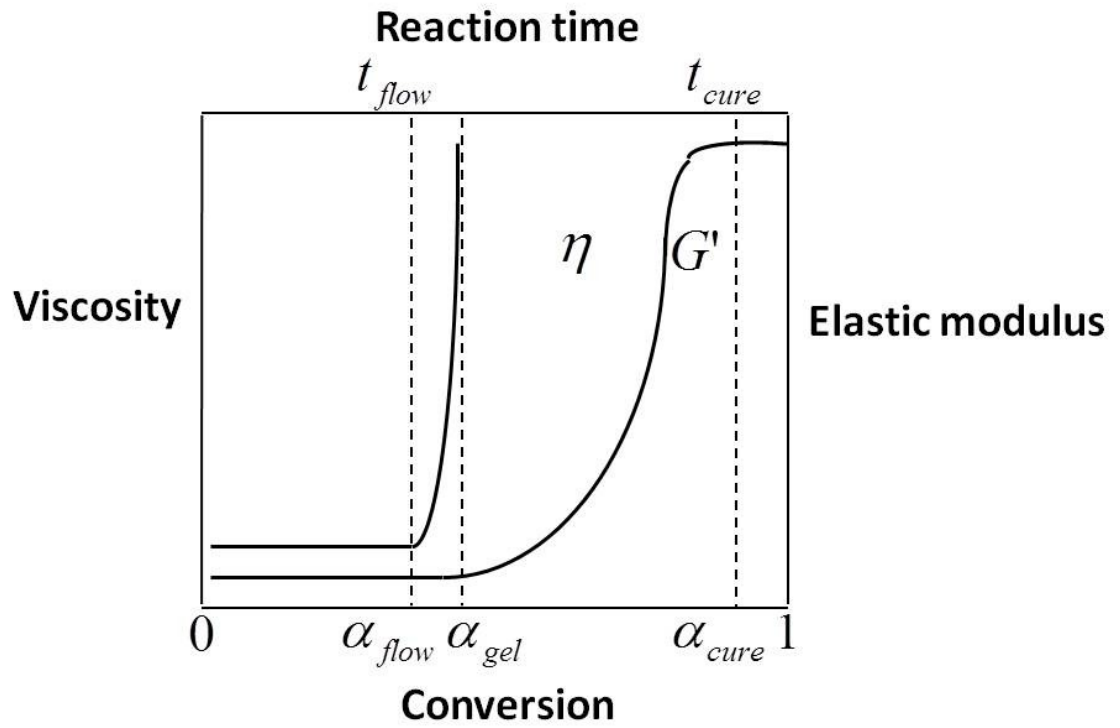
Figure 2. 1 Schematic representation of the change in viscosity and elastic modulus for a typical IMC system during cure

2.2 Experimental

2.2.1 Materials

The commercial in-mold coating resin, Genglaze EC610, provided by OMNOVA Solutions Inc. was used in this study. Genglaze EC610 a liquid, heat activated conductive in-mold coating, is designed to enhance the surface of reinforced plastics, automotive, truck FRP body panels, or any molded part. The components of Genglaze EC610 are listed in Table 2.1. The IMC contains unsaturated oligomers and monomers to give adequate hardness and adhesion to SMC substrates. Hydroxypropyl methacrylate (HPMA) and styrene are used as diluents to decrease the viscosity. Talc is used to improve hardness and decrease shrinkage. Cobalt is employed as an accelerator. The conductive filler used in Genglaze EC610 is carbon black (CB), VULCAN XC72R from CABOT Corp. This resin contains 2.8% of carbon black by weight in order to make the coating conductive. The inhibitor, benzoquinone is used to provide shelf-life and increase flow time. The initiators used in this study are tert-butyl peroxybenzoate (TBPB) from Akzo Nobel. TPBP is the recommended organic peroxide at molding temperatures in the range of 130 to 160 °C which is the typical molding temperature range of compression molded sheet molding compound (SMC) process. The sample was prepared by mixing IMC and 1.0 wt. % of TBPB at room temperature with a stir-bar for 5 min.

17

Genglaze EC610

Epoxy

Styrene

HPMA

Talc

Cobalt

Carbon black

inhibitor

Table 2. 1 Formulation of coating material

2.2.2 Measurements

The chemorheology of IMC coating material was measured with the TA ARES-G2 rheometer using 25 mm disposable parallel plates with a gap of 1mm shown in Figure 2.2. Both steady and dynamic shear flow tests were conducted under isothermal conditions at 100, 110 and 120°C. Steady shear viscosity was measured as a function of reaction time at a shear rate of 0.1 s^{-1} for IMC with 2.8% CB and 5 s^{-1} for IMC with 0% CB. Dynamic shear flow measurements were performed at a frequency of 1Hz and a strain of 0.1%. The time at which the viscosity approaches a very large value is nearly independent of shear rate [18]. Experiments were conducted at shear rates of 0.1, 5 and 10 s^{-1} to study the effect of shear rate on viscosity rise. The time at which viscosity starts to rise is nearly independent of shear rate as shown in Figure 2.3. As the viscosity rises, the tendency of the material to flow out of the gap increases, however, the shear rate needs to be large enough so that the torque is within the equipment measuring range.

Based on that, the shear rate of 0.1 s^{-1} for IMC with 2.8% CB and 5 s^{-1} for IMC with 0% CB were used in the steady shear tests. Our main goal is to study the viscosity rise, the shear rate dependence of the viscosity is only relevant before any reaction has occurred, as this is the period where flow occurs. The linear viscoelastic region was determined through a strain sweep test as shown in Figure 2.4. Strain sweeps were carried out at 1Hz and a strain of 0.1% was used to ensure that the resin samples were within the linear viscoelastic region. In this study, the complex viscosity, elastic modulus and loss modulus were measured as a function of the reaction time.

DSC measurements were performed using a TA Q20 differential scanning calorimeter under the same conditions as the chemorheology tests. The isothermal tests were performed at 100, 110 and 120°C. After the isothermal runs, a dynamic scan was performed at a heating rate of 10°C/min from 30°C to 250°C to determine total heat released during the curing reaction.

In-mold coating experiments during SMC compression molding were conducted at OMNOVA solutions technical center using a 450 ton Hoesch press with a steam heated flat plate mold of 43.18 x 55.88cm (17 x 22 in). The pressing force was 187 during compression molding. During the SMC molding process, 275g of a pre-measured SMC charge was used. The mold temperatures used were 137, 150 and 155°C. After the SMC part was solid enough, the mold was slightly opened (approximately 1 mm) and the coating material was injected using an EMC2 Inc. IMC injection unit. The IMC coated SMC parts were cured at various times, to experimentally obtain the cure time (minimum required mold opening time) by visual inspection.

To determine the minimum mold opening time (cure time) required of molded IMC parts in a more quantitative way, at each mold temperature, the surface quality of molded parts was evaluated using a Wyko NT9100 optical profilometer (Bruker AXS Inc.). The surface roughness (R_a) of every molded part was measured at 10 different locations and averaged. These measurements allowed us to better quantify the minimum required mold opening time than visual inspection of molded parts.
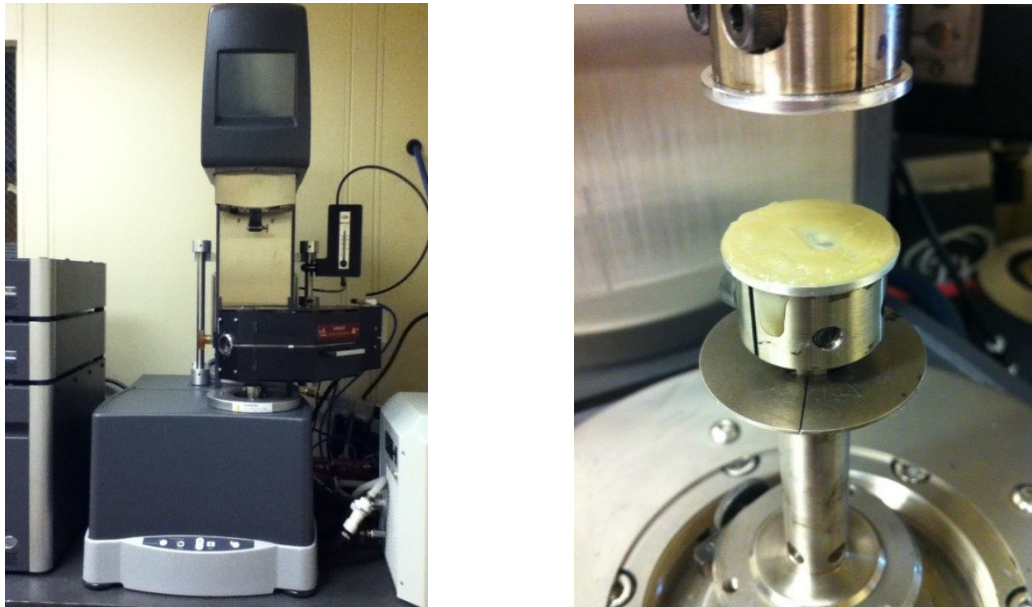
Figure 2. 2 TA ARES-G2 Rheometer
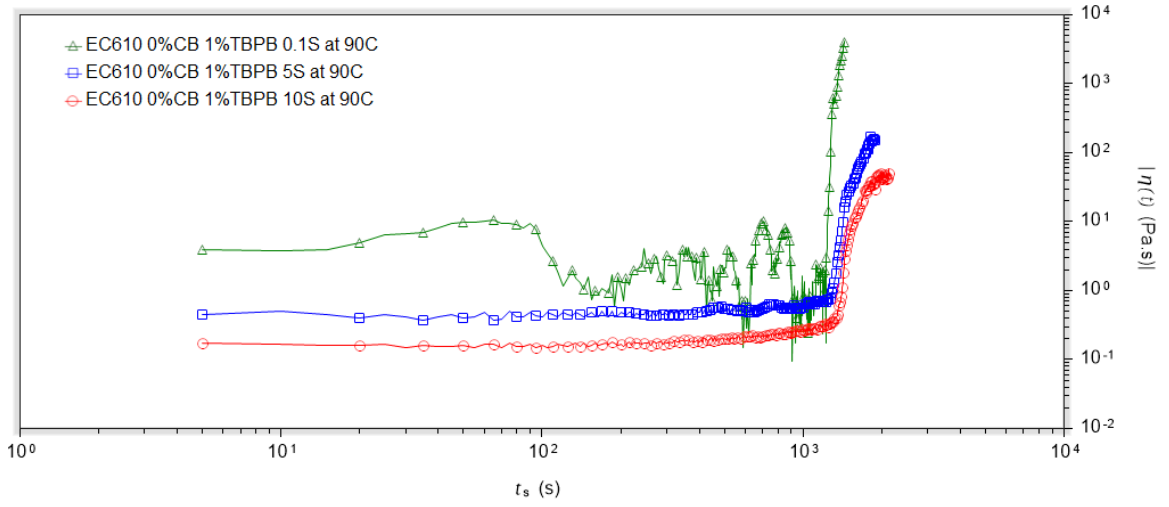
Figure 2. 3 Steady shear viscosity measurements for varying shear rates
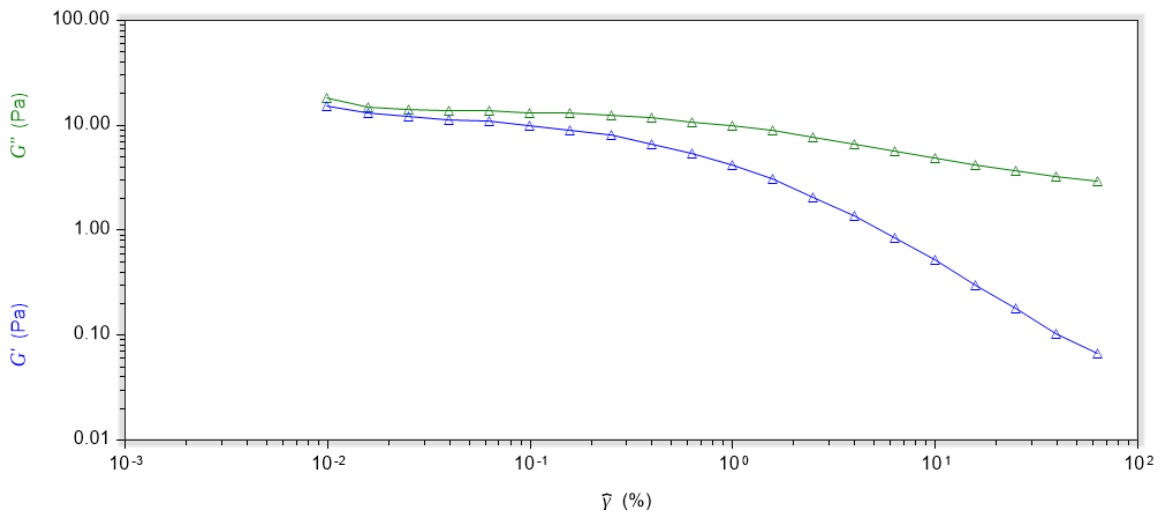
Figure 2. 4 Strain sweep test at a frequency of 1Hz

21

2.3 Results and Discussion

Figure 2.5 shows the viscosity versus reaction time in steady shear at three different temperatures. At the beginning, the viscosity slowly increases with time. At lower temperatures, the viscosity starts higher initially but rises more slowly due to the slower reaction rate. Then, at a certain point a very rapid increase of the viscosity is observed. The gelation occurs during this stage. Gelation corresponds to the forming of an infinite network of cross-linked polymer molecules. In the IMC process, it is critical because the polymer no longer flows after the gel point. In this work, the gelation was assumed to occur at the point at which the viscosity becomes 100 times the initial value.
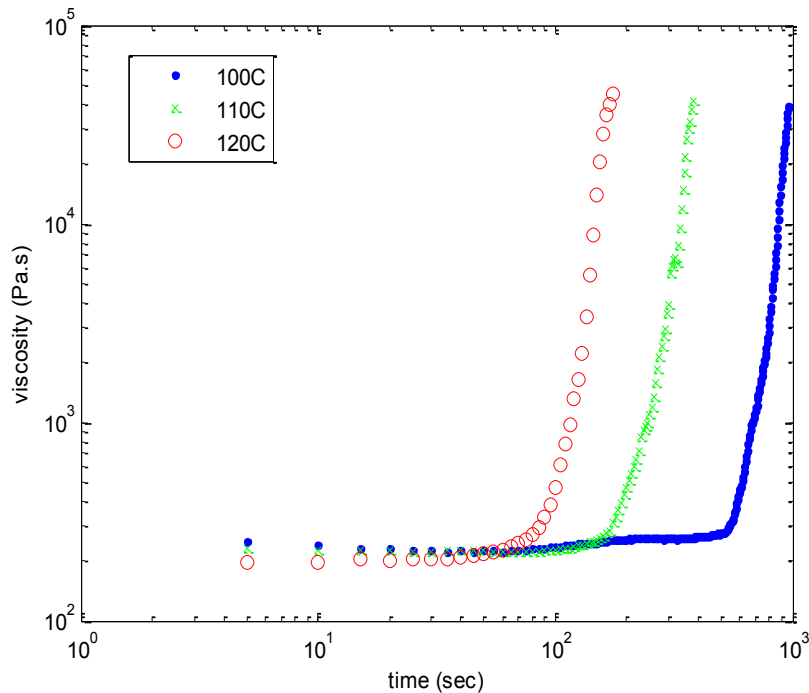
Figure 2. 5 Viscosity versus reaction time in steady shear test

In the IMC process, the mold should be opened when the coating has enough integrity so that the opening occurs without damaging the part surface. The elastic modulus during cure was investigated in the oscillatory shear mode. As reaction the time increases, G' reaches a nearly constant high value as shown in Figure 2.6.
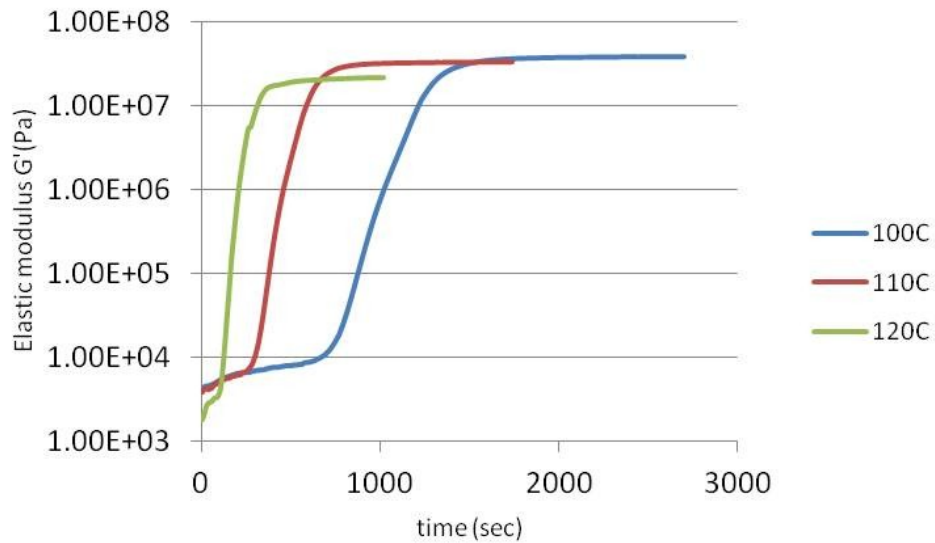
Figure 2. 6 Viscosity versus reaction time in dynamic shear test

In order to predict the time available for flow and the needed mold opening time, we need to relate viscosity and elastic modulus from chemorheology studies to extent of reaction or conversion instead of reaction time. In order to measure extent of reaction we used Differential Scanning Calorimetry (DSC). The basic assumption for applying DSC to predict the extent of reaction is that the dimensionless reaction rate, $d\alpha/dt$, is proportional to the measured heat flow, dH/dt:

$$\frac{d\alpha}{dt} = \frac{1}{H_{total}}\frac{dH}{dt} \tag{2.1}$$

Where if isothermal DSC is used, the total heat for the curing reaction, H_{total}, is given by

$$H_{total} = H_i + H_r \tag{2.2}$$

Where H_i is the heat measured in the isothermal DSC experiments and H_r is the residual heat of the curing reaction after isothermal cure, which can be measured by scanning the isothermally cured samples.

The degree of cure as a function of time is given by:

$$\alpha(t) = \frac{1}{H_{total}}\int_0^t \left(\frac{dH}{dt}\right)dt \tag{2.3}$$

The measured heat flow of a typical isothermal scan is shown in Figure 2.7. The baseline is a straight tangential line to horizontal part of the isothermal DSC curve. The inhibition time was selected as the cross point of baseline and DSC curve where the heat flow starts to increase. In the initial stage, the heat flow remains constant. After all the inhibitor is consumed, the heat flow starts to increase. The reaction rate reaches a maximum and then decreases. By integration of the area under the curve, the total heat flow was calculated.

Sample: IMC SMC
Size: 16.3000 mg
Method: IMC
Comment: Isothermal scan

DSC

File: E:...\IMC(SMC) 1.0%TBPB 100C 120312
Operator: Seunghyun Ko
Run Date: 03-Dec-2012 16:23
Instrument: DSC Q20 V24.9 Build 121
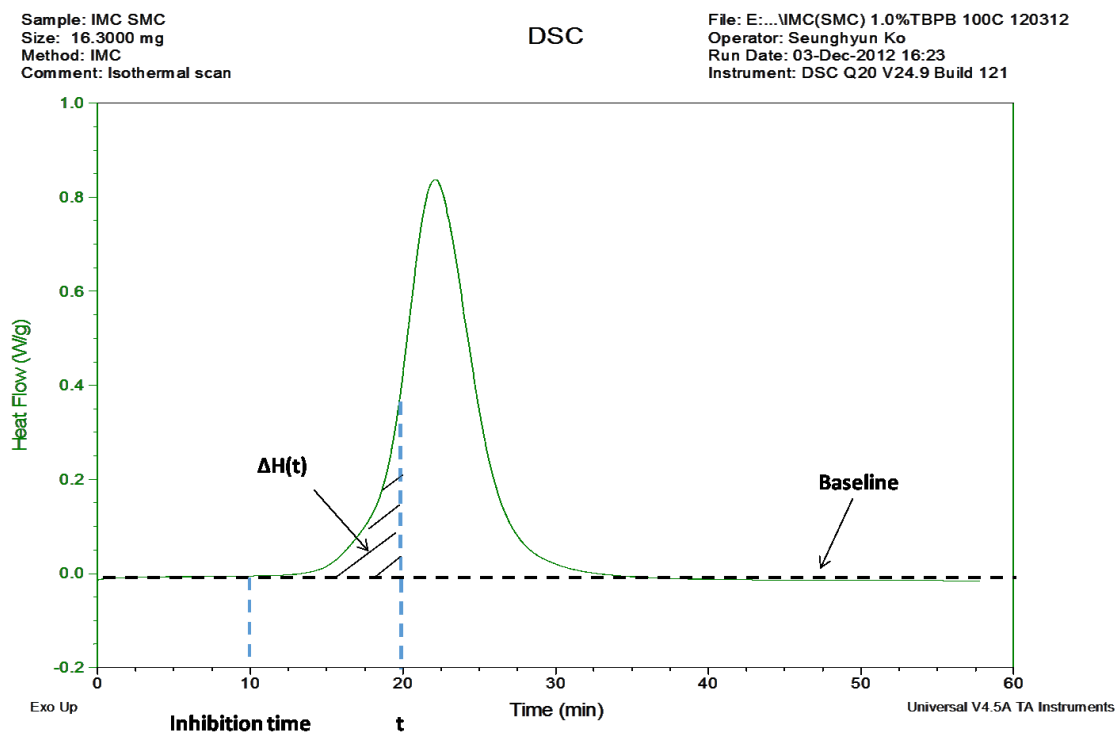
Figure 2. 7 A typical isothermal DSC curing curve of IMC resin

In order to predict conditions others than the measured ones, in particular to select best compromises among performance measures, we need to develop a mathematical model to predict extent of reaction as a function of time and temperature (cure model). The typical IMC compounds have vinyl groups that react by the free radical mechanism. A series of kinetic models for free radical polymerization of IMC coating materials have been developed to describe the reaction mechanism [14-17]. In this study, the free radical polymerization model was used to determine inhibition time, that is the time before the thermosetting reaction starts. Which for the case of one initiator as used in this chapter is given by the following equation:

25

$$t_z = -\frac{1}{k_{do}} \ln \left(1 - \frac{C_{zo}}{2C_{IO}} \right) e^{\frac{E_d}{RT}}$$

(2.4)

Where t_z is the inhibition time, k_{do} is the frequency factor for decomposition, C_{zo} is the initial concentration of inhibitor, C_{IO} is the initial concentration of initiator, E_d is the activation energy of decomposition, R is the ideal gas constant and T is the temperature. Details of the derivation are given in Chapter 3.

After the inhibitor is consumed the curing reaction starts. To predict the conversion versus time and temperature we used the autocatalytic model [13], a phenomenological model since it gave us best results. The parameters of the cure model were fit using the differential scanning calorimeter data shown in Figure 2.8. The model is represented by equation 2.5. Details of the model as well as how is used when to initiators are used, are given in Chapter 3.

$$\frac{d\alpha}{dt} = \left(\alpha_o + k_p \alpha^m \right) (\alpha_{max} - \alpha)^n \text{ where } \alpha_o = 0.001$$

(2.5)

Where k_p is the kinetic rate constant, m and n are reaction orders and α_{max} is maximum conversion. Figure 2.9 shows good agreement between predictions of the model and experimental data. A more relevant test of the model is to compare against data from a DSC scan, over a broad temperature range as these will cover the usual processing conditions for compression molded SMC process. The model does a good job predicting

the conversion during the DSC scan as shown in Figure 2.10. The parameters of the cure

model are given in Table 2.2.
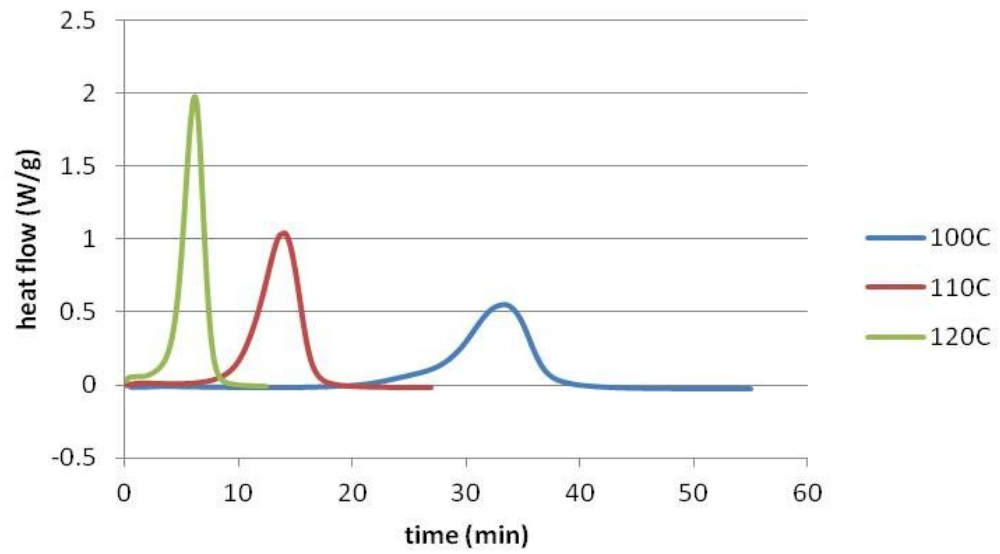
Figure 2. 8 Measured heat flow at different temperatures from DSC tests
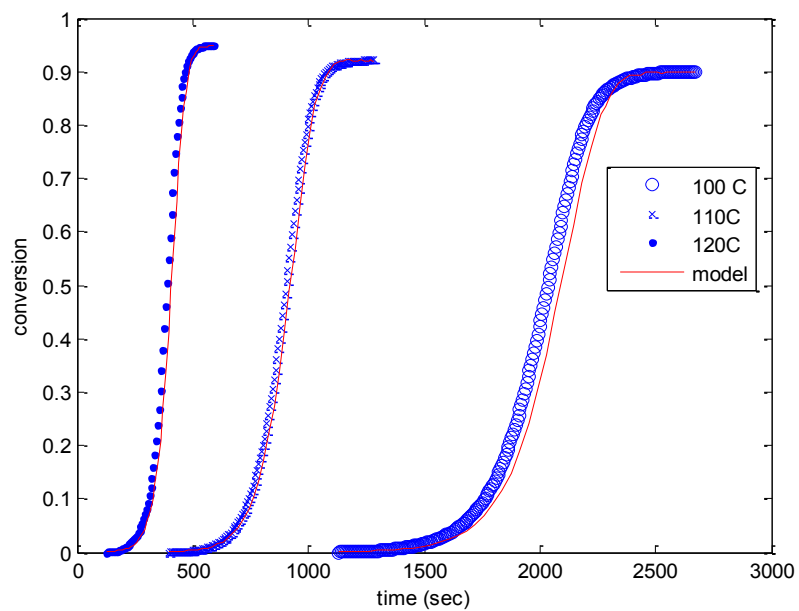
Figure 2. 9 Comparison between isothermal DSC tests and kinetic model
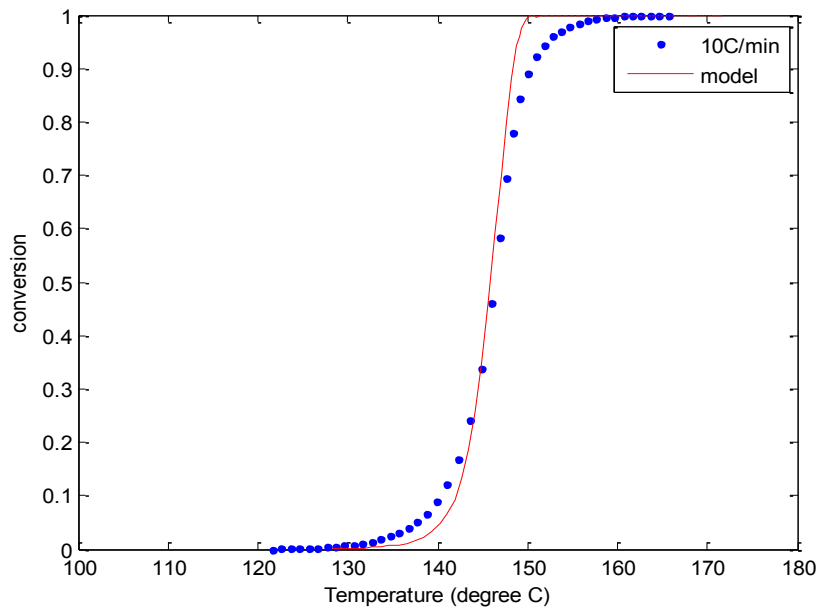
Figure 2. 10 Comparison between non-isothermal DSC scan and kinetic model

Parameters	IMC system
m	0.9998
n	0.7095
k_{p0} $(1/s)$	1.73E+07
E_p (J/mol)	6.63E+04
α_{max}	$0.0024 \times T(kelvin) - 0.0022$
k_{do} $(1/s)$	2.65E+13
E_d (J/mol)	1.32E+05

Table 2. 2 Parameters for cure model

From the rheometer we obtain viscosity and elastic modulus versus time and from the DSC measurements, we obtain the experimental conversion versus time. Combining both, we can obtain both viscosity and modulus versus conversion. Figure 2.11 (a) and (b) show measured viscosity, complex viscosity and conversion as function of reaction time at 120°C. The measured viscosity and complex viscosity was plotted as function of conversion in Figure 2.11 (c). As can be seen in the figure, the viscosity increases as a step function as soon as the conversion becomes non zero (extremely low), contrary to most typical reactive systems, such as the epoxy system discussed in section 2.4. Figure 2.11 (d) shows reduced G' (divided by final value) versus conversion. The reduced G' reached a nearly constant plateau when cured.
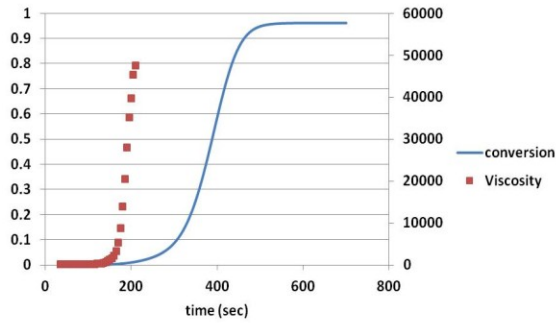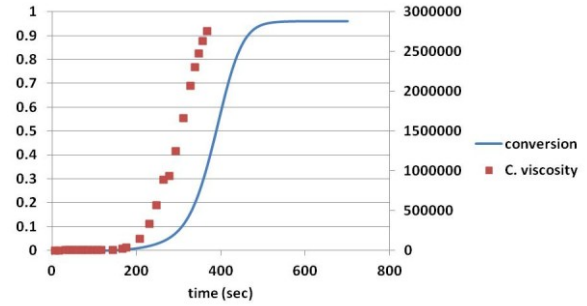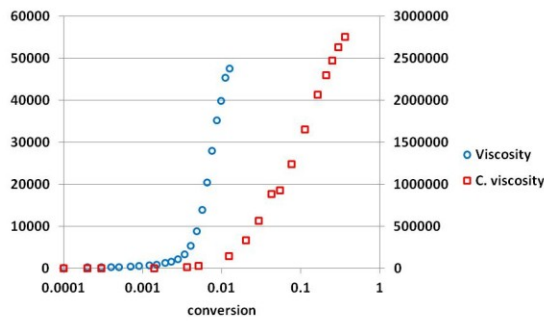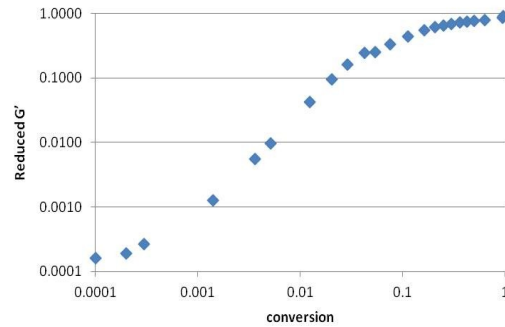
Figure 2. 11 (a) viscosity and conversion versus time (b) complex viscosity and conversion versus time (c) viscosity and complex viscosity versus conversion (d) reduced elastic modulus (G') versus conversion at 120 °C for IMC with 2.8%CB

An important thing to be noted is that when the degree of conversion is 0.01, the viscosity from steady shear measurements increases rapidly and the complex viscosity from dynamic shear flow measurements starts to increase as shown in Figure 2.11 (c). Steady shear measurements can characterize only the initial portion of a thermoset's viscosity range. Near the gel point the steady shear viscosity increases rapidly and becomes unmeasurable due to stiffening the sample fractures. Figure 2.12 shows the reduced viscosity from steady shear measurements for all temperatures for the samples

30

with and without CB as function of conversion. The reduced viscosities do not collapse into a single curve, particularly the ones with CB at 100 and 110 $^{\circ}$C. We can clearly see that the viscosity rises to infinity at a very low conversion value. This behavior is contrasted to an epoxy system in section 2.4.

In contrast, dynamic viscosity measurements can be made beyond the gel point. This is possible because the measurements are done at a strain amplitude low enough to prevent disruption of the gel structure as it is being formed. When the different runs are normalized by dividing by the initial value at the given temperature and plotted against extent of reaction obtained from DSC measurements, two temperatures collapse to a single curve except 100°C as shown in Figure 2.13 but the complex viscosity starts to increase when the conversion is around 0.01 for all temperatures. The results from the tests for IMC with 2.8%CB and 0%CB are plotted in Figure 2.14. It is clearly seen that the reduced viscosity starts to increase at the conversion of 0.01 for all temperatures and carbon black contents.

As we discussed, the viscosity of IMC starts to be increased rapidly at the conversion of 0.01. The inhibition time couldn't be captured above 130 °C in chemorheology and DSC measurements. It takes time before instruments start to measure data because of loading the sample and reaching the set temperature. Therefore, gel test was performed to measure the gel time of IMC and it compared with predicted inhibition time in high temperatures. For the gel test, the IMC resin mixed with 1% TBPB was loaded between preheated hot plate and thin circular aluminum plate of 50 mm in diameter and the time at which the aluminum plate doesn't rotate by hand was measured.

The temperature between hot plate and aluminum plate was measured by thermocouple before loading the sample to check that it is reached to set temperature. Measured gel times for several temperature are summarized in Table 2.3. The predicted inhibition time was close to measured gel times in high temperature regions. It identifies that the developed cure model can be applied to predict inhibition times of IMC resin.

When the IMC gels, it cannot flow, and as seen in the previous figures, the IMC with or without CB and independent of temperature gels at very low conversion values. Thus it can be assumed that the coating gels as soon as the inhibitor is consumed. Therefore, the maximum time available for flow (flow time) can be assumed to be the inhibition time. Since for typical SMC process, the mold temperature can only be controlled within ±5 °C. We defined that flow time is half of inhibition time. The predicted inhibition and flow times for several mold temperatures are summarized in Table 2.3. For example, when the set mold temperature is 150 °C in the molding process, the actual mold temperature can reach to 155 °C. In this case, the inhibition time 4.6 sec at 150 °C will fail to cover the surface since 2.9 sec of the inhibition time at 155 °C is much shorter than the one at 150 °C. If we assumed that the flow time is half of the inhibition time, the time to flow is 2.3 sec and the IMC has enough time to flow to cover the SMC substrate. To predict the flow time, the cure model was used and it was then assumed that flow time is half of inhibition time.
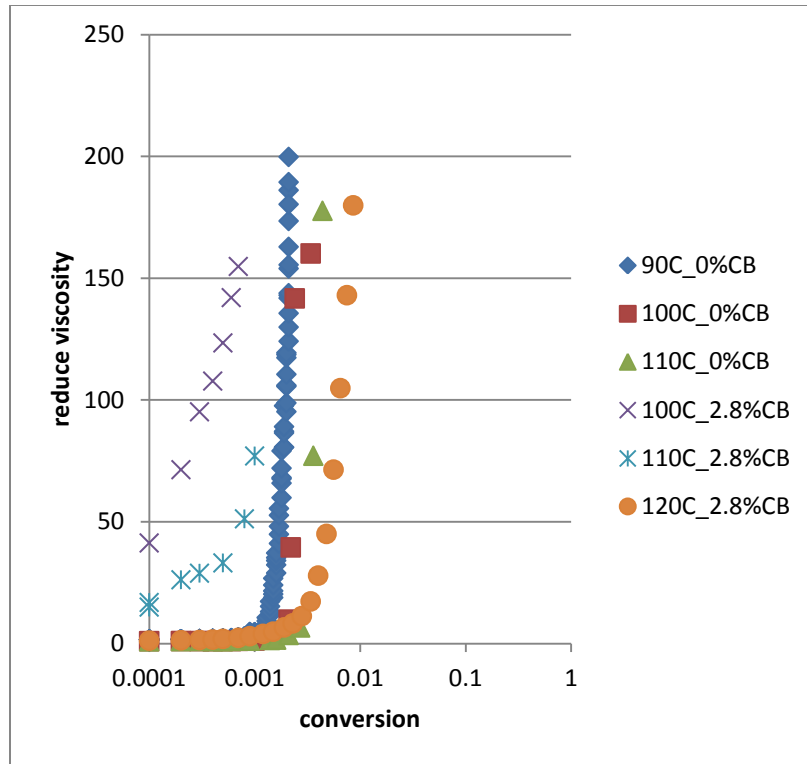
Figure 2. 12 Reduced viscosity versus conversion for IMC with 0% and 2.8%CB at varying temperatures
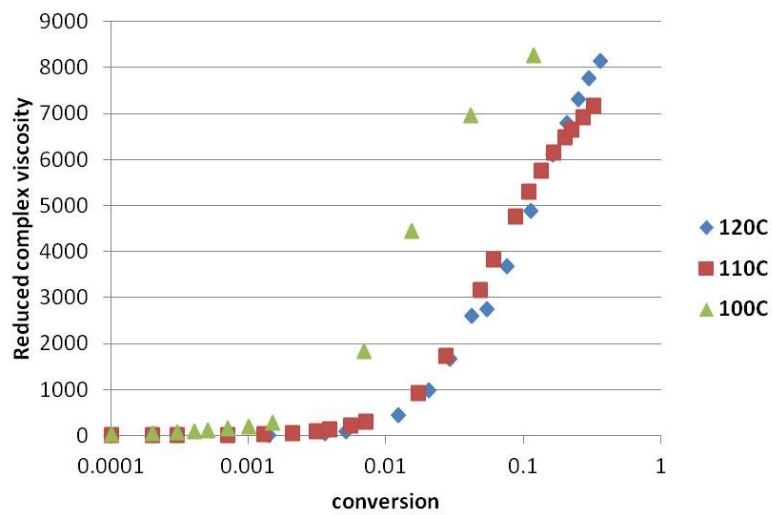
Figure 2. 13 Reduced complex viscosity versus conversion for IMC with 2.8%CB
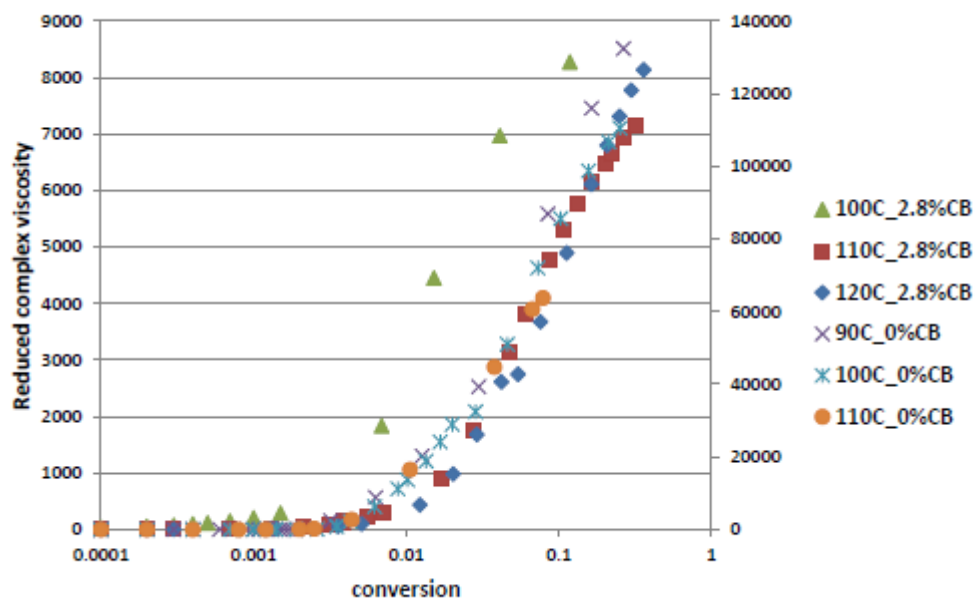
Figure 2. 14 Reduced complex viscosity versus conversion for IMC with 0% and 2.8%CB at varying temperatures.

Mold temperature (°C)	Inhibition time (sec)	Gel time (sec)	Flow time (sec)
120	118	114 - 134	59
130	47.5	47 - 60	23.7
135	27.1	-	13.6
140	15.5	17 - 21	7.7
145	8.9	-	4.4
150	4.6	5 - 7	2.3
155	2.9	-	1.4

Table 2. 3 Predicted inhibition and flow time for varying mold temperatures

In-mold coating experiments for SMC compression molding were conducted using the mold in a 450 ton press, shown in Figure 2.15. Mold opening time was varied at several temperatures, to experimentally obtain the minimum mold opening time, by visual inspection as shown in Figure 2.16 and Table 2.4. Figure 2.17 shows IMC coated compression molded SMC parts cured at a mold temperature of 137°C for 100 and 150 sec. At a mold temperature of 137°C the coating is under cured for 100 sec of cure time. It is fully cured for 150 sec cure time.
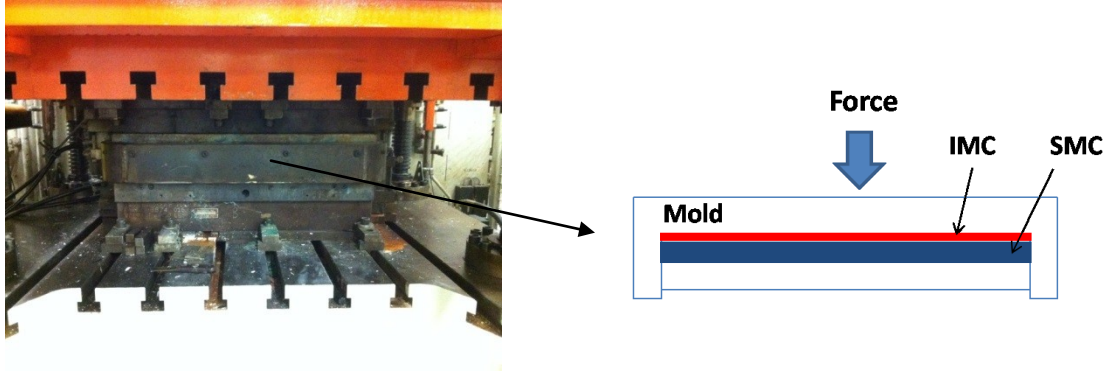
Figure 2. 15 Mold in a 450 ton Hoesch Press at OMNOVA solutions Technical Center
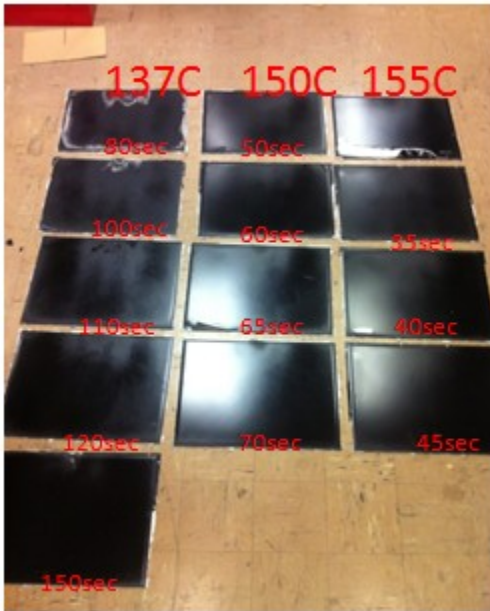
Figure 2. 16 IMC coated SMC parts for varying mold temperature and cure time

<div align="center">(a)   (b)</div>

Figure 2. 17 IMC coated SMC parts at 137°C (a) IMC cure time: 100 sec (b) IMC cure time: 150 sec

Mold temperature (°C)	Cure time of IMC (sec)	Visual inspection of molding part
137	80	Uncured
	100	Under cured
	110	Under cured
	120	Cured
	150	Cured
150	50	Under cured
	60	Under cured
	65	Cured
	70	Cured
155	**35**	Under cured
	40	Cured
	45	Cured

Table 2. 4 IMC coated SMC molding tests

In order to have a more accurate determination of the cure time, the surface quality of molded parts was evaluated using the optical profilometer, shown in Figure

2.18. Figure 2.19 shows measured surface roughness Ra versus cure time at different mold temperatures. Increasing the mold opening time, the measured surface roughness decreased in all mold temperatures. The measured surface roughness at different mold temperatures and varying cure time are summarized in Table 2.5. These measurements allowed us to better quantify the minimum cure time than the visual inspection of molding parts.

Figure 2. 18 Optical profilometer
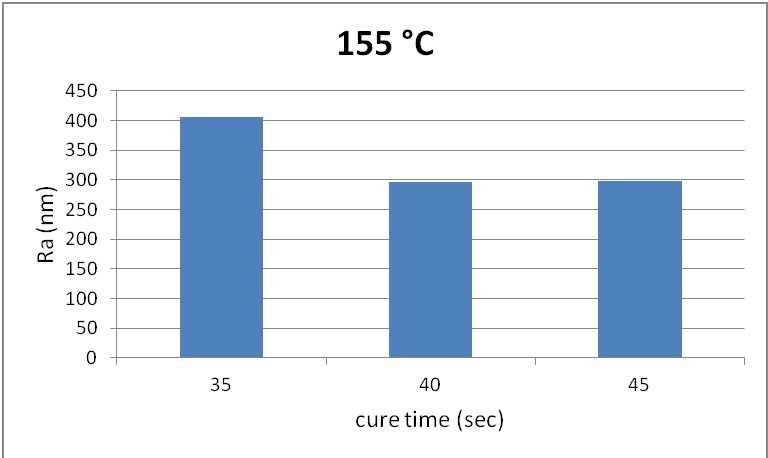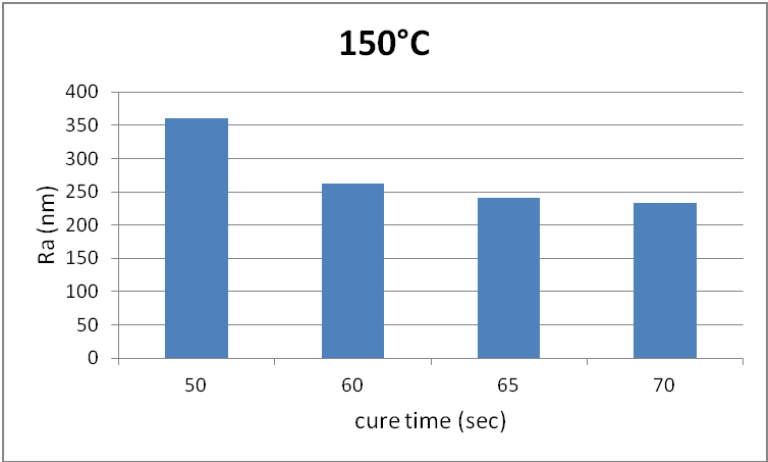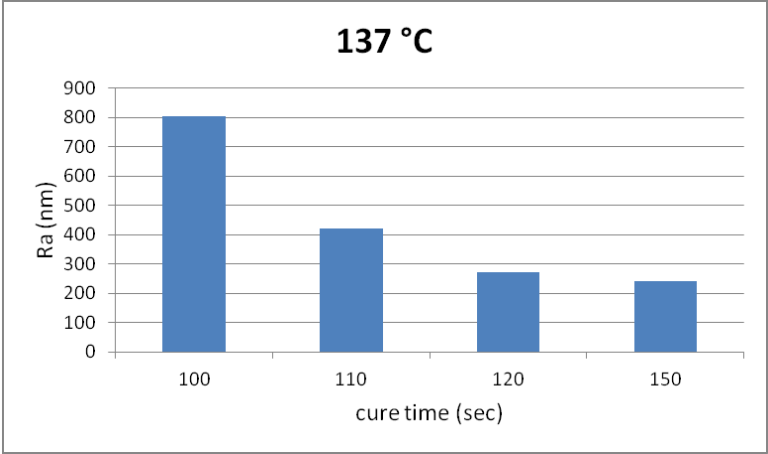
Figure 2. 19 Measured surface roughness at different mold temperatures

Mold temperature (°C)	Cure time of IMC (sec)	R_a (nm)
137	100	938
	110	422
	120	273
	150	243
150	50	360
	60	262
	65	241
	70	216
155	**35**	406
	40	247
	45	277

Table 2. 5 Measured surface roughness at varying mold temperatures and time for cure

Figure 2.20 shows measured surface roughness versus conversion from model predictions at different mold temperatures. At a conversion of 0.9, surface roughness was between 250nm and 300nm for all temperatures and visual observation also agreed with these parts being defect free.

The goal is how to estimate the flow and mold opening times using the cure model developed from the DSC measurements. The time available for flow, is defined as half of inhibition time. As shown previously, the steady shear viscosity nearly becomes infinity as soon as any reaction is detected. The reason for choosing the flow time as half of the inhibition time is to account for the fact that in typical SMC molding operations; the temperature can be controlled to within ±5 °C. As shown in Figures 2.21 and 2.22, the elastic modulus at a conversion of 0.9 has reached a nearly constant plateau for all temperatures and different carbon black contents. This is in good agreement with the value at which the part can be considered properly cure by visual inspection as well as the value at which a plateau of surface roughness is reached. The mold opening time

measured from SMC/IMC molding and predicted by cure model at the 0.9 of conversion summarized in Table 2.6 are in good agreement.

The predicted flow and cure times for IMC/SMC process using EC 610 IMC coating are summarized in Table 2.7. Figure 2.23 shows predicted flow and mold opening times for IMC process at varying temperature ranges compared with gel tests and SMC/IMC molding experiments.
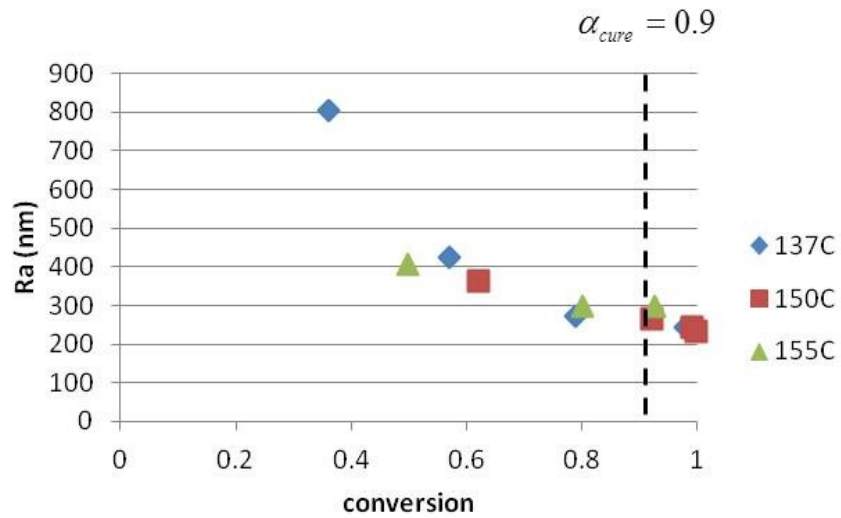
Figure 2. 20 Measured surface roughness versus conversion at varying mold temperature
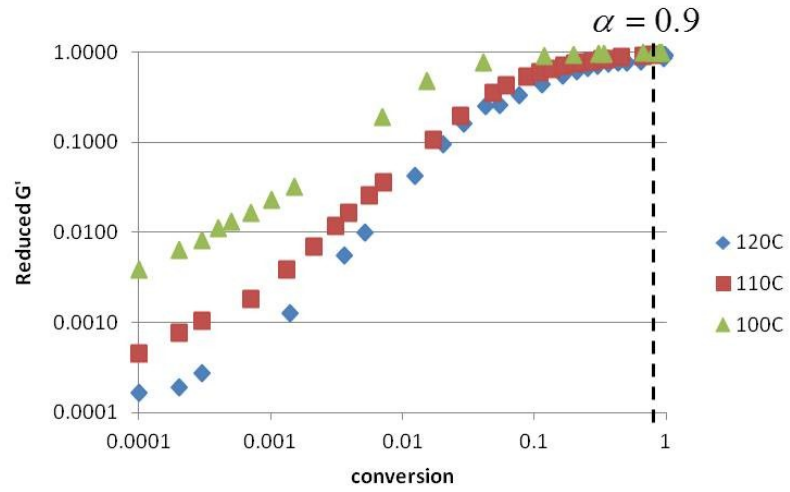
Figure 2. 21 Reduced G' versus conversion for IMC with 2.8%CB
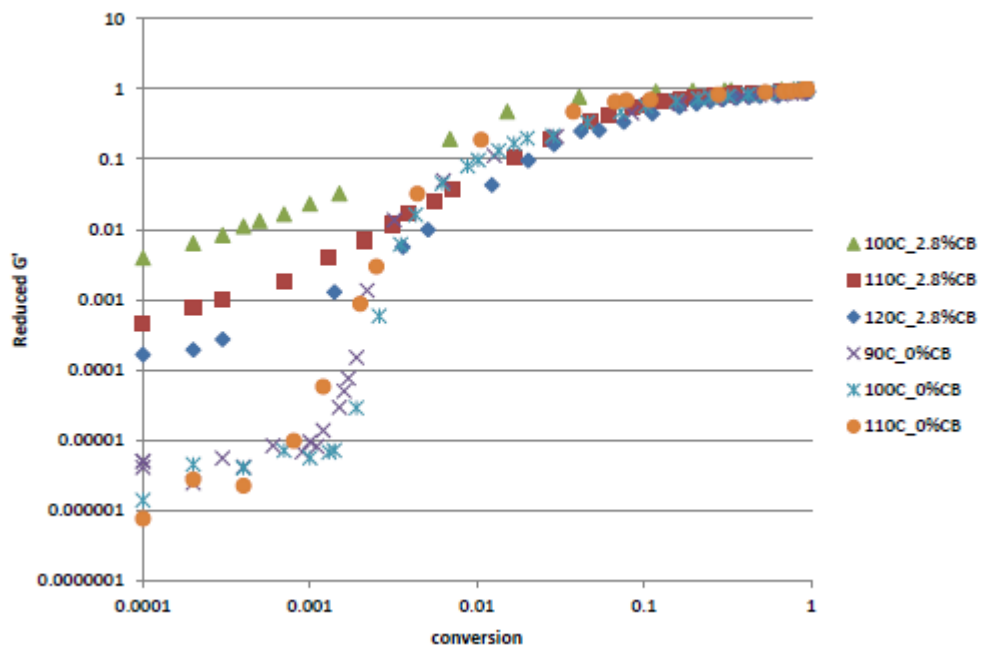
Figure 2. 22 Reduced G' versus conversion for IMC with 0% and 2.8%CB at varying temperatures

Mold temperature (°C)	SMC/IMC molding (sec)	Cure model (sec)
137	110-120	125
150	60-65	59
155	35-40	44

Table 2. 6 Mold opening time from SMC/IMC molding and cure model

Mold temperature (°C)	Flow time (sec)	Mold opening time (sec)
137	8.9	125
150	2.3	59
155	1.4	44

Table 2. 7 Predicted flow and mold opening time of IMC
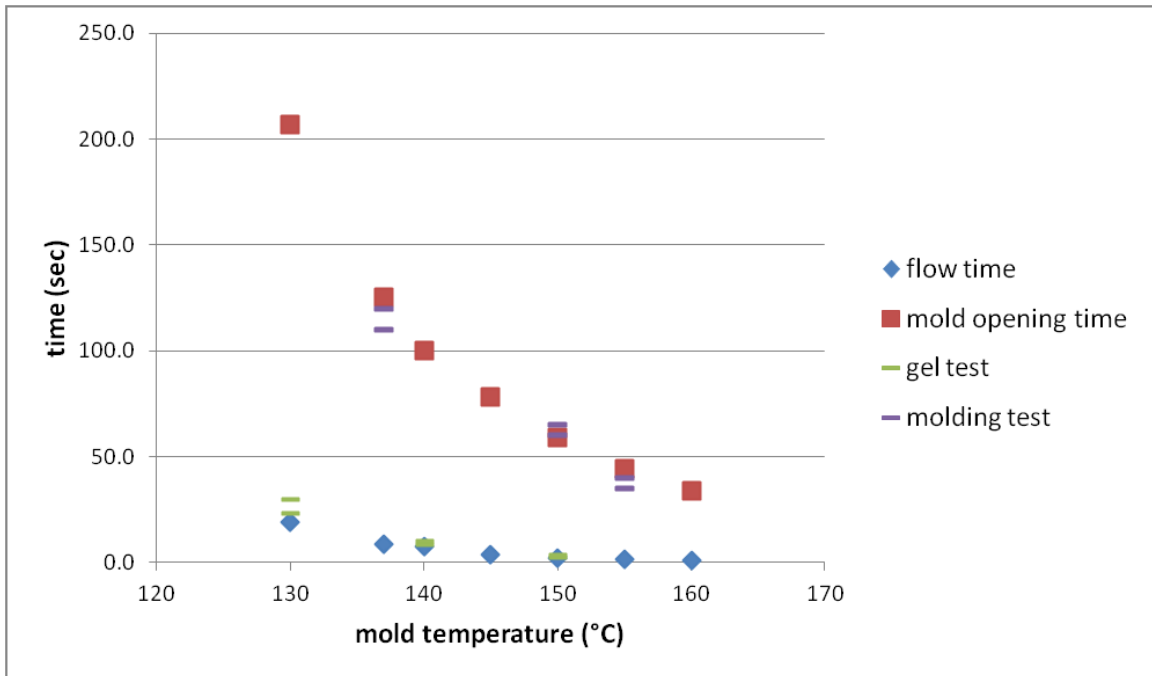
Figure 2. 23 Plot of predicted flow and mold opening time for varying temperatures compared with gel test and SMC/IMC molding experiments

2.4 Chemorheology of Standard Epoxy Resin

For comparison in this section we study a simpler resin system, for which we know its composition. The epoxy resin used was tri-glycidylpara-amino phenol (TGAP) and m-phenylene diamine (m-PDA) was used as the crosslinker. The chemical structure of TGAP is shown in Figure 2.24. The theoretical gel conversion of 0.71 for the epoxy resin was calculated by the following equation [20]:

$$pc = 1/\{r[1 + (fA - 2)][1 + (fb - 2)]\}\text{^}1/2 \hspace{3cm} (2.6)$$

Where,

pc = Conversion of group A at the gel point

fA = Reagent A (epoxy) functionality = 3

fB = Reagent B (m-PDA) functionality = 2

r = Molar ratio of A to B group = 1

Figure 2.25 shows conversion from DSC experiments and steady shear viscosity versus reaction time at 70 and 80 °C. Reduced viscosity versus conversion is plotted in Figure 2.26. The measured gel conversion of 0.75 is very close to the theoretical value.
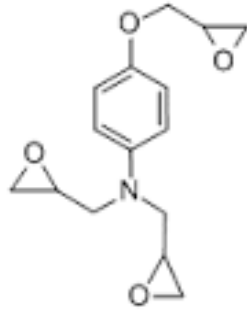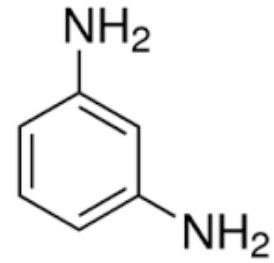
TGAP   m-PDA

Figure 2. 24 Chemical structure of tri-glycidylpara-amino phenol (TGAP) and m-phenylene diamine (m-PDA)
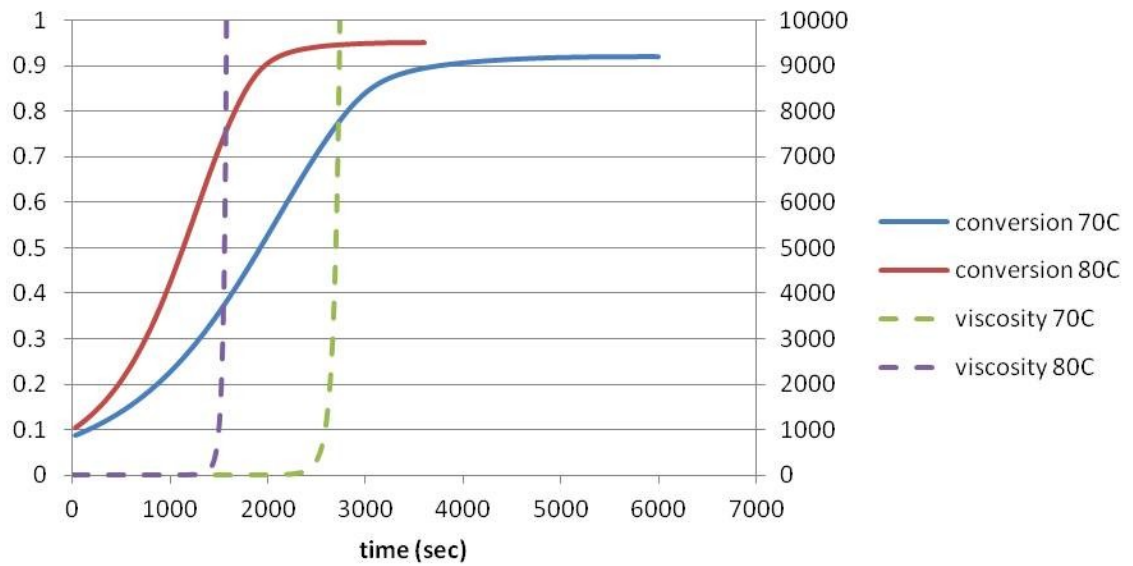
Figure 2. 25 Conversion and steady shear viscosity as reaction time at different temperatures

46
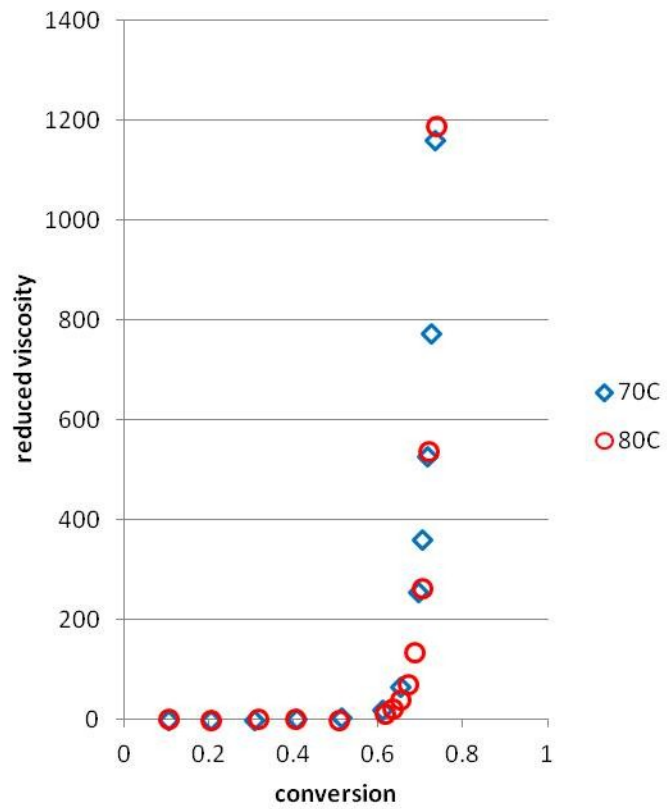
Figure 2. 26 Reduced viscosity versus conversion at 70 and 80 °C

2.5 Conclusions

In this work, the chemorheology of a commercial IMC material (Genglaze EC610) with and without carbon black was investigated using rheological measurements in both steady shear and dynamic oscillation mode. The experimental DSC data were used to obtain the degree of cure as a function of the reaction time. The viscosity, complex viscosity and elastic modulus were correlated with degree of cure (conversion) from the DSC measurements. It was found that gel conversion of IMC was extremely low, 0.01. This phenomenon is very different with the case of a standard epoxy resin system which has 0.75 gel conversion. The viscosity of IMC resin starts to increase as soon as all inhibitor is consumed therefore the maximum flow time should be the inhibition time. It was observed that the elastic modulus at a conversion of 0.9 reached a nearly constant plateau for all temperatures. IMC/SMC molding tests were conducted at varying mold temperatures and several mold opening times. Minimum acceptable mold opening time was determined by investigating surface quality using optical profilometer. A good agreement between the predicted and experimental flow and mold opening times of In-mold coating was obtained. In summary, it is recommended that the time available for flow (flow time) of IMC be half the predicted inhibition time. The IMC coated parts can be de-molded when the extent of reaction reaches 90% (mold opening time).

2.6 References

1.   J. M. Castro and R. M. Griffith, "In-Mold Coating," in *Sheet Molding Compound: Science and Technology,* edited by Hamid G. Kia, Munich: Hanser, 1993, pp. 163-180.

2.   J. M. Castro and R. M. Griffith, *Polym. Eng. Sci.* 30, 677-683 (1990).

3.   H. H. Winter, *Mater. Res. Soc. Bull..* 16, 44-48 (1991).

4.   P. J. Halley and M. E. Mackay, *Polym. Eng. Sci.* 36, 593-609 (1996).

5.   J. Yang, J. Xiao, J. Zeng, C. Peng, X. Feng and B. Hou, *Appl. Compos. Mater*, 19, 573-582 (2012)

6.   K. Raghu Raja Pandiyan and S. Neogi, *J. Appl. Polym. Sci.* 125, 1400-1408 (2012).

7.   A. Terenzi, C. Vedova, G. Lelli, J. Mijovic, L. Torre, L. Valentini and J. M. Kenny, *Comp. Sci.Technol.* 68, 1862-1868 (2008).

8.   H. Yari, M. Mohseni and Z. Ranjbar, *J. Appl. Polym. Sci.* 129, 1929-1938 (2013).

9.   M. Abdalla, D. Dean, P. Robinson and E. Nyairo, *Polymer* 49, 3310-3317 (2008).

10.   M. Monti, D. Puglia, M. Natali, L. Torre and J. M. Kenny, *Comp. Sci.Technol.* 71, 1507-1516 (2011).

11.   Jose M. Castro, "Mold Filling and Curing Studies for the Polyurethane RIM Process", Ph.D. Thesis, University of Minnesota, 1980.

12.   J. M. Castro and C. W. Macosko, *AIChE J.* 28, 250-260 (1982).

13.   J. M. Kenny, *J. Appl. Polym. Sci.* 51, 761-764 (1994).

14.   J. F. Stevenson, *Polym. Eng. Sci.* 28, 746 (1986).

15.   L. J. Lee, *Polym. Eng. Sci.* 21, 483 (1981).

16. J. M. Castro and C. C. Lee, *Polym. Eng. Sci.* 27, 218 (1987).

17. K. S. Zuyev and J. M. Castro, *J. Polym. Eng.* 22, 233-260 (2002).

18. D. H. Chang and W. L. Kwok, *J. Appl. Polym. Sci.* 28, 3155-3183 (1983).

19. Xilian Ouyang, "Surface modified carbon nanoparticle papers and applications on polymer composites", Ph.D. Thesis, The Ohio State University, (2014).

20. Curtis R. Center, "Thermoplastic melt-mixed composition with epoxy-carboxylic acid compound heat stabilizer", Patent WO2013188488 A1, 2013.

Chapter 3: Curing Analysis of In-mold Coating

The curing behavior of a thermoset resin system significantly affects the physical, chemical and mechanical properties of the polymer. Thus, an understanding of the cure during the process is critical for better design and control of the molding process. The in-mold coating (IMC) resin is a thermosetting liquid that when injected onto the surface of the part cures and bonds to provide a smooth surface and required electrical conductivity for electrostatic painting. In order to optimize the IMC process, it is essential to predict the time available for flow (flow time), as well as the time when the coating has enough structural integrity so that the mold can be opened without damaging the part surface (cure time). In Chapter 2, we discussed the relationship between inhibition time and the flow time. We related the chemo-rheological changes of IMC to the cure model and discuss how to best estimate the cure time. In the following section, we discuss the proposed method used to represent the cure model of in mold coating systems. The method is applied to develop the cure rate equations for a typical commercial coating material. The free radical polymerization model was used to determine inhibition time, that is the time before the thermosetting reaction starts. The autocatalytic kinetic model was used to describe the evolution of the extent of reaction or conversion once the inhibitor is consumed. In this study, the cure parameters to represent kinetic model were fitted as function of temperature and contents of initiators by liner regression. Here we

are interested in developing cure model to select best compromises among performance measures using multiple criteria optimization method. The fitted cure parameters were used to predict inhibition time and cure time as function of temperature and initiator contents to optimize IMC process in Chapter 4.

In this chapter, the cure model for IMC with one initiator under isothermal condition was developed. Then, the cure model for IMC with two initiators under isothermal condition was developed to study the effect of two initiators on the cure reaction of IMC. The cure parameters obtained from isothermal DSC data were used to predict the extent of reaction obtained using dynamic DSC data over a broad temperature rage that covers usual processing conditions for sheet molding compound and injection molding. Finally, in the last part of this chapter, we discuss the effect of carbon black on the cure reactions of IMC.

3.1 Introduction

Thermosetting resins, because of their attractive mechanical and chemical properties, play an important role in many industries including automotive, coatings, aerospace and electronics. Many studies have been conducted on the cure kinetics of thermosetting resins and a variety of kinetic models have been proposed to relate the reaction rate to reaction time, temperature and conversion [1-13]. Cure kinetic models are generally developed by analyzing experimental results obtained by different analysis techniques such as differential scanning calorimetry (DSC), infrared spectroscopy (IR), Fourier transform infrared (FTIR) spectroscopy and rheometry. DSC, which measures the

heat evolved from the sample as a function of reaction time at constant or varying temperature, has been used extensively to study the cure kinetics of thermosetting polymers due to its simplicity and ease of use. The basic assumption for applying DSC to kinetic studies is that the dimensionless reaction rate $d\alpha/dt$, is proportional to the measured heat flow, dH/dt:

$$\frac{d\alpha}{dt} = \frac{1}{H_{total}} \frac{dH}{dt}$$
(3.1)

Where if isothermal DSC is used, the total heat for the curing reaction, H_{total}, is given by

$$H_{total} = H_i + H_r$$
(3.2)

where H_i is the heat measured in the isothermal DSC experiments and H_r is the residual heat of the curing reaction after isothermal cure, which can be measured by scanning the isothermally cured samples.

The degree of cure as a function of time is given by:

$$\alpha(t) = \frac{1}{H_{total}} \int_0^t \left(\frac{dH}{dt}\right) dt$$
(3.3)

In general, kinetic models of thermosetting resins fall into two types: phenomenological models and mechanistic models [1, 18]. A phenomenological model is generally expressed in a relatively simple rate equation, and is developed ignoring the details of how the different reactive species take part in the reaction. Although several simultaneous reactions are occurring during the polymerization process, simple models based on the assumption that one reaction can represent the curing process have been

developed for modeling purposes. The simplest model is the nth-order kinetic expression [21]:

$$\frac{d\alpha}{dt} = k(1-\alpha)^n \tag{3.4}$$

where α is conversion, n is the reaction order and k is the rate constant assumed to have an Arrhenius temperature dependence:

$$k = k_0 \exp\left(-\frac{E}{RT}\right) \tag{3.5}$$

However, the nth order model cannot describe the progress of complex reactions of some thermosetting resin systems because it predicts that the maximum reaction rate occurs at time $= 0$. Thus, if the isothermal reaction is characterized by showing a maximum reaction rate at some point other than at the start of reaction, the nth order kinetic model cannot be applied and the autocatalytic model must be used [4, 5]:

$$\frac{d\alpha}{dt} = (k_1 + k_2\alpha^m)(1-\alpha)^n \tag{3.6}$$

where k_1 and k_2 are rate constants with Arrhenius temperature dependency. m and n are reaction orders.

When the isothermal DSC experiments show the existence of inhibition time, the initial cure rate is zero at $t = 0$:

$$\left(\frac{d\alpha}{dt}\right)_{t=0} = k_1$$

The equation (3.6) can be simplified as:

$$\frac{d\alpha}{dt} = k_2\alpha^m(1-\alpha)^n \tag{3.6.1}$$

54

However, equation 3.6.1 starts with α and its derivative equal to zero at time zero. Thus for the reaction to start, we need to set k_1 at least equal to a small value. Here, we used for all cases:

$$\frac{d\alpha}{dt} = (\alpha_o + k_2\alpha^m)(1 - \alpha)^n, where \ \alpha_o = 0.001$$

A series of mechanistic kinetic models for free radical polymerization of IMC materials have been developed by Stevenson [14], Lee [15, 20], and Castro et. all [16-19], to describe the reaction mechanism including initiation, termination and propagation steps. Mechanistic models have the advantage of describing the details of the reaction; however, they are more difficult to fit to experimental data and in some cases too complicated for use in engineering analysis. Furthermore, when the details of the chemical reaction are needed, DSC is not the best analytical method to use. Analytical techniques that follow the details of the appearance or disappearance of the different chemical species such as IR or FTIR should be used.

In the current work, our main objective is to evaluate the chemo-rheological changes of the coating materials during the molding process, that is the evolution of the coating from a liquid to a solid, and as such, be able to predict the time available for flow and the time at which the part can be removed from the mold. Thus we will use a phenomenological model to predict the curing reaction instead of the more complicated mechanistic models. DSC will be used to evaluate the cure parameters. The mechanistic

model will only be used to predict the inhibition time, which is the time needed to consume the inhibitor.

3.2 Cure Model

3.2.1 One Initiator under Isothermal Condition

The main chemical reaction for In-mold coating resins is the breaking of the secondary bond of the vinyl group, depending of the specific coating application, the resin mixture may contain other reacting groups such as epoxy or urethane but for the most part, the vinyl chemistry, describes the cure reaction. The IMC formulation also contains inhibitors, to control the flow time. For the first part of the reaction, that is to predict the inhibition time, we will use a mechanistic model. The reaction can be assumed to proceed by the free radical mechanism [16, 18] as shown below:

$$I \xrightarrow{k_d} 2R \cdot$$
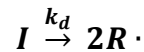
It is assumed that until the inhibitor is consumed, the free radicals react with molecules of inhibitor present in the system:

$$R \cdot + Z \rightarrow RZ$$

After the inhibitor is consumed, the propagation step starts. In propagation step, free radicals react with molecules of monomer to break up the vinyl groups:

$$R \cdot + M \xrightarrow{k_p} RM \cdot$$
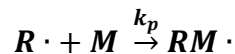
The assumptions of this model are as follows:

- A single initiator and inhibitor are used in the system; in the next section we consider the case where two initiators are used.

56

- No monomer reacts until the number of initiator radicals created is equal to the effective number of inhibitor molecules initially present

- A single reaction rate constant characterizes all propagation reactions

- Monomer diffusion control is less important

- Free radical termination is negligible for times larger than inhibition time

i) $t < t_z$

$$\frac{dC_I}{dt} = -k_d C_I \tag{3.7}$$

where k_d is represented by Arrhenius type equation:

$$k_d = k_{do} e^{-\frac{E_d}{RT}}$$

For isothermal condition, we can integrate the equation 2.7 to get the following:

$$C_I = C_{IO} e^{-k_d t} \tag{3.8}$$

The concentration of free radicals is equal to twice the initial concentration of initiator minus the concentration of initiator at a particular time:

$$C_{R\cdot} = 2(C_{IO} - C_I) \tag{3.9}$$

$$C_{R\cdot} = 2(C_{IO} - C_{IO} e^{-k_d t}) \tag{3.10}$$

$$\therefore\ C_{R\cdot} = 2C_{IO}(1 - e^{-k_d t}) \tag{3.11}$$

At the time when all inhibitor initially present is consumed t_z we have:

ii) $t = t_z$

$$C_{zo} = 2(C_{IO} - C_I(t_z)) \tag{3.12}$$

$$C_{zo} = 2(C_{IO} - C_{IO} e^{-k_d t_z}) \tag{3.13}$$

$$\therefore \ C_{zo} = 2C_{IO}(1 - e^{-k_d t_z}) \tag{3.14}$$

The equation 3.14 means that at the time when all inhibitor is consumed the initial concentration of inhibitor is equal to twice the initial concentration of initiator minus the concentration of initiator at time, t_z.

We can rewrite the equation 3.14 as follows:

$$1 - e^{-k_d t_z} = \frac{C_{zo}}{2C_{IO}} \tag{3.15}$$

$$t_z = -\frac{1}{k_d}\ln\left(1 - \frac{C_{zo}}{2C_{IO}}\right) \tag{3.16}$$

$$\therefore \ t_z = -\frac{1}{k_{do}}\ln\left(1 - \frac{C_{zo}}{2C_{IO}}\right)e^{\frac{E_d}{RT}} \tag{3.17}$$

$$\ln t_z = \ln\left(-\frac{1}{k_{do}}\ln\left(1 - \frac{C_{zo}}{2C_{IO}}\right)\right) + \frac{E_d}{RT} \tag{3.18}$$

If we measure the inhibition times from the DSC experiments; we can plot $\ln t_z$ versus $1/T$ to get a straight line which can be fitted to give us a linear equation. From the slope and intercept, we can get the values of E_d and k_{do}. The concentration of initiator is known, but the concentration of inhibitor is not known, as is added at different stages during the formulation of the commercial IMC resin system. Coating manufacturers usually do not include the value of C_{zo} into material data sheets. The actual concentration of inhibitor present in the formulation is unknown. Some researchers assume a value for

58

the ratio of $\frac{C_{zo}}{2C_{IO}}$, including the inhibitor effectiveness in inactivating free radicals [15-17]. It can also be considered a fitting parameter, in our case; we assume that the concentration of inhibitor is 0.0002 wt. %, which is consistent with the work of Lee and Stevenson [15]. The model with this assumption showed a good agreement between experimental data and prediction.

iii) $t > t_z$

As discussed previously, we will use the autocatalytic model instead of the free radical model:

$$\frac{d\alpha}{dt} = \left(\alpha_o + k_p \alpha^m\right)(\alpha_{max} - \alpha)^n, where \; \alpha_o = 0.001$$

where m and n are the reaction orders, α_{max} is the maximum conversion and k_p is the rate constant given by an Arrhenius temperature dependence:

$$k_p = k_{po} e^{-\frac{E_P}{RT}}$$

where k_{po} is the pre-exponential constant, E_P is the activation energy and T is the absolute temperature.

Several methods have been proposed to determine kinetic parameters from experimental data. Ryan and Dutta proposed a numerical method base one the zero initial reaction rate and on the maximum of the reaction rate curve for epoxy systems. However, they assumed that total reaction order is m+n=2. Some researcher used the nonlinear regression analysis to obtain kinetic parameters. In this dissertation, the kinetic parameters of the autocatalytic model are determined using the graphic-analytical method proposed by Kenny et al [5]. The procedure is illustrated in appendix B. After estimating

the kinetic parameters, the relationship between the cure time and conversion can be obtained by integrating equation 3.6.1. Since an algebraic integration of equation 3.6.1 is not possible, it is necessary to implement the numerical integration. In this procedure, the Runge- Kutta numerical method was employed to solve the differential equation using MATLAB function to provide an accurate solution. The autocatalytic kinetic model applied in this research can be expressed as:

$$t < t_z: \quad \frac{d\alpha}{dt} = 0$$

$$t \geq t_z: \quad \frac{d\alpha}{dt} = (\alpha_o + k_p \alpha^m)(\alpha_{max} - \alpha)^n, where \; \alpha_o = 0.001$$

3.2.2 One Initiator under Non-isothermal Condition

If the curing temperature is a function of time, that is, $T = T(t)$, and assuming that the temperature varies linearly with time (such as in the DSC scanning mode) we have:

$T = T_o + \beta t \; where \; \beta = \frac{dT}{dt} = constant$ is the heating rate.

$i) \; t < t_z$

$$\frac{dC_I}{dt} = -k_d(t)C_I \; where \; k_d(t) = k_{do}e^{-\frac{E_d}{RT}} \tag{3.19}$$

$$C_I(t) = C_{IO}e^{-\int_0^t k_d(t)dt} \tag{3.20}$$

$$\therefore C_I(t) = C_{IO}e^{-\int_0^t k_{do}e^{-\frac{E_d}{R(T_o+\beta t)}}dt} \tag{3.21}$$

$ii) \ t = t_z$

$$C_{zo} = 2(C_{IO} - C_I(t_z)) \tag{3.22}$$

$$C_{zo} = 2(C_{IO} - C_{IO}e^{-\int_0^{t_z} k_{do}e^{-\frac{E_d}{R(T_o+\beta t)}}dt}) \tag{3.23}$$

$$C_{zo} = 2C_{IO}(1 - e^{-\int_0^{t_z} k_{do}e^{-\frac{E_d}{R(T_o+\beta t)}}dt}) \tag{3.24}$$

$$\therefore \ -\int_0^{t_z} k_{do}e^{-\frac{E_d}{R(T_o+\beta t)}}dt = \ln\left(1 - \frac{C_{zo}}{2C_{IO}}\right) \tag{3.25}$$

For the non-isothermal case, if the kinetic parameters are known, t_z can be calculate using the equation 3.25.

$iii) \ t > t_z$

$$\frac{d\alpha}{dt} = (\alpha_o + k_p(t)\alpha^m)(\alpha_{max}(t) - \alpha)^n \tag{3.26}$$

where $k_p(t) = k_{po}e^{-\frac{E_p}{R(T_o+\beta t)}}$

$\alpha_{max}(t) = C_1 + C_2 T = C_1 + C_2(T_o + \beta t) \qquad C_1, C_2 : constant$

3.2.3 Two Initiators under Isothermal Condition

When two initiators are used during the initiation step, initiator 1 and initiator 2 decompose to give free radicals. Those free radicals react with molecules of inhibitor present in the system until all the inhibitor is consumed. Once the inhibitor is consumed, in the propagation step, free radicals react with molecules of monomer. It is assumed that R_1 and R_2 are equivalent, thus we will use R as the sum of R_1 and R_2:

$$I_1 \xrightarrow{k_{d_1}} 2R_1 \cdot$$

$$I_2 \xrightarrow{k_{d_2}} 2R_2 \cdot$$

$$R \cdot + Z \rightarrow RZ$$

$$R \cdot + M \xrightarrow{k_p} RM \cdot$$
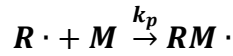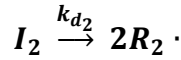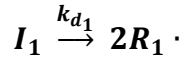
i) $t < t_z$

$$\frac{dC_{I_1}}{dt} = -k_{d_1} C_{I_1} \tag{3.27}$$

$$\frac{dC_{I_2}}{dt} = -k_{d_2} C_{I_2} \tag{3.28}$$

For isothermal conditions, we can integrate each equation 3.27 and 3.28 to get the following:

$$C_{I_1} = C_{I_1 0} e^{-k_{d_1} t} \tag{3.29}$$

$$C_{I_2} = C_{I_2 0} e^{-k_{d_2} t} \tag{3.30}$$

The concentration of total free radicals is the sum of R_1 and R_2 :

$$C_{R \cdot} = C_{R_1} \cdot + C_{R_2} \cdot \tag{3.31}$$

$$C_{R.} = 2(C_{I_1 0} - C_{I_1}) + 2(C_{I_2 0} - C_{I_2}) \tag{3.32}$$

By substituting equation 2.29 and 2.30 into equation 2.32:

$$C_{R.} = 2C_{I_1 0}(1 - e^{-k_{d_1} t}) + 2C_{I_2 0}(1 - e^{-k_{d_2} t}) \tag{3.33}$$

ii) $t = t_z$

$$C_{ZO} = 2(C_{I_1 0} - C_{I_1}(t_z)) + 2(C_{I_2 0} - C_{I_2}(t_z)) \tag{3.34}$$

$$C_{ZO} = 2C_{I_1 0}(1 - e^{-k_{d_1} t_z}) + 2C_{I_2 0}(1 - e^{-k_{d_2} t_z}) \tag{3.35}$$

The values of k_{d_1} and C_{ZO} are known from the kinetic model using a single initiator. Thus, for easiness of writing, we set:

$$2C_{I_1 0}(1 - e^{-k_{d_1} t_z}) = C_1 \tag{3.36}$$

and write the equation 3.36 as:

$$C_{ZO} = C_1 + 2C_{I_2 0}(1 - e^{-k_{d_2} t_z}) \tag{3.37}$$

$$k_{d_2} = -\frac{1}{t_z} \ln\left(1 - \frac{C_{ZO} - C_1}{2C_{I_2 0}}\right) \tag{3.38}$$

from the values of t_z at the given temperature we can calculate k_{d_2} versus temperature, then assuming an Arrhenius temperature dependence:

$$k_{d_2} = k_{d_2 0} e^{-\frac{E_{d_2}}{RT}} \tag{3.39}$$

63

$$lnk_{d_2} = lnk_{d_2o} - \frac{E_{d_2}}{RT} \qquad (3.40)$$

The values of k_{d_2o} and E_{d_2} can be calculated from the plot of lnk_{d_2} versus $1/T$.

$$t_z = -\frac{1}{k_{d_2}}\ln\left(1 - \frac{C_{ZO} - C_1}{2C_{I_2O}}\right) \qquad (3.41)$$

$$\therefore \ t_z = -\frac{1}{k_{d_2o}}\ln\left(1 - \frac{C_{ZO} - C_1}{2C_{I_2O}}\right)e^{\frac{E_{d_2}}{RT}} \qquad (3.42)$$

$iii) \ t > t_z$

$$\frac{d\alpha}{dt} = (\alpha_o + k_p\alpha^m)(\alpha_{max} - \alpha)^n \qquad (3.43)$$

$$where \ k_p = k_{po}e^{-\frac{E_P}{RT}}$$

$$lnk_p = lnk_{po} - \frac{E_P}{RT} \qquad (3.44)$$

The values of k_{po} and E_P can be calculated from the plot of lnk_p versus $1/T$ from isothermal DSC tests. The determination of autocatalytic kinetic parameters can be found in Appendix B.

3.2.4 Two Initiators under Non-isothermal Condition

$$Let. T = T_o + \beta t \ where \ \beta = \frac{dT}{dt}$$

$i) \ t < t_z$

$$\frac{dC_{I_1}}{dt} = -k_{d_1}(t)C_{I_1} \qquad (3.45)$$

$$\frac{dC_{I_2}}{dt} = -k_{d_2}(t)C_{I_2} \qquad (3.46)$$

where,

$$k_{d_1}(t) = k_{d_1o}e^{-\frac{E_{d_1}}{R(T_o+\beta t)}}$$

$$k_{d_2}(t) = k_{d_2o}e^{-\frac{E_{d_2}}{R(T_o+\beta t)}}$$

$$\therefore\ C_{I_1}(t) = C_{I_1O}e^{-\int_0^t -k_{d_1}(t)dt} \qquad (3.47)$$

$$\therefore\ C_{I_2}(t) = C_{I_2O}e^{-\int_0^t -k_{d_2}(t)dt} \qquad (3.48)$$

$ii)\ t = t_z$

$$C_{ZO} = 2\big(C_{I_1O} - C_{I_1}(t_z)\big) + 2\big(C_{I_2O} - C_{I_2}(t_z)\big) \qquad (3.49)$$

$$\therefore\ C_{I_1O}e^{-\int_0^{t_z} -k_{d_1}(t)dt} + C_{I_2O}e^{-\int_0^{t_z} -k_{d_2}(t)dt} = C_{I_1O} + C_{I_2O} - \frac{C_{ZO}}{2} \qquad (3.50)$$

In the non-isothermal case, the inhibition time can be determined by satisfying the equation 3.50.

$iii)\ t > t_z$

$$\frac{d\alpha}{dt} = \big(\alpha_o + k_p(t)\alpha^m\big)(\alpha_{max}(t) - \alpha)^n \qquad (3.51)$$

where $k_p(t) = k_{po}e^{-\frac{E_p}{R(T_o+\beta t)}}$

$$\alpha_{max}(t) = C_1 + C_2 T = C_1 + C_2(T_o + \beta t) \qquad C_1, C_2 : constant$$

3.3 DSC Experiments

3.3.1 IMC Resin Systems

The coating material used is a commercial IMC (Genglaze EC610) supplied by OMNOVA Solutions Inc. The components of Genglaze EC610 are listed in Table 3.1. The IMC contains unsaturated oligomers and monomers to give adequate hot hardness and adhesion to SMC or thermoplastic substrates. Hydroxypropyl methacrylate (HPMA) and styrene are used as diluents to decrease the viscosity. Talc is used to improve hardness and decrease shrinkage. Cobalt is employed as an accelerator. The conductive filler used in Genglaze EC610 is carbon black (CB), VULCAN XC72R from CABOT Corp. Most of the kinetics studies were done using the resin system without CB; at the end of the chapter the effect of CB on the curing reaction is evaluated. The inhibitor, Benzoquinone is used to provide shelf-life and increase flow time. The initiators used in this study are tert-butyl peroxybenzoate (TBPB) from Akzo Nobel and tert-butyl peroxy-2-ethylhexanoate (TBPE) from Arkema.

Genglaze EC610

Epoxy

Styrene

HPMA

Talc

Cobalt

Carbon black

inhibitor

Table 3. 1 Formulation of coating material

3.3.2 DSC Measurements

The reaction rate of neat IMC resin was measured using a DSC Q20 (TA instruments). The sample was prepared by adding the required quantity of initiator to the IMC resin and thoroughly mixed. About 10-15 mg of the sample was placed in a Tzero hermetic sample pan and sealed. The selection of sample size for DSC measurements can be found in Appendix C. Isothermal DSC experiments were conducted at 90, 100 and 110 °C followed by a dynamic DSC scan from 30 °C to 250 °C to measure the residual reaction heat. Non-isothermal DSC scans were performed with a heating rate 10 °C/min from 30 °C to 250 °C. The measured heat flow of a typical isothermal scan is shown in Figure 3.1. The baseline is a straight tangential line to horizontal part of the isothermal DSC curve. The inhibition time was selected as the cross point of baseline and DSC curve where the heat flow starts to increase.

In the initial stage, the heat flow remains constant. After all the inhibitor is consumed, the heat flow starts to increase. The reaction rate reaches a maximum and then decreases. By integration of the area under the curve, the total heat flow was calculated.
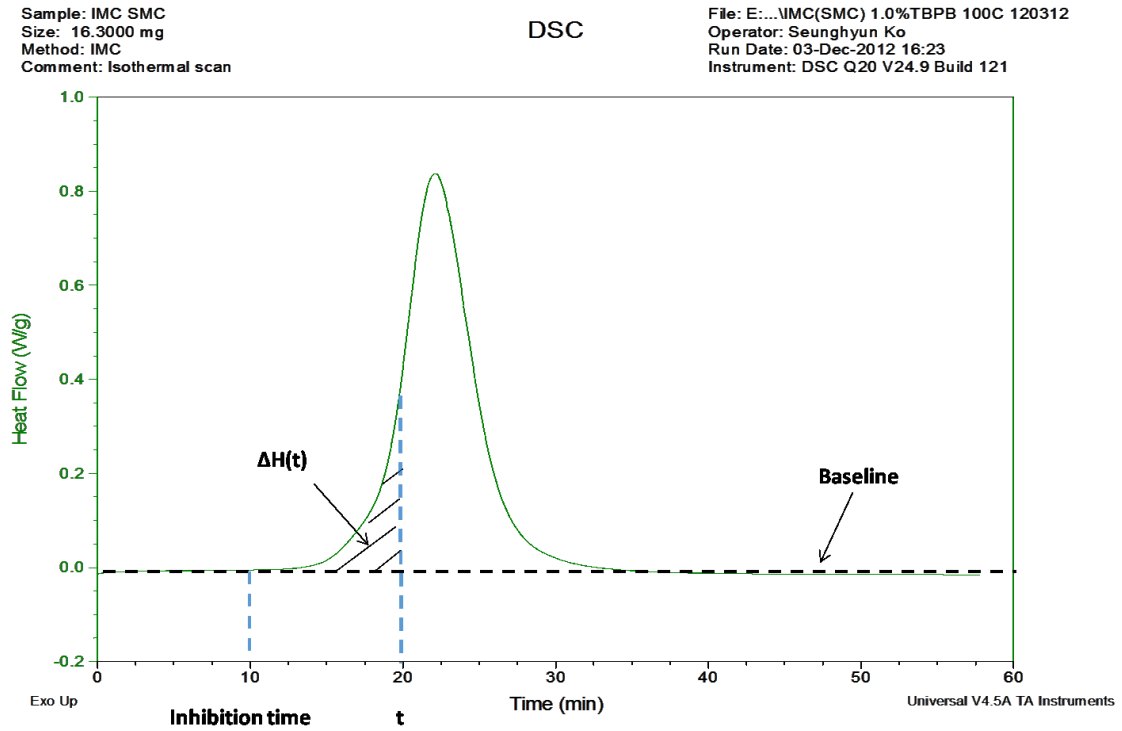
Figure 3. 1 A typical isothermal DSC curing curve of IMC resin

3.4 Effect of Initiators on the Curing of IMC

3.4.1 Cure Models with One Initiator

The experimental data obtained from DSC for IMC with one initiator is summarized in Table 3.2. The inhibition time (t_z) is calculated as the intersection between the horizontal right base line and heat flow curve. It can be seen that as the cure temperature is increased, H_i increases, while H_r decreases. At higher temperature a

higher maximum conversion, α_{max} is achieved. Since we know the inhibition time - time when the reaction starts from the DSC experiments, we can plot lnt_z versus 1/T to get a straight line which can be fitted to give us a linear equation as shown in Figure 3.2. From the slope of the equation, we can get the value for E_d and from the intercept we can get the value for k_{do}. The values of E_d and k_{do} for each initiator concentration are reported in Table 3.3.

TBPB (wt. %)	T (°C)	t_z(sec)	H_i (J/g)	H_r(J/g)	H_{total}(J/g)	α_{max}
	90	1944	263.8	20.69	284.49	0.9244
1	100	574	272.1	16.25	288.35	0.9416
	110	232	289.1	13.55	302.65	0.9545
	90	1403	262.7	24.85	287.55	0.9121
1.75	100	304	275.4	23.36	298.76	0.922
	110	158	289.5	14.41	303.91	0.9507
	90	1054	259.7	35.19	294.89	0.8711
2.5	100	222	276.2	31.94	308.14	0.8964
	110	110	288.2	22.98	311.18	0.9255

Table 3. 2 DSC results for isothermal experiments with one initiator
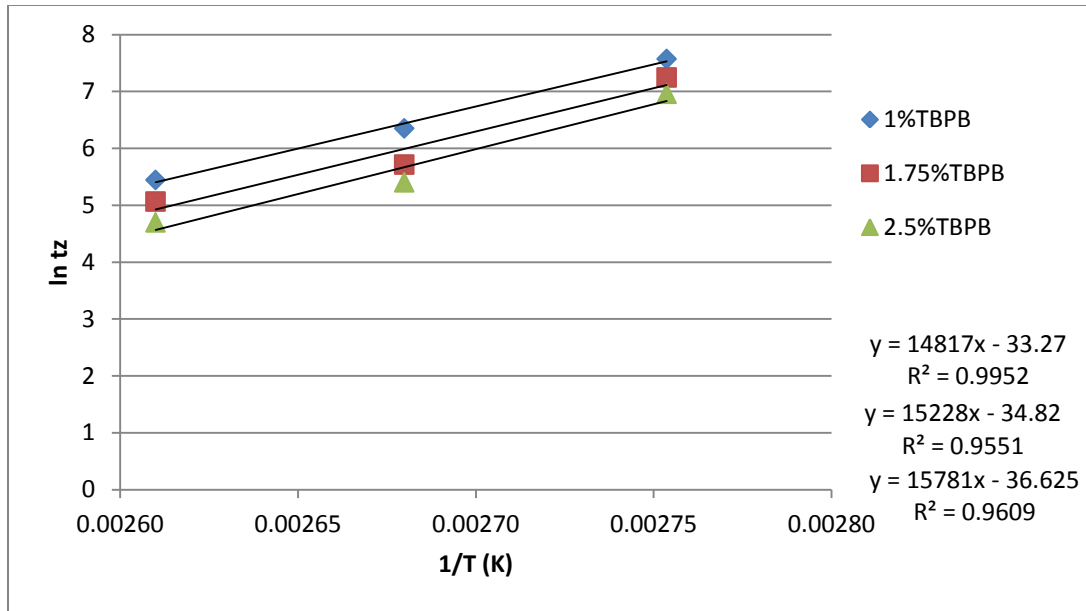
Figure 3. 2 Plot of lnt_z versus 1/T

TBPB (wt. %)	k_{do}	E_d
1	2.83E+12	1.23E+05
1.75	7.57E+12	1.27E+05
2.5	3.29E+13	1.31E+05

Table 3. 3 Cure parameters to calculate inhibition time from DSC experiments

Figures 3.3 and 3.4 show E_d and k_{do} as a function of initiator weight percent, the fitted linear equation can be used to predict inhibition time as a function of initiator content as shown in Table 3.4.
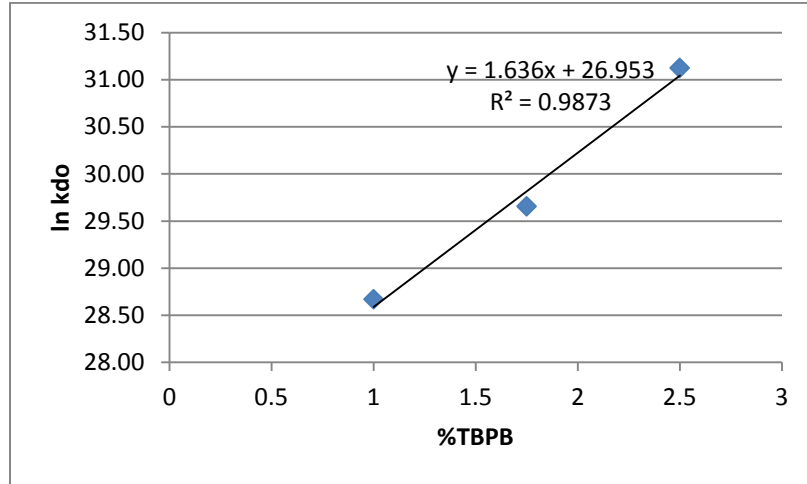
Figure 3. 3 E_d as a function of initiator contents
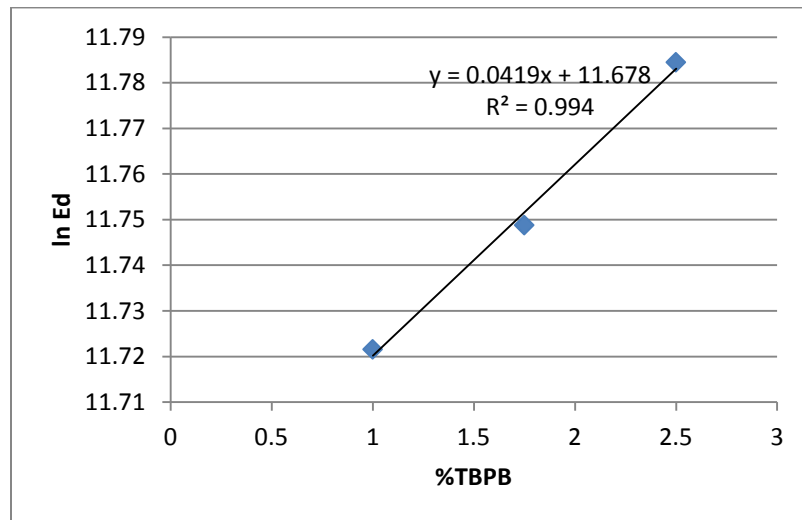
Figure 3. 4 k_{do} as a function of initiator contents

71

k_{do}	$e^{(1.636\times\%TBPB+26.953)}$
E_d	$e^{(0.0419\times\%TBPB+11.678)}$

Table 3. 4 Cure parameter to calculate inhibition time as a function of initiator weight percent

Thus, in summary we can write:

$$t_z = -\frac{1}{k_{do}}\ln\left(1 - \frac{C_{zo}}{2C_{IO}}\right)e^{\frac{E_d}{RT}}$$

where,

$$k_{do} = e^{(1.636\times\%TBPB+26.953)}, E_d = e^{(0.0419\times\%TBPB+11.678)}$$
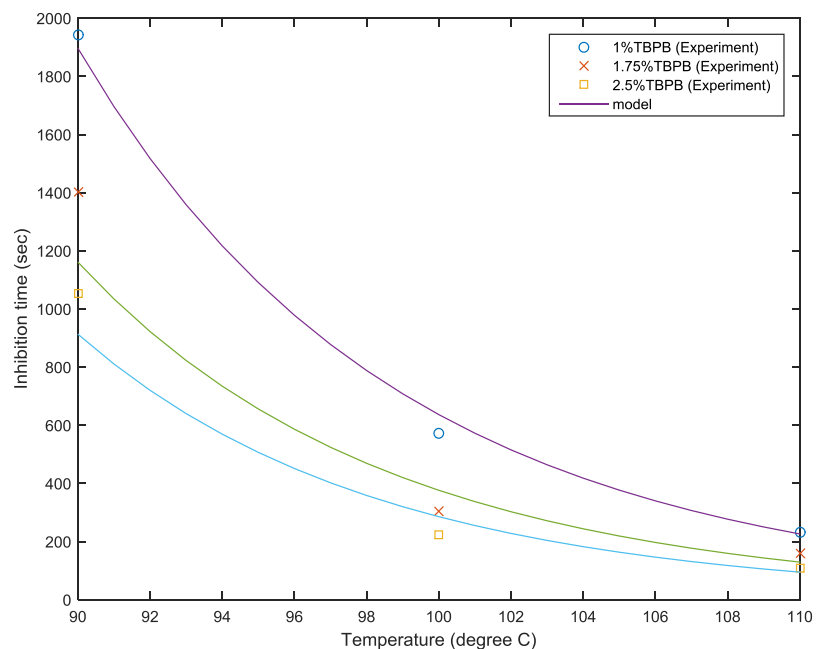
(a)
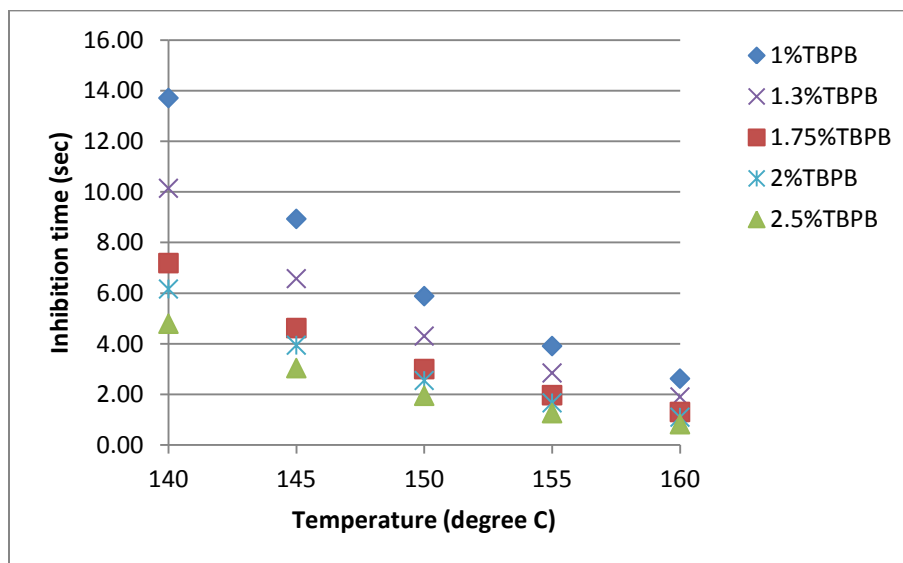
(b)

Figure 3. 5 Plot of inhibition time as a function of temperature and initiator concentration (weight percent) (a) at low temperature range (b) high temperature range

73

Figure 3.5 shows predicted inhibition times from 90°C to 160°C compared with DSC experimental results. From the equation, the inhibition time can be predicted as function of temperature and concentration of initiator. The experimental and predicted inhibition times are summarized in the table 3.5.

%TBPB	T (°C)	t_z (sec) Experiment	t_z (sec) Prediction
1	90	1944	1897.16
	100	574	636.76
	110	232	226.26
	120	-	84.74
	130	-	33.32
	140	-	13.71
	150	-	5.88
	160	-	2.62
1.75	90	1403	1164.25
	100	304	377.39
	110	158	129.74
	120	-	47.09
	130	-	17.97
	140	-	7.19
	150	-	3.00
	160	-	1.31
2.5	90	1054	913.53
	100	222	285.65
	110	110	94.91
	120	-	33.35
	130	-	12.34
	140	-	4.79
	150	-	1.95
	160	-	0.82

Table 3. 5 Experimental and predicted inhibition time as function of temperature and concentration of initiator

The autocatalytic kinetic model was fit using DSC data as proposed by Kenny et al. [5]:

$$\frac{d\alpha}{dt} = (\alpha_o + k_p\alpha^m)(\alpha_{max} - \alpha)^n$$

$$where \; k_p = k_{po}e^{-\frac{E_P}{RT}}$$

k_p is the kinetic rate constant, assumed to have an Arrhenius temperature dependence, m and n are the reaction rate orders. α_{max} is the maximum conversion. The activation energy and the pre-exponential factor can be obtained from the kinetic rate constant k_p at different temperatures:

$$ln k_p = ln k_{po} - \frac{E_P}{RT}$$

The activation energy is calculated from the plot of $ln k_p$ versus $1/T$ as shown in Figure 3.6. Table 3.6 shows kinetic parameters of the autocatalytic model from isothermal DSC experimental data.
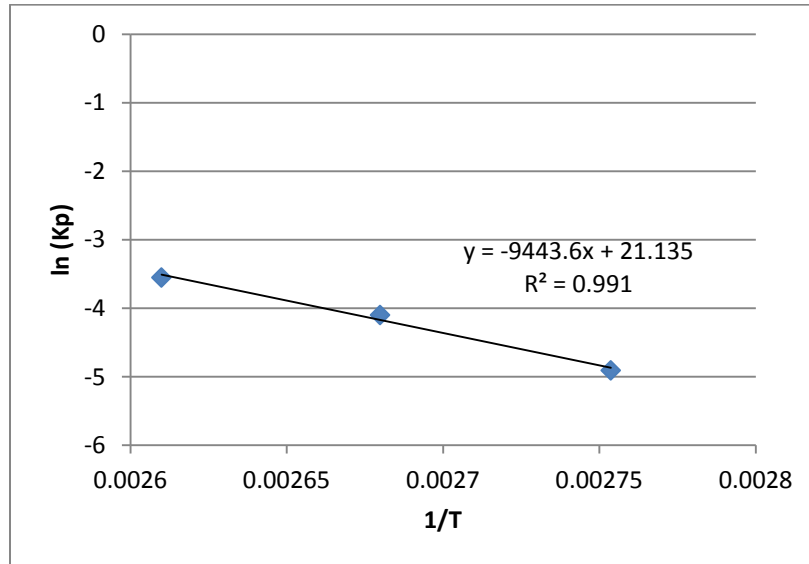
Figure 3. 6 IMC with 1% of TBPB

%TBPB	T (°C)	m	n	k_p	k_{po}	E_P
1	90		1.0926	0.0074	1.51E+09	7.85E+04
	100		1.1285	0.0166		
	110		1.1027	0.0287		
1.75	90	1	0.9966	0.0098	2.63E+08	7.22E+04
	100		1.1491	0.0244		
	110		1.066	0.034		
2.5	90		0.975	0.0117	3.54E+06	5.86E+04
	100		1.0975	0.0271		
	110		1.0226	0.0334		

Table 3. 6 Cure parameters of the autocatalytic model from isothermal DSC experiments

m	1
n	1.1
k_{po}	$e^{(0.2548 \times \%TBPB + 18.095)}$
E_P	$6.98E + 04$
α_{max}	$0.1565 + 0.0021 \times T(K)$

Table 3. 7 Cure parameters of the autocatalytic model as a function of initiator concentration and temperature

Table 3.7 shows the fit of the cure parameters for the autocatalytic model as a function of initiator concentration and temperature. These can be used to interpolate in between the ranges tested. Figure 3.7 shows good agreement between experimental results and model predictions at varying temperatures; the results are also shown in Table 3.8. In this study, the cure time is assumed to be the time when the extent of reaction (conversion) reaches 0.9. The reason why we selected this conversion value was justified through chemorheology in the Chapter 2.
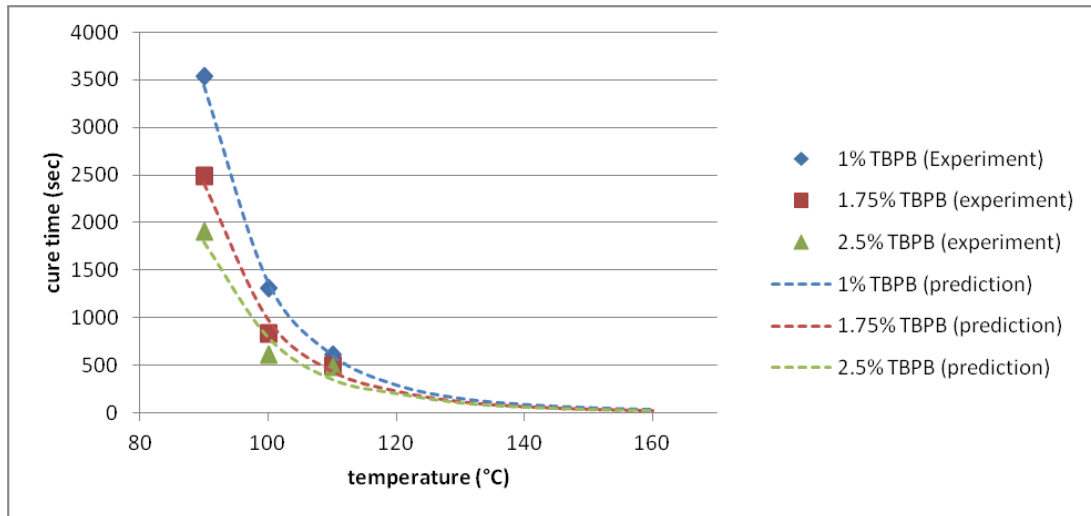
Figure 3. 7 Comparison between experimental and predicted curing time at different temperatures

%TBPB	T (°C)	t_c (sec) Experiment	t_c (sec) Prediction
1	90	3540	3436
	100	1302	1369
	110	606	602
	120	-	287
	130	-	146
	140	-	82
	150	-	48
	160	-	29
1.75	90	2490	2410
	100	828	981
	110	492	436
	120	-	228
	130	-	117
	140	-	65
	150	-	38
	160	-	23
2.5	90	1908	1796
	100	612	792
	110	480	348
	120	-	200
	130	-	101
	140	-	56
	150	-	32
	160	-	19

Table 3. 8 The experimental and predicted cure time as function of temperature and concentration of initiator

3.4.2 Cure Models with Two Initiators

   The effect of using two initiators on the cure models of IMC is discussed in this section. The DSC experiments were performed under the same condition as for one initiator. In this study, tert-butyl peroxy-2-ethylhexanoate (TBPE) along with tert-butyl peroxybenzoate (TBPB) were used as the two initiators. TBPE is a liquid organic peroxide recommended for molding temperatures between 105 and 135 °C. The sample was prepared by mixing the IMC with the required quantities of TBPB and TBPE. The experimental results measured using DSC are summarized in Table 3.9.

TBPB (%)	TBPE (%)	T (°C)	t_z(sec)	t_c(sec) $\alpha = 0.9$	α_{max}
1		90	1290	2326	0.9164
		100	390	967	0.9322
		110	132	452	0.9562
1.75	0.1	90	708	1550	0.9004
		100	156	610	0.918
		110	42	278	0.9489
2.5		90	462	1230	0.8849
		100	108	501	0.8975
		110	24	245	0.9191
1		90	852	1707	0.9133
		100	228	711	0.937
		110	66	349	0.9695
1.75	0.2	90	522	1279	0.8965
		100	108	515	0.9177
		110	24	255	0.9411
2.5		90	276	967	0.8752
		100	72	375	0.9067
		110	6	183	0.9287

Table 3. 9 Experimental DSC results for isothermal experiments with two initiators

Table 3.10 shows the cure parameters to predict inhibition time from isothermal DSC data. The cure parameters, E_{d1} and k_{d1o} are already known from the tests with one initiator. The two cure parameters for the second initiator, E_{d2} and k_{d2o} were obtained by plotting lnk_2 versus $1/T$. The predicted inhibition times for the two initiator systems are given in Table 3.12 using the general cure parameters listed in Table 3.11. The activation energy and the pre-exponential factor can be obtained from the kinetic rate constant k_p measured at different temperatures assuming an Arrhenius temperature dependence and are given in Table 3.13. The concentration of inhibitor as discussed previously was assumed 0.0002 wt. %. Table 3.14 shows the fitted cure parameters to predict cure time. As mentioned earlier, the determined kinetic parameters from DSC data were fitted as function of temperature and initiator concentrations by linear regression to predict inhibition and cure time. There is good agreement between experiments and model predictions as shown in Table 3.15 using the general cure parameters listed in Table 3.14. The combination of two initiators, TBPB and TBPE was found to have a synergistic effect on the reaction of the IMC resin system. Figure 3.8 shows the effect of initiators on cure time. When a high temperature initiator (TBPB) was mixed with 0.1 to 0.2 wt.% of low temperature initiator (TBPE), a 34 to 51% of reduction in cure time at 90 °C was obtained.

A more relevant test of the model is to compare against data from a DSC scan, over a broad temperature range covering the usual processing conditions for the compression molded SMC process. The cure model, with parameters determined from isothermal DSC data, was successfully used to predict the conversion obtained from DSC

scan data, over a broad temperature range. The model does a good job predicting the

conversion during the DSC scan as shown in Figure 3.9.

TBPB (%)	TBPE (%)	E_{d_1}	$k_{d_1 o}$	E_{d_2}	$k_{d_2 o}$
1		1.23E+05	2.83E+12	1.48E+05	5.35E+16
1.75	0.1	1.27E+05	7.57E+12	1.93E+05	3.49E+23
2.5		1.31E+05	3.29E+13	1.99E+05	4.73E+24
1		1.23E+05	2.83E+12	1.66E+05	2.73E+19
1.75	0.2	1.27E+05	7.57E+12	1.96E+05	1.02E+24
2.5		1.31E+05	3.29E+13	2.17E+05	1.64E+27

Table 3. 10 Cure parameters to calculate inhibition time from DSC experiments

E_{d_1}	$e^{(0.0419 \times \%TBPB + 11.678)}$
$k_{d_1 o}$	$e^{(1.636 \times \%TBPB + 26.953)}$
E_{d_2}	$e^{(0.188 \times \%TBPB + 0.723 * \%TBPE + 11.7)}$
$k_{d_2 o}$	$e^{(12.1 \times \%TBPB + 43.9 * \%TBPE + 24.3)}$

Table 3. 11 General cure parameters of the autocatalytic model for practical applications
of coating material

TBPB (%)	TBPE (%)	T (°C)	t_z(sec) Experiment	t_z(sec) Prediction
1	0.1	90	1290	1253
		100	390	414
		110	132	128
1.75		90	708	673
		100	156	175
		110	42	40
2.5		90	462	479
		100	108	102
		110	24	24
1	0.2	90	852	854
		100	228	229
		110	66	64
1.75		90	522	503
		100	108	114
		110	24	24
2.5		90	276	328
		100	72	51
		110	6	10

Table 3. 12 Predicted inhibition time with two initiators

TBPB (%)	TBPE (%)	k_{po}	E_P
1		8.98E+06	6.21E+04
1.75	0.1	2.76E+07	6.46E+04
2.5		1.97E+07	6.30E+04
1		1.09E+06	5.51E+04
1.75	0.2	5.93E+06	5.95E+04
2.5		1.87E+07	6.24E+04

Table 3. 13 Cure parameters from DSC experiments to predict cure time

m	*1*
n	*1.1*
k_{po}	$e^{(17.3305+0.31338\times\%TBPB-12.3167\times\%TBPE)}$
E_P	$e^{(11.1246-0.696493\times\%TBPE)}$
α_{max}	$0.0985312 - 0.023611 \times \%TBPB + 0.013444 \times \%TBPE + 0.0023 \times T(K)$

Table 3. 14 General cure parameters to predict cure time

TBPB (%)	TBPE (%)	T (°C)	t_c(sec) Experiments	t_c(sec) Prediction
1	0.1	90	2326	2280
1	0.1	100	967	958
1	0.1	110	452	430
1.75	0.1	90	1550	1536
1.75	0.1	100	610	628
1.75	0.1	110	278	291
2.5	0.1	90	1230	1211
2.5	0.1	100	501	489
2.5	0.1	110	245	233
1	0.2	90	1707	1699
1	0.2	100	711	701
1	0.2	110	349	337
1.75	0.2	90	1279	1224
1.75	0.2	100	515	507
1.75	0.2	110	255	250
2.5	0.2	90	967	940
2.5	0.2	100	375	382
2.5	0.2	110	183	198

Table 3. 15 Experimental and predicted cure time using general cure parameters
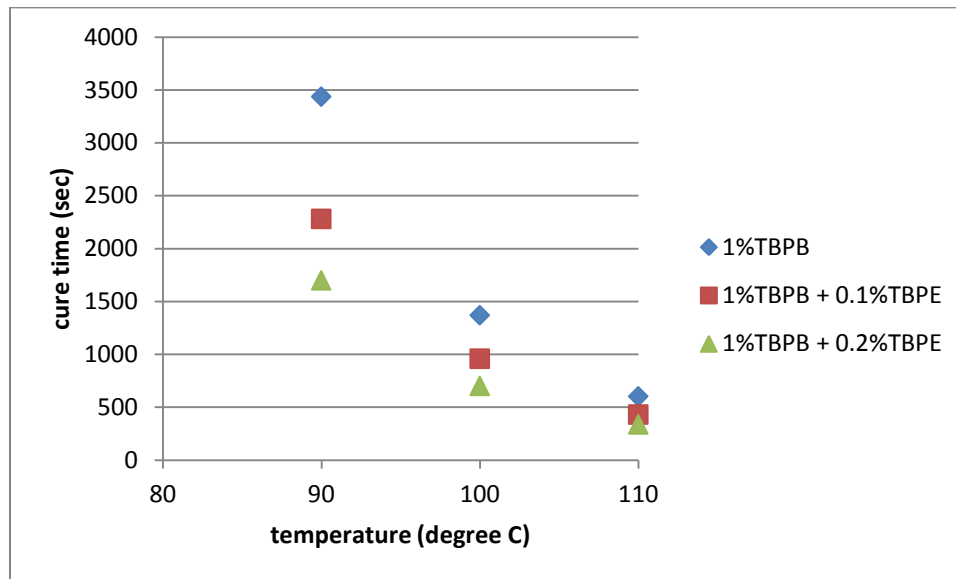
Figure 3. 8 The effect of initiators on cure time
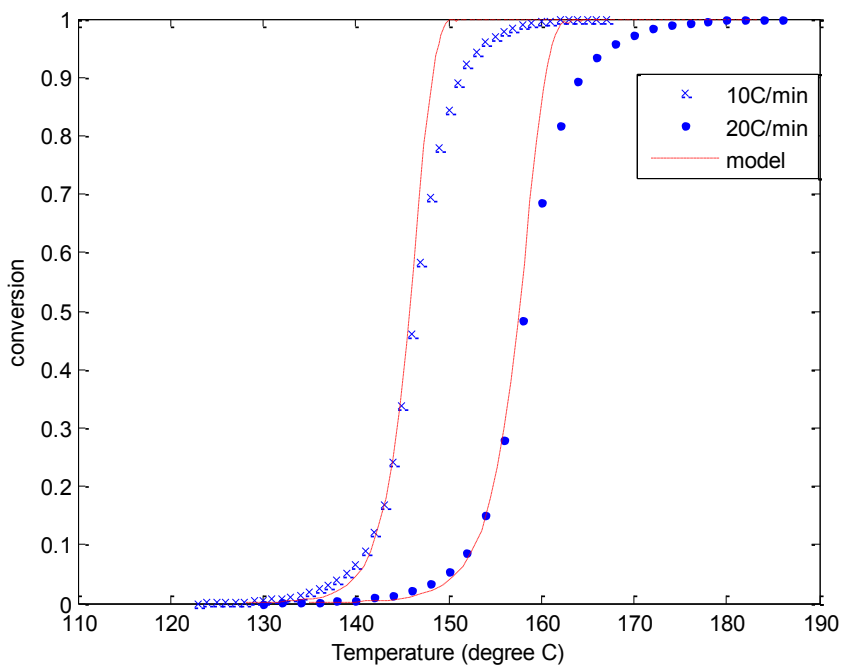
Figure 3. 9 Comparison between model predictions and experimental results obtained in dynamic DSC tests for neat IMC with 1%TBPB

3.5 Effect of Carbon Black filler on the Curing of IMC Systems

One of the reasons IMC is used; is to make the surface conductive so that it can be painted electrostatically. In the case of IMC, CB is used as the conductive filler to provide the required conductivity for electrostatic painting. Several researchers have studied the effect of carbon black, carbon nanofibers, and carbon nanotubes on the curing process of thermosetting resins [23-31]. An understanding of the effect of filler content on the curing process is important for the optimization of inhibition time, cure time and processing conditions. The higher the conductivity the higher the paint transfer efficiency, however, the viscosity of the coating also increases to a point where coating flow is not feasible, as discussed in Chapter 5. In actual manufacturing, the higher

85

percent that can be used is about 3% by weight. Actually the commercial EC 610 formulation has 2.8% CB. In this section we investigate the effect of adding CB to the IMC resin on the curing kinetics using DSC.

The resin (Genglaze EC610) was supplied by OMNOVA solutions with two levels of carbon black, namely 1 and 3 wt. %. The sample for DSC analysis was prepared by thoroughly mixing 1.75 wt. % of TBPB with the IMC. About 10-15 mg of the sample were placed in a Tzero hermetic pan and sealed. The isothermal DSC experiments were conducted at 90, 100 and 110 °C followed by a dynamic DSC scan from 30 °C to 250 °C to measure residual reaction heat. DSC scans were performed with a heating rate 10 °C/min from 30 °C to 250 °C. The heat flow evolved during the isothermal runs is shown as function of reaction time in Figure 3.10 for the two different carbon black contents, as well as the data for the resin without CB, from the previous section.
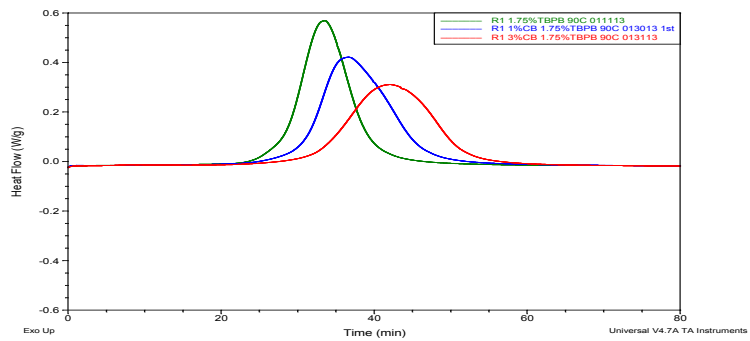
(a)
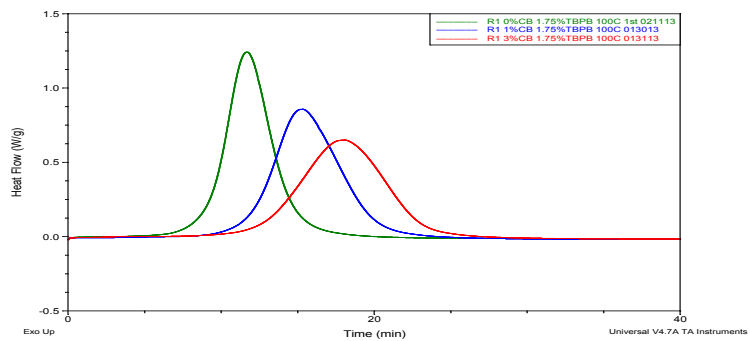
(b)
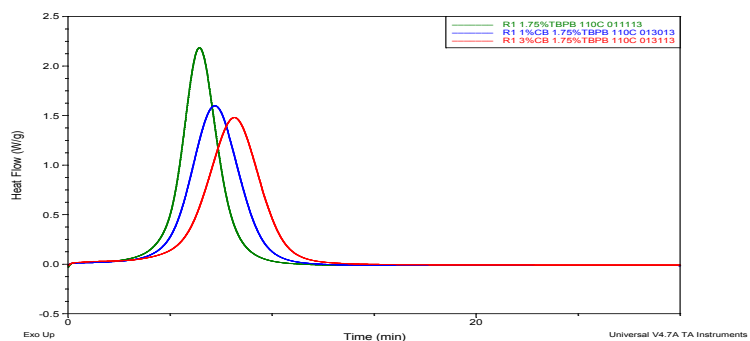
(c)

Figure 3. 10 Isothermal DSC scans for (a) 90 °C (b) 100 °C (c) 110 °C of 0, 1 and 3% by weight carbon black

87

% CB	Temperature (°C)	t_z (sec)	t_c(sec) $\alpha = 0.9$	H_i	H_r	H_{Total}	α_{max}
0	90	1404	2490	262.7	24.85	287.55	0.9136
	100	304	828	275.4	23.36	298.76	0.9206
	110	158	492	289.5	14.41	303.91	0.9512
1	90	1423	2880	263.4	26.14	289.54	0.9114
	100	432	1212	271.6	20.49	292.09	0.9296
	110	173	546	279.8	12.5	292.3	0.9562
3	90	1435	3204	248.9	24.24	273.14	0.9127
	100	473	1392	258.1	20.74	278.84	0.9258
	110	191	610	275.7	13.34	289.04	0.9530

Table 3. 16 DSC results for isothermal tests

In general we can see that the carbon black inhibits the coating reaction, the effect is more noticeable at lower temperatures. Similar results have been obtained in our group for IMC with CNF [19]. Table 3.16, shows the values of inhibition time, cure time, heat liberated during isothermal scan and the residual heat, for all conditions. Even though Figure 3.10, shows that the heat flow (reaction rate), is affected by the amount of carbon black, the effect on inhibition time is small. In Figure 3.11, the degree of conversion from experimental DSC data at 90 °C was plotted as function of reaction time for 0, 1 and 3 wt. % carbon black. As it can be seen in the figure, cure time ($\alpha = 0.9$) increases when increasing the carbon black content.
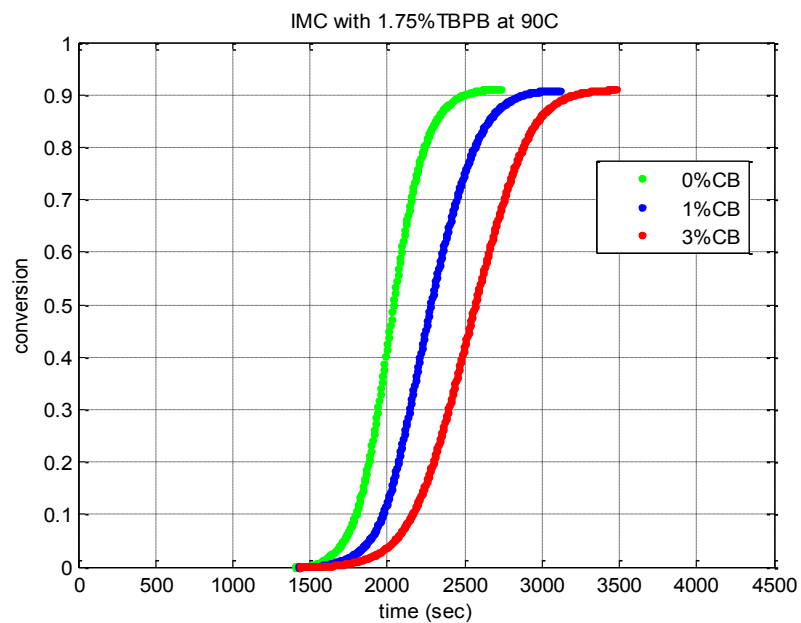
Figure 3. 11 Conversion vs. reaction time for 0 to 3 wt. % of carbon black

% CB	Temperature (°C)	n	m	K
0	90	1.0125	0.9381	0.0092
	100	1.0679	0.9816	0.0229
	110	0.9752	1.0255	0.0323
1	90	0.8966	0.8339	0.0056
	100	0.9863	0.9233	0.0131
	110	0.9353	0.9118	0.0216
3	90	0.9872	0.8801	0.0051
	100	0.9088	0.89	0.0094
	110	0.8943	0.9377	0.0198

Table 3. 17 Cure parameters for isothermal scans

%CB	k_{do}	E_d	k_{po}	E_p	m	n
0	7.57E+12	1.27E+05	3.09E+08	7.29E+04	1.02	0.98
1	3.53E+11	1.18E+05	1.06E+09	7.82E+04	0.94	0.89
3	2.55E+11	1.17E+05	9.30E+08	7.84E+04	0.93	0.90

Table 3. 18 General cure parameters to predict inhibition time and cure time

The cure parameters for IMC with carbon black at different isothermal temperatures are reported in Table 3.17. The general cure parameters to predict inhibition and cure time are summarized in Table 3.18. This cure model successfully predicts the cure reaction with time as shown in Figure 3.12. The cure reaction is delayed with increasing the CB contents.
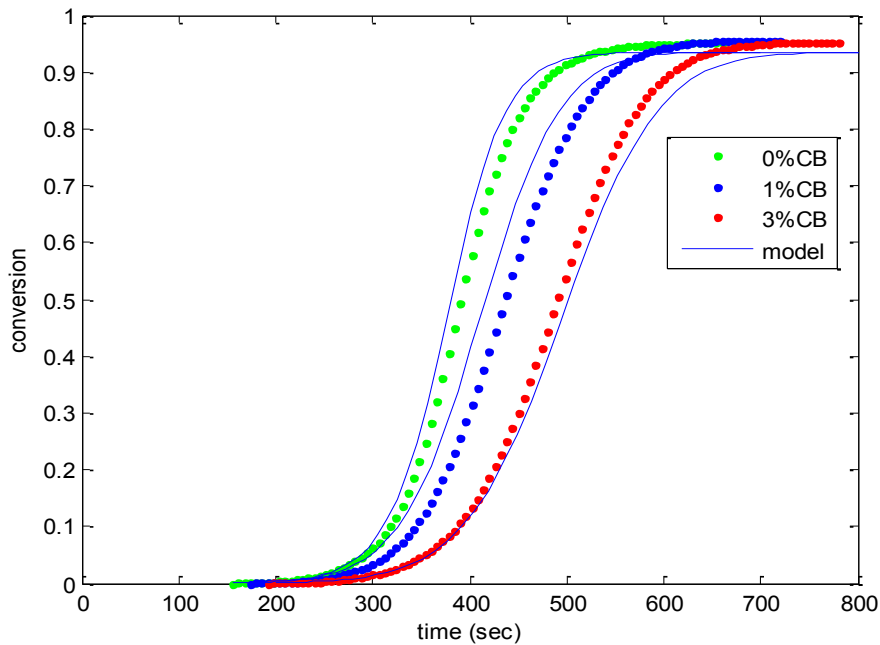
Figure 3. 12 Comparison between model predictions and experimental results obtained in isothermal DSC tests at 110°C for IMC with 0, 1 and 3 wt.% CB

To find the relationship between cure time and CB content, the cure time is normalized by the cure time at 90 °C for each CB content:

$$t_c' = \frac{t_c}{t_c \ at \ 90°C} \tag{3.52}$$

Figure 3.13 shows the normalized cure time (t_c') as function of temperature for varying CB contents. As can be seen in the figure, the normalized cure time can be fitted to a one curve as function of temperature for all CB contents. If we know the cure time at 90 °C, the cure time for unknown CB contents can be predicted. Since we know the cure times for 0, 1 and 3 wt. % CB content at 90 °C, the cure time at 90 °C for each CB contents is normalized by the cure time of 0 wt.% CB:

91

$$t_c'' = \frac{t_c}{t_c \ at \ 0 \ wt.\% \ CB} \quad at \ 90 \ °C \qquad\qquad (3.53)$$

Figure 3.14 shows the plot of normalized cure time (t_c'') versus CB contents which can be fitted to a linear equation. Now we can predict the cure time for different levels of CB contents with 1.75% TBPB. Figure 3.15 shows predicted cure time for 2 wt. % CB contents as function of temperature. This method offers a good compromise to predict the cure time for different CB contents and temperature without additional DSC tests.
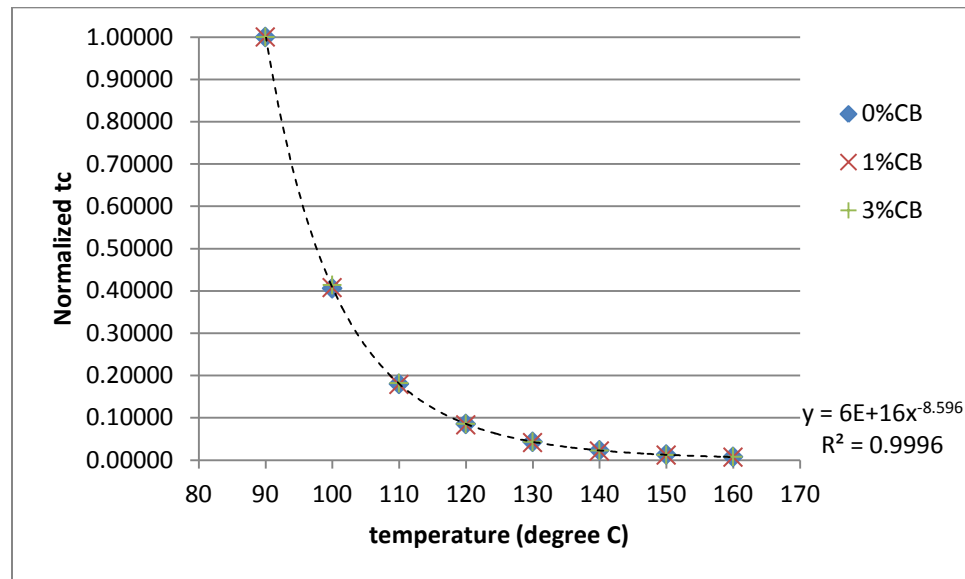
Figure 3. 13 Normalized cure time versus temperature for 0,1 and 3 wt.% CB
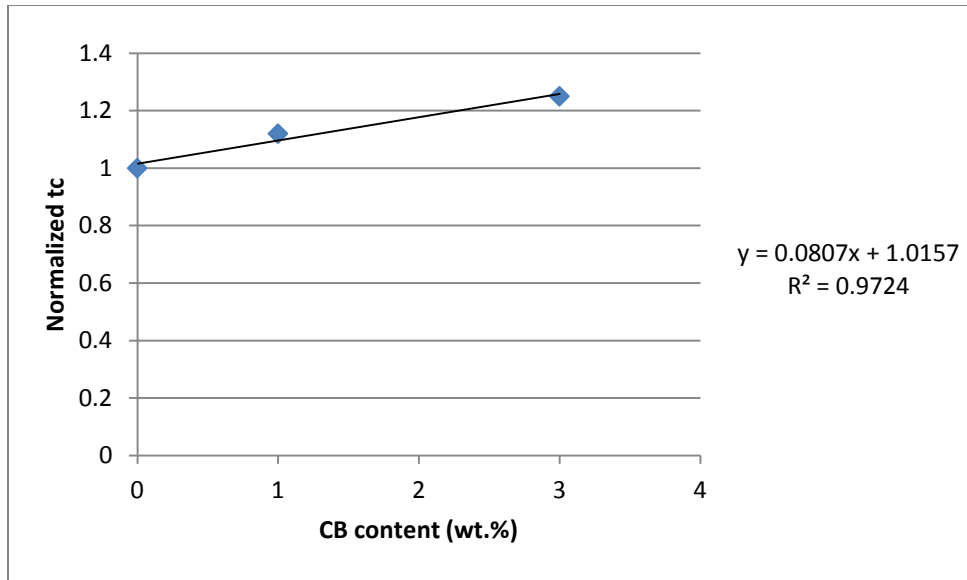
Figure 3. 14 Normalized cure time versus CB contents by weight at 90 °C
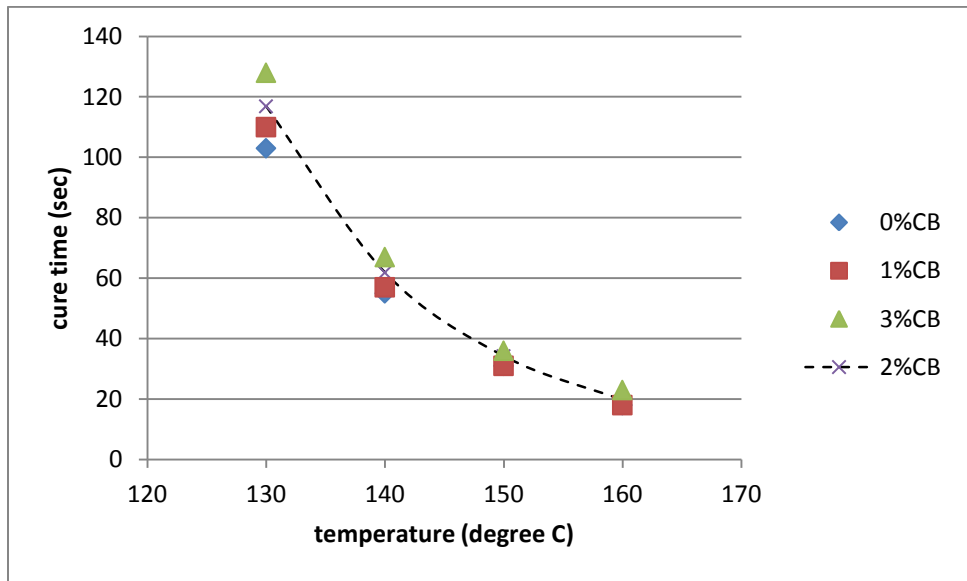
Figure 3. 15 Cure time versus temperature for CB contents by weight

3.6 Conclusions

The cure of a commercial in-mold coating resin system was studied using both isothermal and non-isothermal differential scanning calorimetry. A mechanistic kinetic model based on the free radical polymerization was used to predict inhibition time and the autocatalytic kinetic model was used to predict the conversion for both one initiator and two initiators. The fitted cure model showed good agreement with experimental data over all curing temperatures and initiator levels. Using a dual initiator system, can provide a shorter cycle time at low processing temperature. The cure parameters determined from isothermal DSC data do a good job in predicting dynamic DSC data over a broad temperature range.

The effect of carbon black on the curing of IMC resin was investigated and the results were fitted by the cure model. It was observed that the presence of carbon black in IMC resin have a negligible effect on inhibition time. However, the DSC results have shown that the addition of carbon black to the IMC resin produces a delay in the cure reaction and increases the activation energy of IMC systems.

3.7 References

1. A. Yousefi and P. G. Lafleur, Polymer Composites, Vol. 18, No. 2, 1997

2. S. Vyazovkin, A. K. Burnham, J. M. Criado, L. A. Perez-Maqueda, C. Popescu and N. Sbirrazzuoli, Thermochimica Acta, 520, 1-19, 2011

3. L. Zhao and X. Hu, Polymer, Vol. 51, 3814-3820, 2010

4. S. Park, M. Seo and J. Lee, Journal of Polymer Science, Vol. 38, 2945-2956, 2000

5. J. M. Kenny, Journal of Applied Polymer Science, Vol. 51, 761-764, 1994

6. S. Sourour and M. R. Kamal, Thermochimica Acta, 14, 41-59, 1976

7. N. W. Manthey, F. Cardona and T. Aravinthan, Vol. 125, E511-E517, 2012

8. J. Y. Lee, H. K. Choi, M. J. Shim and S. W. Kim, Thermochimica Acta, 343, 111-117, 2000

9. K. Tao, S. Yang, J. C. Grunlan, Y. Kim, B. Dang, Y. Deng, R. L. Thomas, B. L. Wilson and X. Wei, Journal of Applied Polymer Science, Vol. 102, 5248-5254, 2006

10. P. Lei, Y. Yu and X. Yang, Journal of Applied Polymer Science, Vol. 109, 2539-2545, 2008

11. J. Bae, J. Jang and S. Hoon, Macromol. Chem. Phys, 203, 2196-2204, 2002

12. M. Monti, D. Puglia, M. Natlai, L. Torre and J. M. Kenny, Composites Science and Technology, 71, 1507-1516, 2011

13. X. Huang and B. Batham, , Journal of Applied Polymer Science, Vol. 127, 1959-1996, 2013

14. J. F. Stevenson, *Polym. Eng. Sci.* **28**, 746 (1986).

15. L. J. Lee, *Polym. Eng. Sci.* **21**, 483 (1981).

16. J. M. Castro and C. C. Lee, *Polym. Eng. Sci.* **27**, 218 (1987).

17. K. S. Zuyev and J. M. Castro, *J. Polym. Eng.* **22**, 233-260 (2002).

18. J. M. Castro and R. M. Griffith, "In-Mold Coating," in *Sheet Molding Compound: Science and Technology,* edited by Hamid G. Kia, Munich: Hanser, 1993, pp. 163-180.

19. J. M. Castro and R. M. Griffith, *Polym. Eng. Sci.* **30**, 677-683 (1990).

20. J. D. Fan, J. M. Marinelli and L. J. Lee, Polymer Composites, Vol. 7, No. 4, 1986

21. J. M. Barton, Advances in Polymer Science, Vol. 72, 1985.

22. A. Dutta and M. E. Ryan, Journal of Applied Polymer Science, Vol. 24, 635-649, 1979

23. Abdalla M, Dean D, Robinson P and Nyairo E, Polymer, 49, 3310-7, 2008

24. N. L. Ranikumar, K. K. Kar, S. Sarkar and D. Sathyamoorthy, Polymer Composites, 2010

25. Terenzi A, Vedova C, Lelli G et al., Compos. Sci. Technol., 68, 1862-8, 2008

26. Xu L and James Lee L, Polym. Eng. Sci.,45, 496-509, 2005

27. Movva, Journal of Composites Materials, 43, 611, 2009

28. Xie et al., Journal of Applied Polymer Science, 96, 329-335, 2005

29. Chou, Composite Science and Technology, 70, 1, 2009

30. J. Wu and D.D.L. Chung, Carbon, 42, 3003-3042, 2004

31. S.B.Susin, V. Pistor, S. C. Amico, L. A. F. Coelho et al., Journal of Applied Polymer Science, 2014

Chapter 4: Application of Multiple Criteria Optimization Method to In-mold Coating Process

This chapter presents the application of the multiple criteria optimization method developed by Villarreal [9] to the In-mold coating process. The approach is based on Design of Experiments (DOE) and linear regression metamodels which are used to speed up the prediction of the performance measures. DEA is used to identify non-dominated solutions which are then predicted using the physics based simulation model. The newly predicted values are used to update the metamodels. In section 4.2 an overview of the multiple criteria optimization method is given using an example case. In section 4.3, the method is applied to IMC process for compression molded SMC, for two cases: (1) to find the best compromises among inhibition and cure time for typical SMC conditions and (2) finding the best compromises among inhibition and cure time for low mold temperature molding.

4.1 Introduction

The interrelationship between controllable variables and performance measures in the in-mold coating process is very complex. Figure 4.1 shows a schematic representation of the case considered in this chapter. As was discussed in the introduction section, and can be seen in Figure 1.5, there are a large number of controllable variables and

performance measures. Here, we would focus on the controllable variables that are accessible to the molder. The resin system is selected for proper adhesion to the substrate and cosmetic effects. The molder can select the initiator level (1 or 2) and mold temperature. The performance measures available to the molder are inhibition time and cure time. The interactions between controllable variables and performance measures are summarized in Figure 4.2. Increasing the content of initiators decreases the cure time but the inhibition time will also be decreased. Higher mold temperature will decrease the cure time as well as the inhibition time. For the IMC process, it is desired to maximize the inhibition time and minimize the cure time so as to maximize the time available for flow and minimize the cycle time, which clearly show conflictive behavior.
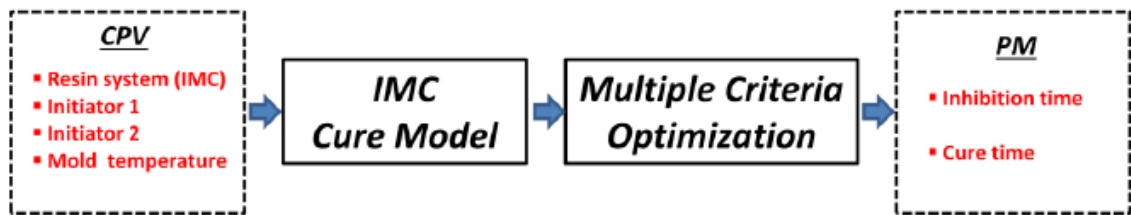
Figure 4. 1 Schematic representation of the system for In-Mold Coating process for SMC
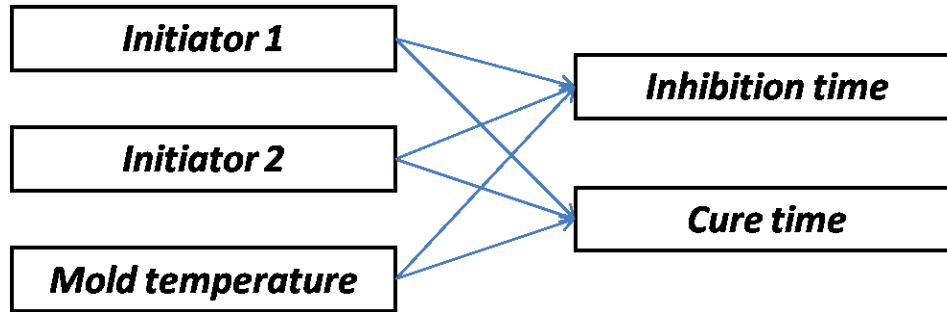
Figure 4. 2 Summary of the interaction between controllable variables and performance measures

The most widely used approach to determine the process setting is to optimize performances measures as functions of the input variables. This is done by using a model to relate the behavior of the performance measures to controllable process and design variables and then using these models to solve the desired optimization problem. [1-6].

In this chapter, the iterative multiple criteria optimization method developed by Villarreal [9] is applied to identify the best compromises between performance measures. The method starts by performing a design of experiments to collect a set of initial data which is used to fit a metamodel for each performance measures. Then, the metamodels are used to estimate the performance for a large set of input combinations and a Pareto frontier is identified. The Pareto set corresponding to the approximated Pareto frontier is evaluated using the physics based simulation model, and as new information is available the metamodels are updated.

4.2 Multiple Criteria Optimization Method

4.2.1 Design of Experiments

Design of experiments is a collection of statistical tools that deal with planning experiments so that appropriate data can be collected and analyzed by statistical models. An experiment can be defined as a test or a series of tests in which control changes are made to the controllable factors of a process or system so that we may observe and identify the reasons of changes in the output response. One of the most popular design of experiments used to construct second order polynomial models are Central Composite Designs (CCD). A general CCD with d factors consists of a 2^d factorial design, 2d axial runs, and c replications of the central point, c is usually between 3 and 5 [10]. Figure 4.3 shows an example of a CCD of 2 factors which in our case are the initiator level (weight percent) and mold temperature (^{o}C).
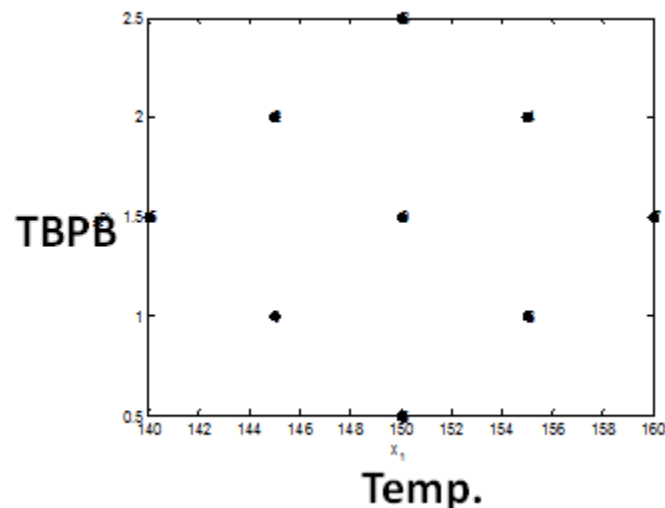
Figure 4. 3 Example of central composite design

100

4.2.2 Metamodeling

An empirical model or a metamodel is a mathematical equation that relates the output response to the controllable variables (inputs). The parameters of the model are fitted using a sample of data points which are commonly generated using an experimental design. Metamodels are commonly used to predict the output responses at unobserved inputs, and to find the input combinations that optimize the output responses. One of the most traditional metamodeling techniques is linear regression models and more modern approaches are Kriging metamodels and Artificial Neural Networks [11-12]. The general form of a first order regression model is defined as follows:

$$y = \beta_0 + \beta_1 x_1 + \beta_2 x_2 + \cdots + \beta_n x_n + \varepsilon$$

The parameters β_i are called the regression coefficients. β_i describe the expected change in output y per unit change in input x_i when all of the other input variables are held constant [7]. A linear regression model may contain terms that are second order or higher. Any form of this equation that is linear with respect to the regression coefficients is referred to as linear regression. The goal of the linear regression model is to determine the regression coefficients that minimize the sum of the squared errors between the regression model output and PM data that it is intended to represent. For this study second order regression model was used and the method of least squares was used to estimate the regression coefficients of the linear regression model.

4.2.3 Data Envelopment Analysis (DEA)

Once the metamodels were obtained, they were used to generate a large data set which then became the subject of a multiple criteria optimization. The method used in this research to solve the multiple criteria optimization problem is called Data Envelopment Analysis (DEA). The goal of DEA is to determine the data points which dominate the rest of the dataset. These are the points that cannot be improved with respect to any one PM without negative effect on another. The combination of these points makes up the efficient frontier. The number of PMs considered determines the dimensionality of a multiple criteria problem. The efficient frontier can only be visualized graphically in two or three dimensions.

The efficient frontier found by DEA of a sample dataset with two PMs is shown in Figure 4.4. In this figure, each point represents a candidate system solution in terms of their PM values: for example injection pressure and electrical conductivity. The aims are to minimize injection pressure and to maximize conductivity of an in-mold coating operation. In other words, it is desirable to move the left on the x axis and move up on the y axis. Ideally, it is desirable to move towards the top left region of the dataset which is the ideal solutions. An ideal solution would be in the northwest corner of the graph; however there is no solution there. The efficient solutions are found on the frontier generated by the desirable directions of both PMs.
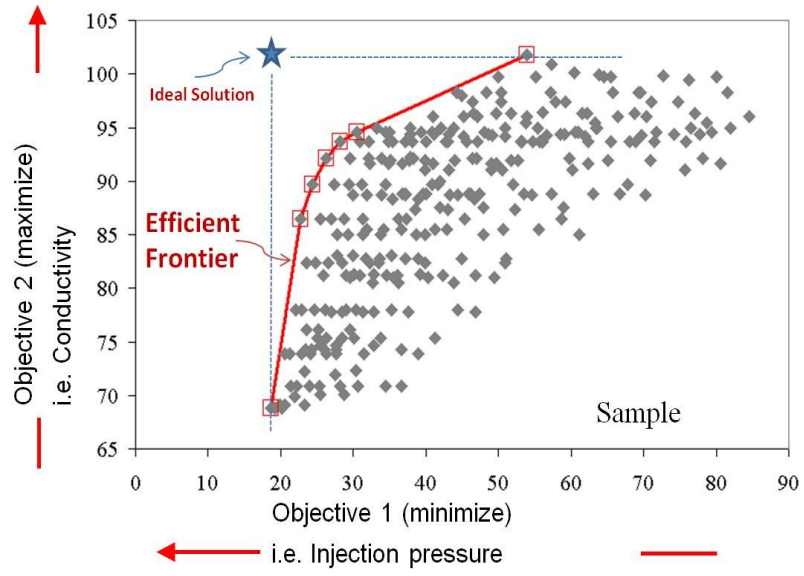
Figure 4. 4 Schematic of efficient frontier for two PMs [9]
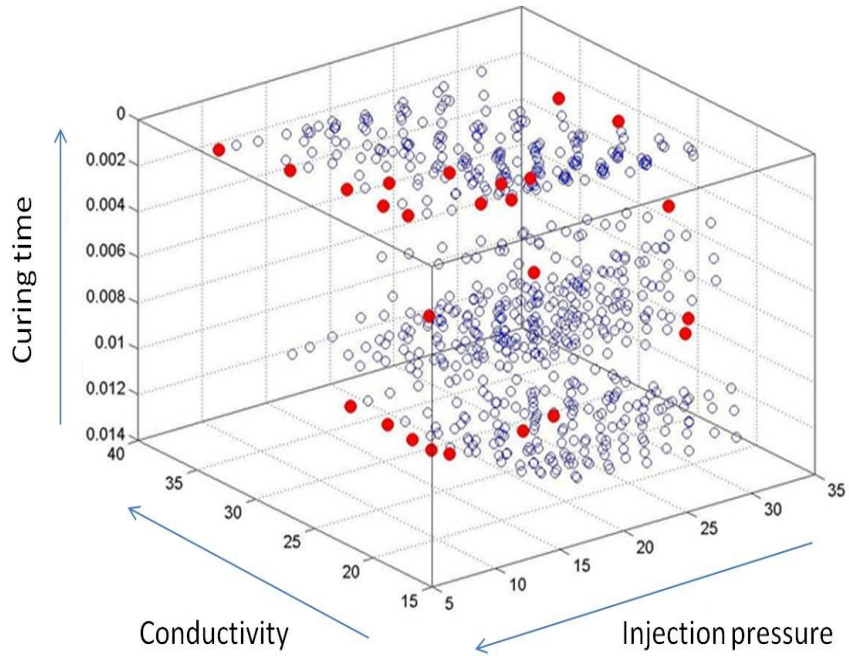
Figure 4. 5 Schematic of efficient frontiers for three PMs [9]

In a two-dimensional case, it is easy to visualize the envelop that the efficient frontier forms over the data, hence the name Data Envelopment Analysis. Any data point not located on the efficient frontier could be improved with respect to injection pressure without hurting the electrical conductivity or vice-versa. Figure 4.5 shows a schematic presentation of efficient frontiers for three performance measures.

4.2.4 Multiple Criteria Optimization Method

The steps of the multiple criteria optimization method proposed by Villarreal-Marroquin, M. G. from our group; to find the best compromises between several PMs are shown in Figure 4.6. The optimization method has several steps. The method starts with an experimental design for which a simulation run is performed at each design point. Then, the set of best compromises between all performance measures is found, and is called incumbent Pareto frontier. A metamodel for each performance measure is constructed at each iteration using all the available information. Then, the metamodels are used to predict the values of the performance measures at a grid of input combinations. The solutions that form the piece-wise linear envelop of the evaluated data are identified via DEA. These solutions are a subset of the non-dominated solutions of the evaluated data, and are called here non-dominated predicted solutions. The non-dominated predicted solutions are then simulated and compared against the incumbent Pareto frontier for updating purposes. A series of stopping criteria are evaluated: (1) if the coefficient of determination, R^2, for all metamodels is larger than $(1 - \varepsilon)$, ε small number (2); (2) if the incumbent Pareto frontier does not change after a given number of

iteration. If at least one is met, the method stops and reports the incumbent Pareto frontier, otherwise, the new simulated points are added to the existing set of points and a new iteration begins. At each iteration the metamodels are updated to obtain good approximations of the output responses closer to the Pareto frontier.
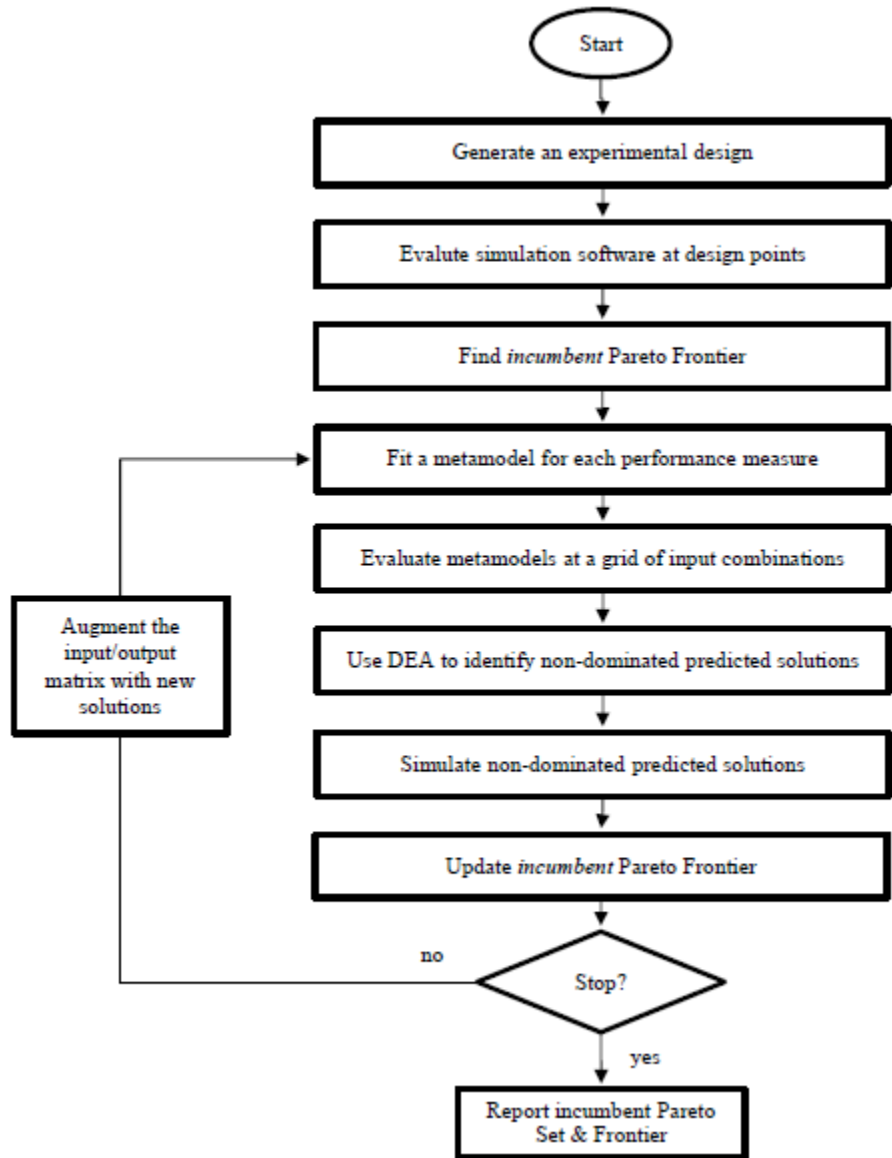
Figure 4. 6 Flow chart of the multiple criteria optimization method [9]

Next we explain the MCO method using the following example of three controllable variables and two performance measures. Mold temperature (x_1), initiator 1 (x_2) and initiator 2 (x_3) were considered as controllable variables and are varied in the ranges of $[100,140]°C$, $[0.5,2.5]$wt.% and $[0,1]$wt.% respectively. Performance measures are inhibition time (t_z) and cure time (t_c) in sec. In this example, we are interested in finding the processing conditions that maximize the inhibition time and minimize the cure time to reduce the cycle time. The cure model and kinetic parameters characterizing the model were obtained by Konstantin [13] and simplified here, to facilitate the explanation of the method.

The inhibition time (t_z) is given by the equation (4.1):

$$t_z = -\frac{1}{2.98 \times (1 + x_3)} \ln\left(1 - \frac{0.0001}{x_2}\right) e^{\frac{30644.072}{8.31 \times x_1}} \tag{4.1}$$

The cure time (t_c) is assumed to be the time when the degree of conversion (α) is 0.9. The degree of conversion as a function of time is calculated using equation (4.2).

$$\alpha(t) = 1 - e^{-A_1 e^{-\frac{2\times10^6 \times x_2 + 108555}{8.31 \times x_1}(t + \frac{1}{k_d}e^{-k_d(t-t_z)} - t_z - \frac{1}{k_d})}} \tag{4.2}$$

where $A_1 = 2e^{588.05 \times x_2 + 38.2} x_2 e^{-k_d t_z}$ and $k_d = 2.98(1 + x_3)e^{-\frac{30644.072}{8.31 \times x_1}}$

The optimization problem is defined as follows:

Find x_1 (*mold temperature*), x_2 (*initiator* 1) and x_3 (*initiator* 2) to
Maximize t_z (inhibition time)
Minimize t_c (cure time)
Subject to $100 \leq x_1 \leq 140$
$\qquad\quad 0.5 \leq x_2 \leq 2.5$
$\qquad\quad 0 \leq x_3 \leq 1$

To solve the above problem, the proposed multiple criteria optimization method was applied. The steps are as follows.

Step 1. Generate an experimental design for the controllable variables. The design used in this example is the CCD with 15 points shown in Figure 4.7.
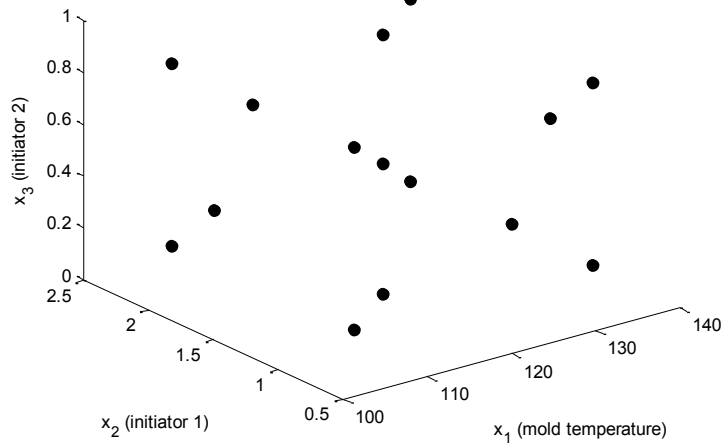
Figure 4. 7 Initial design of experiments (CCD)

Step 2. Run physics based simulation (IMC cure model) at initial design points. Figure 4.8 shows the performance measures for each of the corresponding input points.
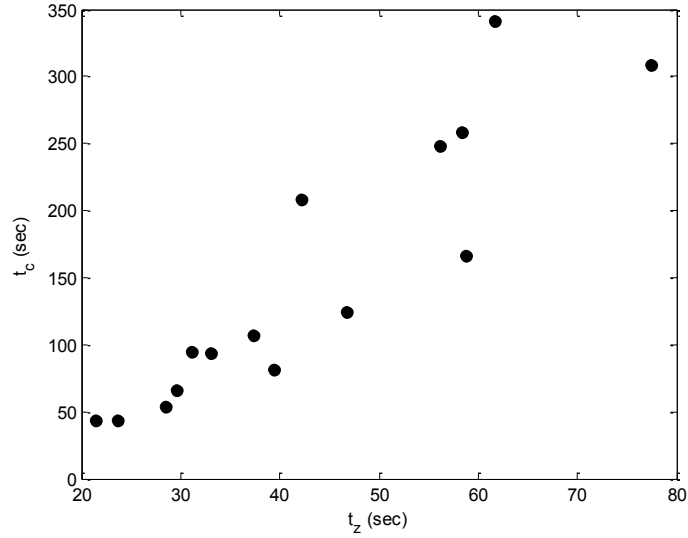
Figure 4. 8 Performance measures at initial experimental design points

Step 3. Find the incumbent Pareto Frontier from the current simulated data. The red circles represent the incumbent Pareto Frontier for the initial DOE in Figure 4.9.
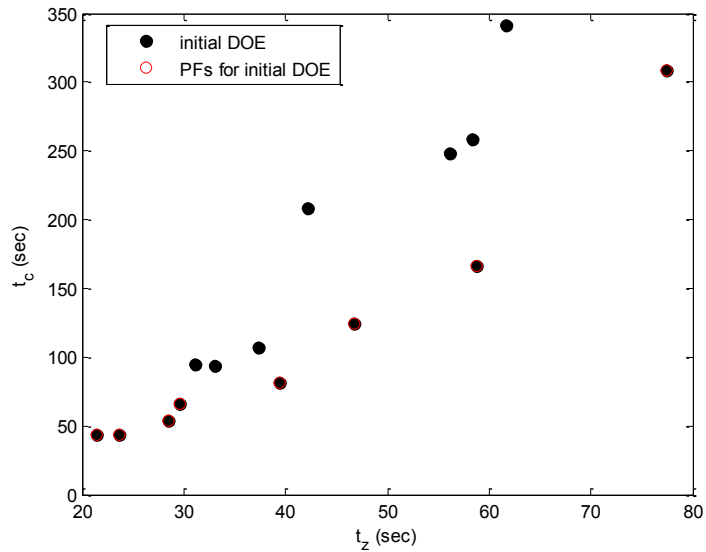
Figure 4. 9 Incumbent Pareto Frontier for initial DOE

109

Step 4. Construct a multiple linear regression model (metamodel) for each performance measure using all available information as shown in Figure 4.10.

Step 5. Evaluate the metamodels to identify predicted Pareto set using DEA in Figure 4.11.
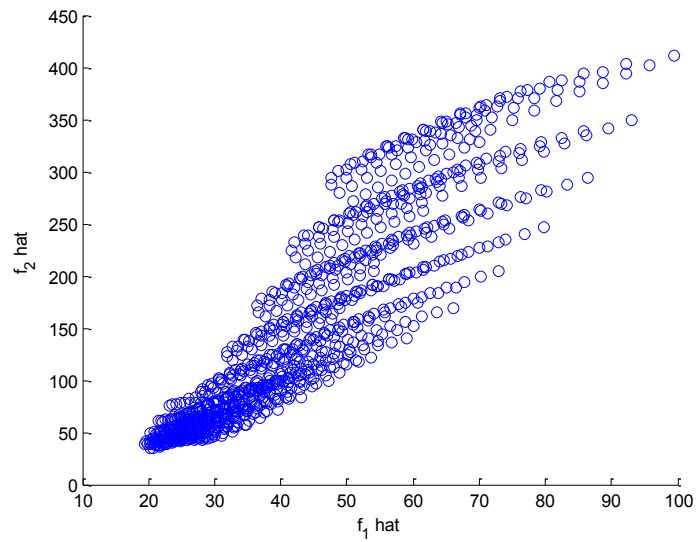
Figure 4. 10 A multiple linear regression model for each performance measure using all available information
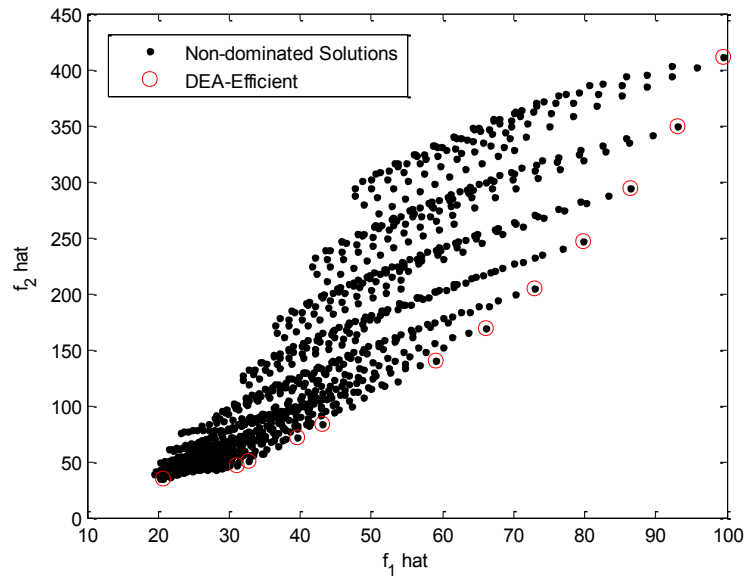
Figure 4. 11 Evaluation of metamodels at each input combination

Step 6. Update the incumbent efficient frontier. Evaluate stopping criteria. Figure 4.12 compares the performance measure for initial DOE and final Pareto solutions by applying multiple criteria optimization method. In this example, the inhibition time should be maximized and the cure time should be minimized therefore the ideal solutions should be located right-lower region. Figure 4.13 and Figure 4.14 show the final Pareto set and frontier respectively. The Pareto frontier found suggests that in order to maximize the inhibition time we should use low mold temperatures with only 0.5 wt.% of initiator 1 (green points). On the other hand, to minimize the cure time we need to use high mold temperatures in the range of 130 - 140 °C (blue points) with higher contents of initiators. Red points are the compromise between inhibition time and cure time. In the next section, we discuss the application of the multiple criteria method to determine multiobjective

111

optimization problems using the cure model developed in Chapter 3 for In-mold coating

process for SMC.
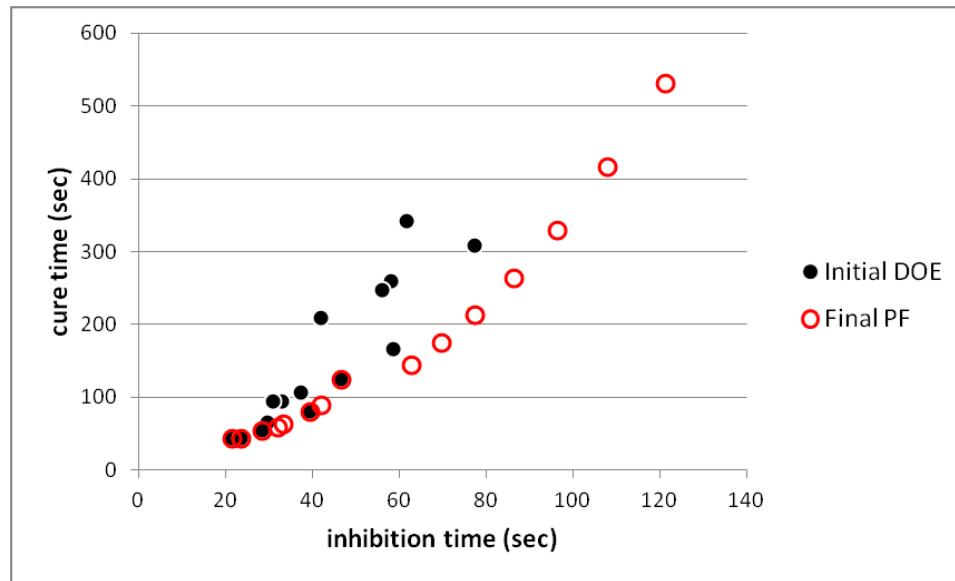
Figure 4. 12 The crosses are the simulated values of the selected predicted Pareto set. The circles are the evaluation of the original design points
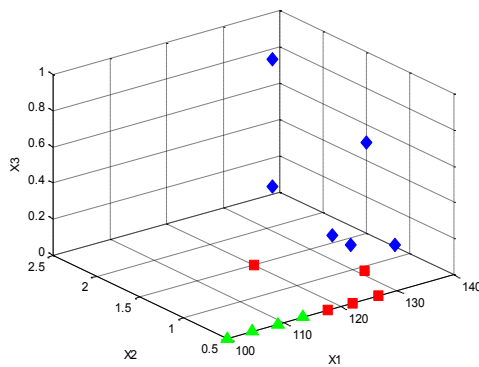
Figure 4. 13 Final Pareto set
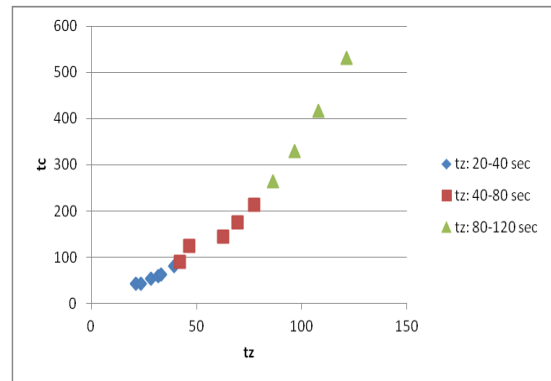
Figure 4. 14 Final Pareto frontier

4.3 Application of Proposed Optimization Method to the In-mold Coating Process

The multiple criteria optimization method was applied to select the best compromises for the In-mold coating process. Here we are interested in finding In-mold coating process conditions that maximize the inhibition time and minimize the cure time. The controllable process variables were: (1) mold temperature (2) weight percent of initiator 1 (TBPB) and (3) weight percent of initiator 2 (TBPE). The performance measures are the inhibition time and cure time of IMC resin. The cure parameters obtained in Chapter 3 are used to predict the inhibition and cure time as a function of the controllable variables.

4.3.1 Case Study 1: Inhibition and Cure Time for Typical SMC Conditions

The controllable variables as discussed above are mold temperature (°C), weight percent of initiator 1 (TBPB) and initiator 2 (TBPE). They are varied in the range of [140, 160]°C, [0.5, 2.5]wt.% and [0, 0.2]wt.%. The performance measures are inhibition time (sec) and cure time (sec). To solve this case, the multiple criteria optimization method was applied using two additional sub cases to increase the number of solutions in the pareto frontier. First, typical SMC conditions were studied in Case 1 following the steps explained in the previous example. Secondly, only the two controllable variables of mold temperature and initiator 1 with the same range as in case 1 were considered (Case 1A). Finally, the reduced range of controllable process variables were tested using multiple criteria optimization method in Case 1B, this allowed us to find more points in the efficient frontier. The optimization problem is defined as follows:

Find the mold temperature, wt.% of initiator 1 (TBPB) and wt.% of initiator 2 (TBPE) to
Maximize   Inhibition time (t_z)
Minimize   Cure time (t_c)
Subject to $140 \leq$ Mold temperature ≤ 160
                   $0.5 \leq$ TBPB ≤ 2.5
                      $0 \leq$ TBPE ≤ 0.2
Case 1:
Subject to $140 \leq$ Mold temperature ≤ 160
                   $0.5 \leq$ TBPB ≤ 2.5
                      $0 \leq$ TBPE ≤ 0.2

Case 1A:
Subject to $140 \leq$ Mold temperature ≤ 160
                   $0.5 \leq$ TBPB ≤ 2.5

Case 1B:
Subject to $140 \leq$ Mold temperature ≤ 160
                   $0.5 \leq$ TBPB ≤ 1.0
                      $0 \leq$ TBPE ≤ 0.1

The initial experimental design used in this case is a CCD. For each design point,

the developed cure model in Chapter 3 was applied to predict the inhibition and cure

time. A series of stopping criteria are evaluated and, if at least one is met, the method

stops and reports the incumbent Pareto frontier, otherwise the new simulated points are

added to existing set of points and a new iteration begins. At each iteration, the

metamodels are updated to obtain good approximations of the output responses close to

the Pareto frontier. Figure 4.15-4.17 shows the final Pareto solutions for each case where

the K represents the number of iteration used to update the incumbent Pareto frontier.

From Figure 4.15 we can see that in order to maximize the inhibition time we need to use

controllable variables for area A and to minimize the cure time for area B but there are no

compromising solutions between A and B. Therefore, we tested two additional sub cases

of case1A and case1B to find more solutions in Pareto frontier. Figure 4.16 and 4.17

shows the final Pareto frontier for Case 1A and Case 1B, respectively. All cases are

plotted in Figure 4.18. The line represents the Pareto frontier.

.
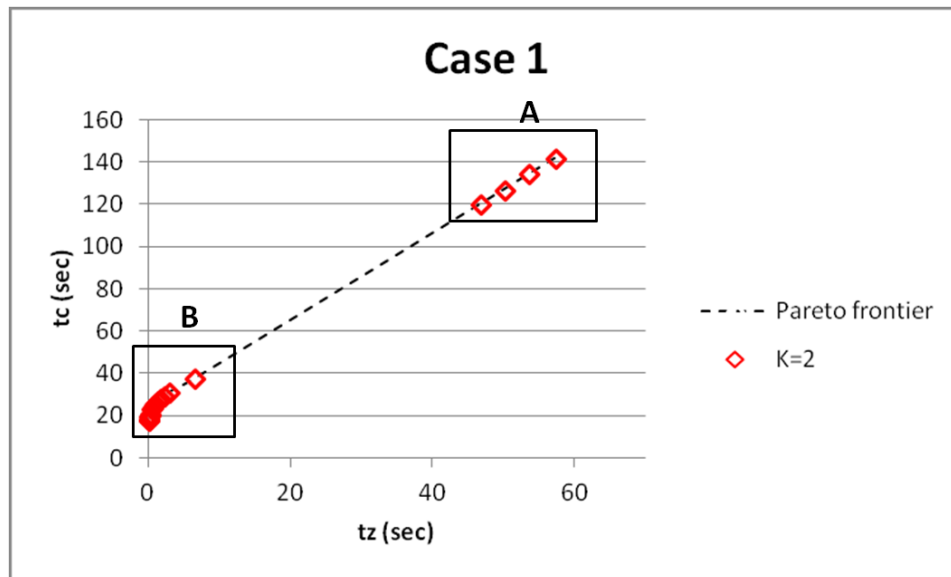
Figure 4. 15 Final Pareto frontier of Case 1
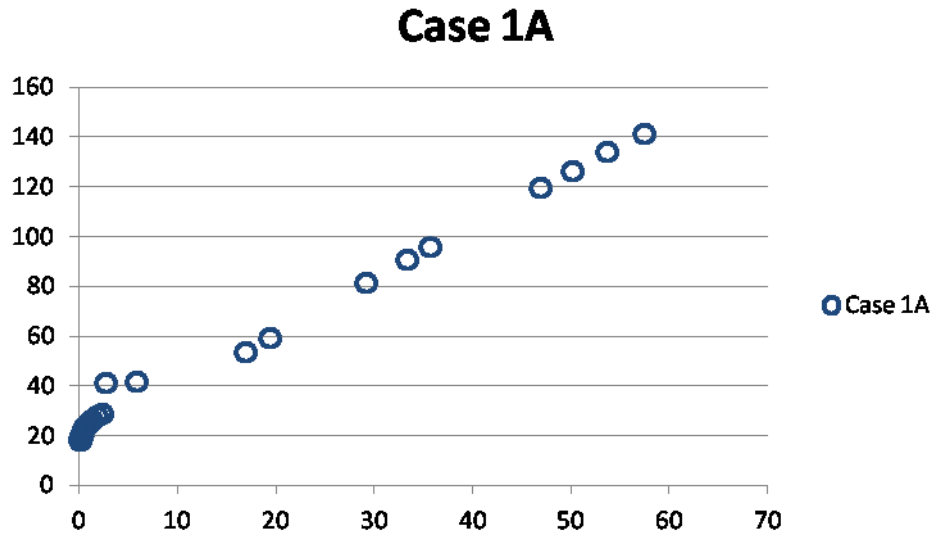
Figure 4. 16 Final Pareto frontier of Case 1A
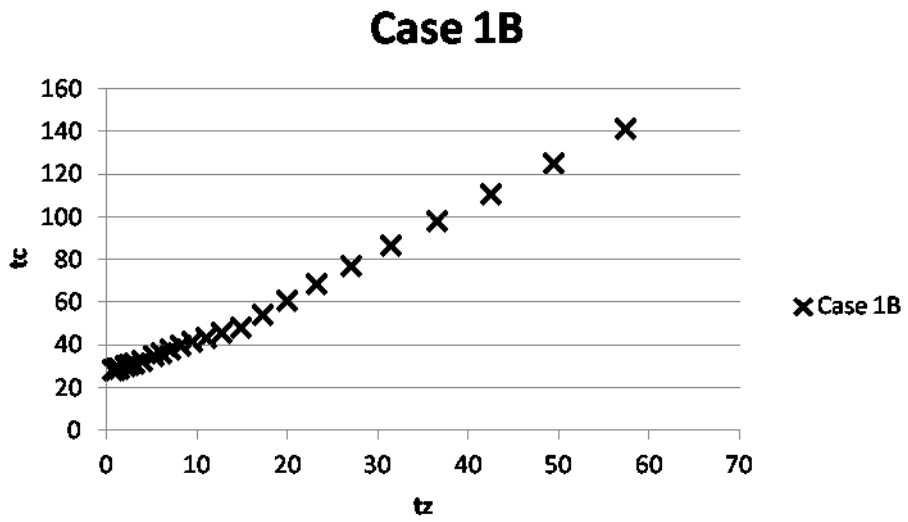
Figure 4. 17 Final Pareto of Case 1B
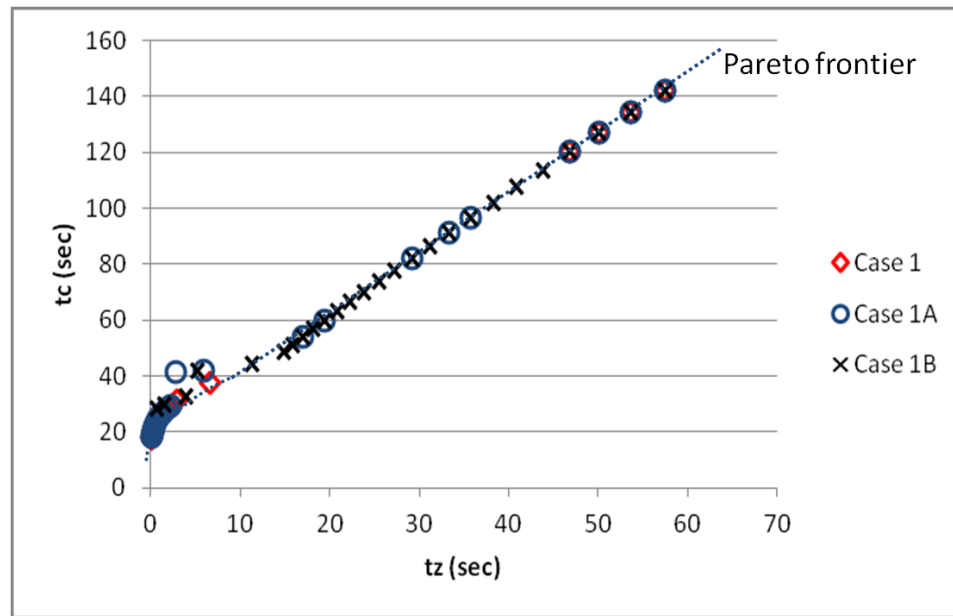
Figure 4. 18 Final Pareto frontier for standard SMC conditions: Case study 1

Figure 4.19 and Figure 4.20 show the final Pareto set and frontier, respectively. From the final Pareto set and Frontier, we can see that in order to maximize inhibition time and to minimize cure time, we need to set the In-mold coating process at the highest molding temperature and the weight percent of initiator 1 (TBPB) should be between 0.5 and 1.5. The results are listed in Table 4.1. It should be noticed that the level of initiator 2 (TBPE) is 0 in the final Pareto frontier for the given level of controllable variables. The inhibition time and cure time on the pareto frontier are dominated by mold temperature and weight percent of initiator 1.
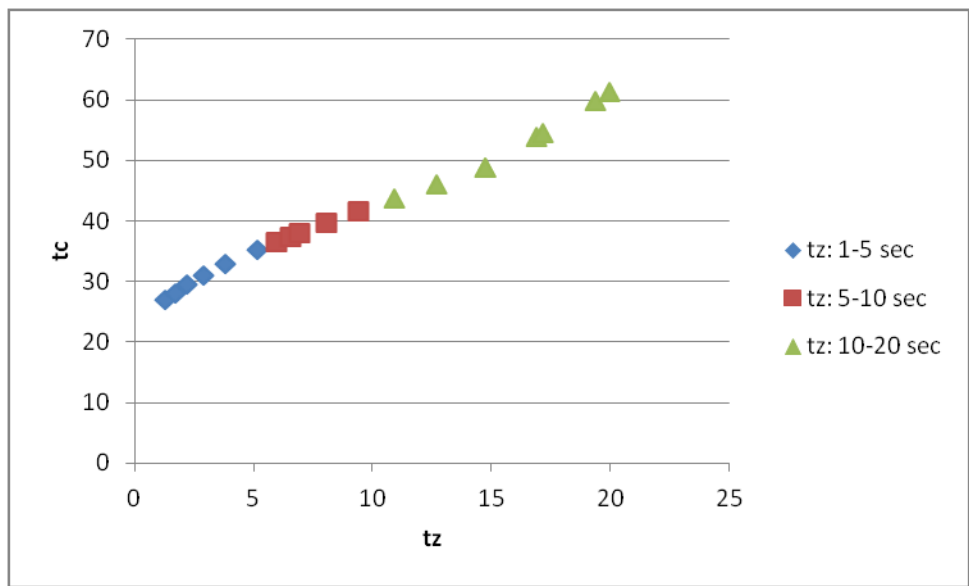
Figure 4. 19 Final Pareto Frontier: performance measure of inhibition and cure time for typical SMC conditions

Figure 4. 20 Final Pareto set: controllable process variables for typical SMC conditions
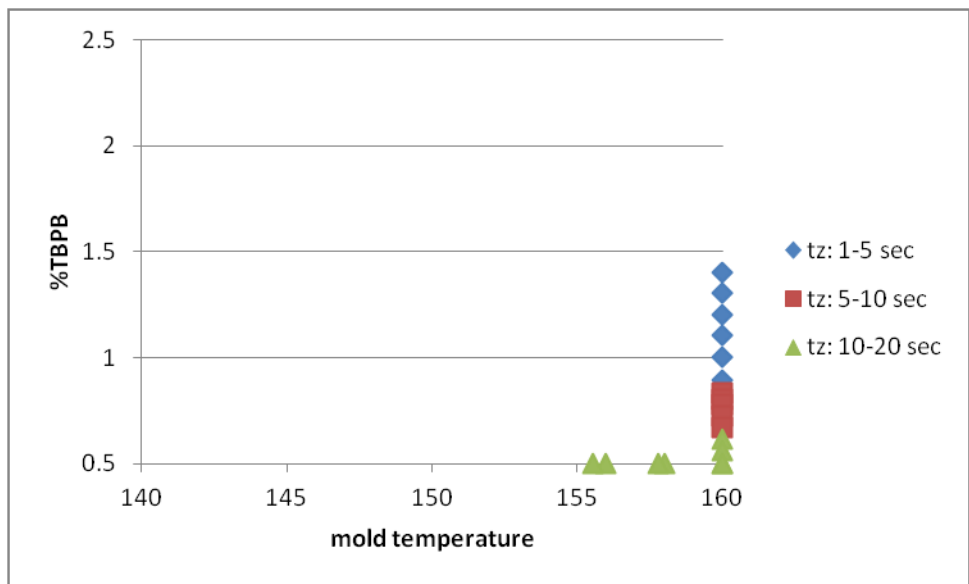
Temperature	%TBPB	%TBPE	Inhibition time	Cure time
160	0.8	0	6.5482	37.5
160	1.1	0	2.9067	31.08
160	1.2	0	2.2173	29.52
160	1.3	0	1.6914	28.15
160	1.4	0	1.2902	26.94
156	0.5	0	19.3555	59.88
158	0.5	0	16.8976	54
160	0.5	0	14.7518	48.75
160	0.5	0	14.7518	48.75
160	0.555556	0	12.6919	46.11
160	0.611111	0	10.9196	43.76
160	0.666667	0	9.3948	41.67
160	0.722222	0	8.0829	39.8
160	0.777778	0	6.9542	38.12
160	0.833333	0	5.9831	36.61
160	0.888889	0	5.1477	35.25
155.5556	0.5	0	19.9486	61.28
157.7778	0.5	0	17.1545	54.62
160	1	0	3.8104	32.88

Table 4. 1 Final Pareto set and Pareto frontier for case study 1 using proposed optimization method with CCD design

4.3.2 Case Study 2: Inhibition and Cure Time at Lower Mold Temperature Range

This analysis is presented to show the benefits of the low temperature initiator, for cases when lower mold temperature is used, such as Reactive Liquid Molding, Resin Transfer Molding, Injection Molding or low temperature SMC. Case study 2 is similar to the first one. The controllable process variables and performance measure are the same the range of mold temperature is changed to a lower temperature range; that is between 90 and 100°C.

The controllable variables are mold temperature (°C), weight percent of initiator 1 (TBPB) and initiator 2 (TBPE). They are varied in the range of [90, 110]°C, [0.5, 2.5]wt.% and [0, 0.2]wt.%. The performance measures are inhibition time (sec) and cure time (sec). The optimization problem is defined as follows:

Find   Mold temperature, wt.% of initiator 1 (TBPB) and wt.% of initiator 2 (TBPE) to
Maximize   Inhibition time (t_z)
Minimize   Cure time (t_c)
Subject to $90 \leq$ Mold temperature ≤ 110
                $0.5 \leq \text{TBPB} \leq 2.5$
                  $0 \leq \text{TBPE} \leq 0.2$
Case 1A:
Subject to $90 \leq$ Mold temperature ≤ 110
                $0.5 \leq \text{TBPB} \leq 2.5$
Case 1:
Subject to $90 \leq$ Mold temperature ≤ 110
                $0.5 \leq \text{TBPB} \leq 2.5$
                  $0 \leq \text{TBPE} \leq 0.2$

As in the previous case, the optimization method was applied for two different conditions. First, one controllable process variable initiator 1 (TBPB) was studied and the second two controllable process variables of initiator 1 and initiator 2 keeping the same range of molding temperature. After following the same steps as in the previous case, the

final Pareto frontier of the two different conditions are shown in Figure 4.21 and Figure 4.22. For large values of inhibition and cure time, they look similar. In Figure 4.23 we can see the effect of initiator 2 for low inhibition and cure times in the area A. Figure 4.24 shows the final Pareto frontier for the two different cases with and without initiator 2. in area A. It was found that initiator 2 does not affect the performance measures at high molding temperature as in the previous section. We can see that the points of the final Pareto frontier set moves to left-lower side in this case study. It means that the inhibition and cure time is decreased when including the initiator 2. Although the inhibition time is decreased, we can reduce the cure time and cycle.

Figure 4.25 and 4.26 show the final Pareto set and frontier for the given processing conditions. The corresponding values are summarized in the Table 4.2. From the results we can see that the mold temperature should be high around 110°C. In order to have the inhibition time between 30 and 45 sec, the initiator 1 should be in the range of 1.4 to 2.1 and the initiator 2 in the range of 0.1 to 0.2. If we want to decrease inhibition time between 5 and 15, the level of initiator 1 should be 2.1 to 2.5 and the one of initiator 2 is 0.15 to 0.2.
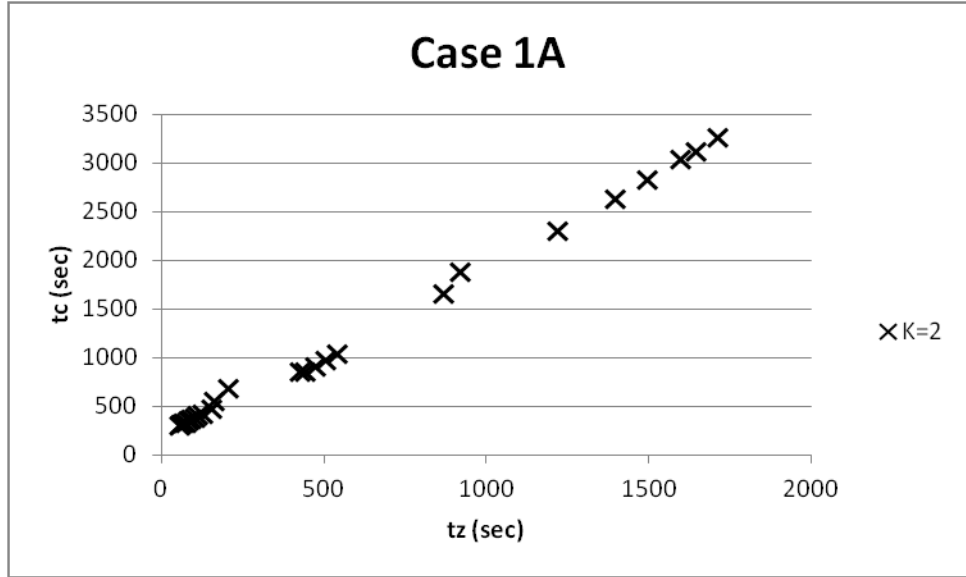
Figure 4. 21 Final PFs: $90 \leq T \leq 110$, $0.5 \leq TBPB \leq 2.5$
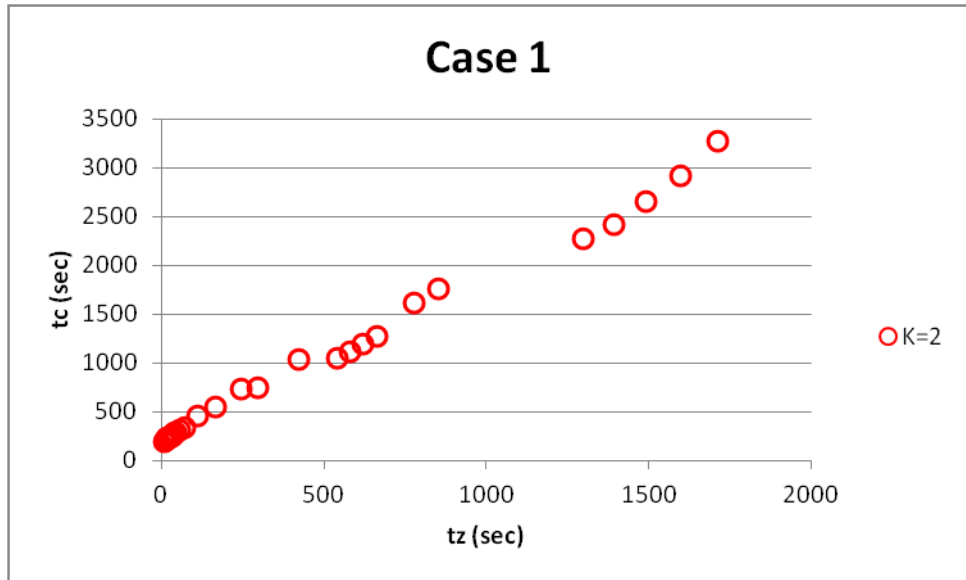
Figure 4. 22 Final PFs: $90 \leq T \leq 110$, $0.5 \leq TBPB \leq 2.5$, $0 \leq TBPE \leq 0.2$

122
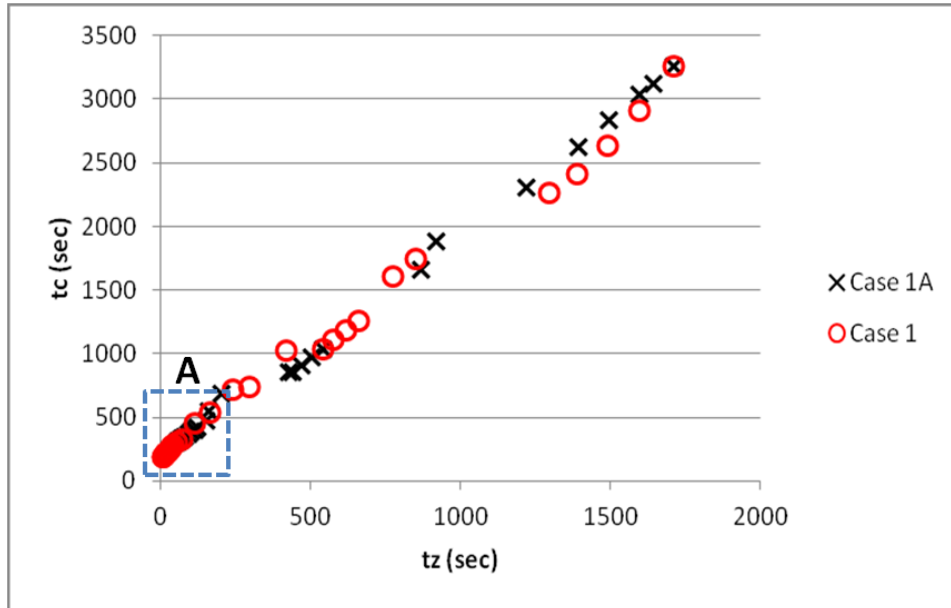
Figure 4. 23 Comparison between Case 1A and Case 1
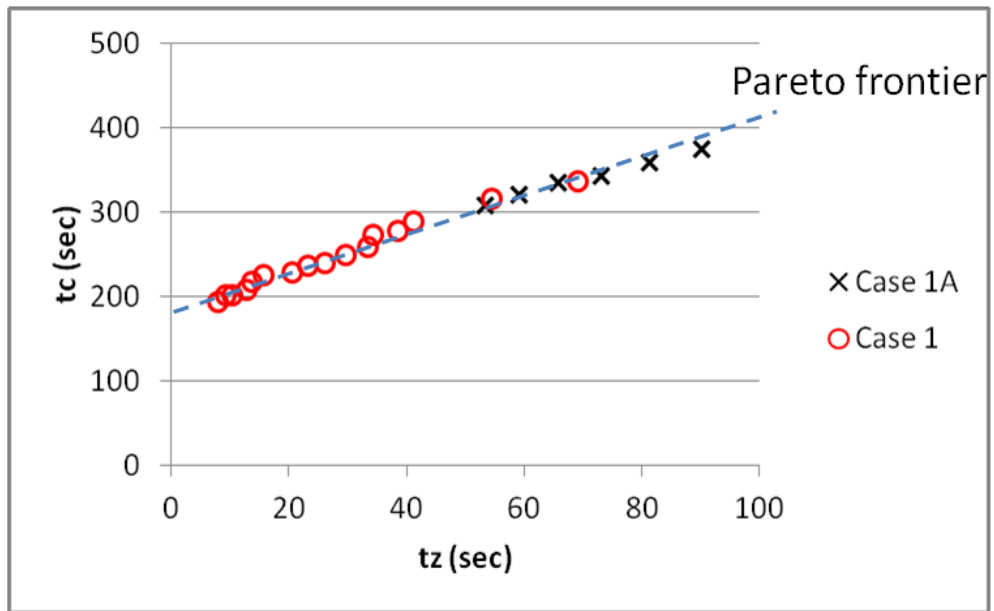
Figure 4. 24 PFs: The effect of initiator 2 (TBPE) at low molding temperature
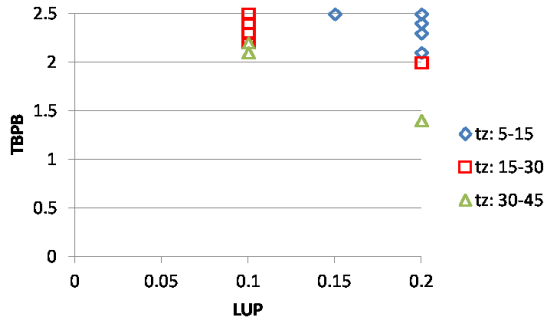
Figure 4. 25 Final Pareto set
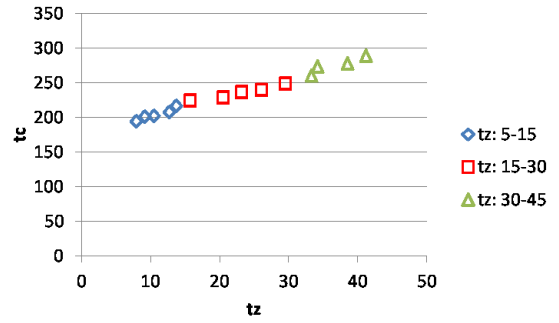
Figure 4. 26 Final Pareto frontier

Temperature	%TBPB	%TBPE	Inhibition time	Cure time
110	2.5	0.2	7.8	195.6
110	2.4	0.2	9	202.3
110	2.3	0.2	10.3	203.4
110	2.5	0.15	12.6	208.4
110	2.1	0.2	13.6	217.9
110	2	0.2	15.6	225.8
110	2.5	0.1	20.4	229.3
110	2.4	0.1	23	237.9
110	2.3	0.1	26	240.7
110	2.2	0.1	29.4	250.2
110	2.1	0.1	33.2	260.4
109	2.2	0.1	34.1	274.3
109	2.1	0.1	38.4	278.4
110	1.4	0.2	41.1	289.8

Table 4. 2 Final Pareto set and Pareto frontier for case study 2 using proposed optimization method with CCD design

4.4 Conclusions

We used the multiple criteria optimization method to solve in-mold coating case studies: (1) inhibition and cure time at high temperature for SMC and (2) inhibition and cure time at low temperature. Mold temperature, initiator 1 and initiator 2 were considered as controllable variables to maximize inhibition time and minimize cure time. . In both cases, we were able to observe how the Pareto frontier was improved. From the first case study we found that in order to maximize inhibition time and minimize cure time, we need to set the in-mold coating process variables at high mold temperature and vary the content of initiator 1 either low or middle range, depending on which performance measure is more import. It was fond that there was no effect of initiator 2 at high mold temperature. On the other hand, for low mold temperatures we identified that small amount of initiator 2 can reduce the cure time in the range of desired inhibition time.

4.5 References

1. Rosen, S., Harmonsky, C. M. and Trand, M, "Optimization of systems with multiple performance measures via simulation: survey and recommendation", Computers and industrial engineering, 52(2), 327-339, 2008.

2. Sevenson, J. D., "Computer experiments: multiobjective optimization and sensitivity analysis", Ph. D. Thesis, The Ohio State University, 2011.

3. Evans, G., Stuckman, B. & Mollaghasemi, M., 1991. Multicriteria optimization of simulation models. *Proceedings of the 1991 Winter Simulation Conference,* pp. 894-900.

4. Dellino, G., Kleijnen, J. & Meloni, C., 2009. Robust Simuation-Optimization using metamodels. *Proceedings of the 2009 Winter Simulation Conference*, pp. 540-550.

5. Zakerifar, M., Biles, W. & Evens, G., 2009. Kriging Metamodeling in Multi-Objective Simulation Optimization. *Proceedings of the 2009 Winter Simulation Conference*, pp. 2115-2122.

6. Ryu, J.-H., Kim, S. & Wan, H., 2009. Pareto front approximation with adaptive weighted sum method in multiobjective simulation optimization. *Proceedings of the 2009 Winter Simulation Conference*, pp. 623-633.

7. Mauricio Cabrera Rios, "Multiple criteria optimization studies in reactive in-mold coating", Ph.D. Thesis, The Ohio State University, (2002)

8. Carlos E. Castro, " Optimization and analysis of variability in high precision injection molding", M.S. Thesis, The Ohio State University, (2005)

9. Maria G. Villareal-Mirroquin, "A metamodel based multiple criteria optimization vis simulation method for polymer processing", Ph.D. Thesis, The Ohio State University, (2012)

10. Montgomery, D. C., 2005. *Design and Analysis of Experiment.* 6th ed. s.l.:John Wiley & Sons, Inc..

11. Barton, R. R., 2009. Simulation optimization using metamodels. *Proceedings of the 2009 Winter Simulation Conferenc*e, pp. 230-238.

12. Simpson, T., Poplinski, J., Koch, P. N. & Allen, J., 2001b. Metamodels for computer-based engineering design: Survey and recommendations. *Engineering with Computers,* 14(2), pp. 129-150.

13. Konstantin S. Zuyev, "Processing studies in reactive in-mold coating for thermoplastic substrates", Ph. D. Dissertation, The Ohio State University, 2006.

Chapter 5: Electrical Conductivity and Injection Pressure for IMC Process of Thermoplastic Parts

In-Mold Coating (IMC) has been applied for many years to Sheet Molding Compound (SMC) as an environmentally friendly alternative to make the surface conductive; for subsequent electrostatic painting operations. Due to its successful application to exterior body panels made from compression molded SMC, the application of In-Mold Coating for injection molded thermoplastic parts is being developed. In order to make the coating conductive, the filler used in IMC is carbon black (CB). However, the injection pressure needed to coat the part is significantly affected by the amount of CB in the coating material. Due to the mold differences between typical injection molds and SMC compression molding (land versus shear edges), as mentioned in chapter 1, predicting injection pressures for IMC of thermoplastic parts is more critical than for IMC of SMC. The clamping force needs to be larger than the hydraulic force generated as the coating flows. If this is not the case, leakage will occur and the part will not be fully coated. To predict the coating pressures we need to measure the effect of CB on the IMC viscosity. In the present work, we studied the effect of CB on electrical conductivity and viscosity. The pressures needed for coating a typical IMC part with the required conductivity level are estimated

5.1 Introduction

Plastics are by nature very good insulators. This inherent electrical insulation causes the plastic to hold electrostatic charges, allow electromagnetic / radio frequency interference (EMI/RFI) to pass through and cannot be painted electrostatically, a usual requirement for materials to be used as exterior automotive body panels. Plastics are increasingly becoming the material of choice for many applications where light weight is critical but require conductivity. This is true not only for the automotive and aerospace industries but also in electronics and telecommunications. Thus, the challenge is to convert inherently insulating thermoplastic materials to a product that would provide antistatic or electrostatic dissipative or EMR/RFI shielding or a combination of these properties. The surface conductivity requirements vary depending on the desired application. For EMI shielding, surface conductivity larger than 10S/m are required. For electrostatic painting, values larger than 0.0001S/m are needed and for electrostatic dissipation values above 0.00005S/m are needed [1]. In the case of electrostatic paining for example, the larger the conductivity the larger the paint transfer efficiency.

For many years, In-Mold Coating has been commercially applied to SMC as an environmentally friendly approach to minimize problems with porosity; improve the surface quality and to provide the required conductivity for electrostatic painting [2]. In order to make the coating conductive, carbon black is used in IMC as conductive filler. In the IMC process, a liquid heat activated reactive thermosetting mixture is injected onto the surface of the SMC substrate at the end of the molding process while the part is still in the mold. After the coating material has reached enough surface integrity (cured) by

the chemical reaction, the coated SMC part is removed from the mold. Fully reacted IMC is 100% solid material and, therefore, no volatile chemicals are released during the process [3]. The IMC stage is an integral part of the manufacturing process of compression molded SMC exterior automotive body panels.

To date, the use of IMC as a conductive primer for SMC parts requiring painting is a standard practice. This success has attracted the interest of thermoplastic manufacturers to use IMC as a conductive primer. The IMC cycle for thermoplastics is composed of three stages: filling, packing and curing. The coating is injected once the thermoplastic has reached enough mechanical integrity. During the filling stage, the coating flows by compressing the substrate and spreads until it reaches the mold end, as shown schematically in Figure 5.1. In the packing stage, more coating is introduced until the volume needed for the desired coating thickness is injected. During the curing stage, the coating solidifies by chemical reaction. Figure 5.2 depicts the stages for IMC during the injection molding process.

The application of IMC to thermoplastic substrates is more challenging than the application of IMC to SMC compression molded body panels [5]. Unlike its SMC counterparts, most thermoplastic injection molds, with the exception of the ones used for injection compression, have no shear edges as shown in the Figure 5.3. Any opening of the mold caused by injection of the liquid coating will result in coating leakage. To avoid this problem, the clamping tonnage needs to be greater than the hydraulic force generated by the injected coating material at any time. Thus predicting pressures during the injection stage of the coating process is critical. The key material property needed to

predict coating pressure is the viscosity, which is greatly affected by the amount of CB in the IMC resin.

Increasing the amount of CB will increase the surface conductivity of the coated part, thus improving the paint transfer efficiency [6, 7]. However the need for a higher conductivity needs to be balanced with the needs to have a reasonable viscosity for adequate coating. In this research the effect of the CB level on conductivity and viscosity were measured. Other fillers such as carbon nanofibers (CNF) and carbon nanotubes (CNT) are more conductive than CB but their cost will make them prohibitive for automotive applications [8, 9]. Coating pressures are also predicted for a typical part.
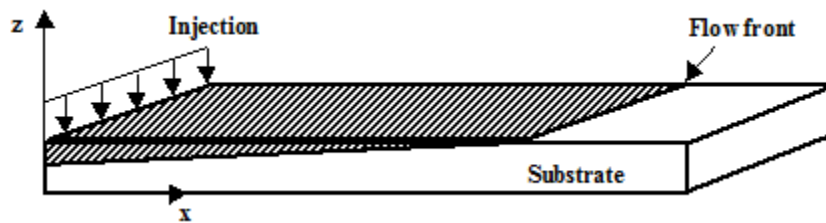
Figure 5. 1 Schematic of 1D IMC flow [4]
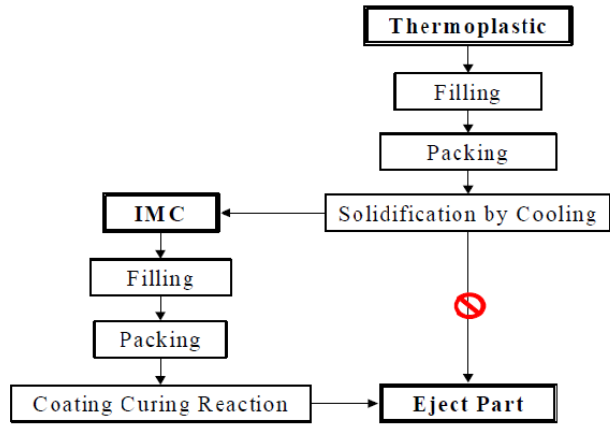
Figure 5. 2 Schematic representation of the stages of IMC for injection molding process of thermoplastic substrates [4]
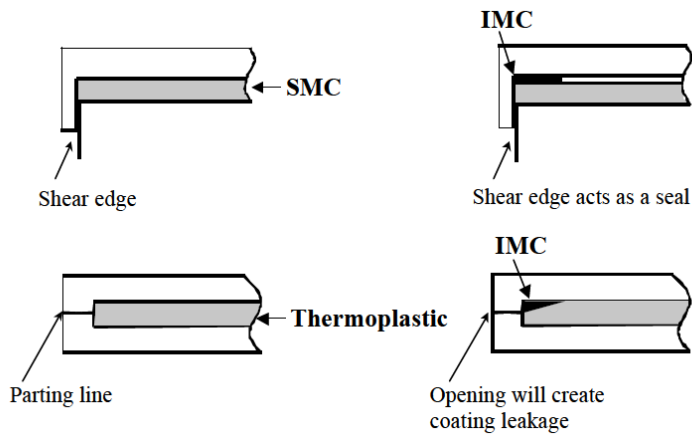
Figure 5. 3 Tooling difference between IMC for SMC and IMC for thermoplastic [4]

132

5.2 Materials

The coating material used was a one component system for thermoplastic applications, Genglaze 2623AM supplied by OMNOVA Solutions Inc. The resin is an acrylated urethane. Hexanediol diacrylate is used as the diluent to decrease viscosity. Cobalt is used as accelerator. The conductive filler used in this study is carbon black, VULCAN XC72R from CABOT Corp. Typical coating formulations can be found in reference [2]. The IMC resin is a thermosetting material that reacts by the free radical mechanism. The initiator used was tert-butyl peroxybenzoate (TBPB).

5.3 Electrical Conductivity Measurements

To facilitate sample preparation, previously molded thermoplastic polyolefin (TPO) 15.2cm by 15.2cm flat plates were blade coated with IMC catalyzed with 1.75% TBPB. After coating, the plates were cured in an oven at 70°C. The coating thickness was measured to be between 0.1 and 0.2 mm. CB level was varied from 1% up to 6% by weight. From the plates, square samples of 25.4 mm sides were cut. The electrical conductivity of IMC coated thermoplastic parts was measured using a KEITHLEY series 2400 source meter according to the Van der Pauw technique (four points contact method) [10]. Figure 5.4 shows the samples used to measure the electrical conductivity of IMC coated thermoplastic parts. Van der Pauw showed that the sheet resistance of samples with arbitrary shapes can be determined from two of these resistances - one measured along a vertical edge and a corresponding one measured along a horizontal edge. Silver paste was used as the conductive medium between the conductive surface and the four measuring probes.

Figure 5.5 shows the measured electrical conductivity versus carbon black weight fractions of 1 to 6%. It is observed that the electrical conductivity of IMC coated thermoplastic parts increases by adding carbon black and the measured electrical conductivity is in the level required for electrostatic painting application. The larger the conductivity increases the paint transfer efficiency. However, even with 6% CB, the minimum conductivity level needed for EMI shielding is not achieved. If EMI shielding is required the levels of CB needed would be such that the viscosity of the coating will be to large, to allow for complete part coating. Preliminary results show that even using

CNF, the levels needed for EMI shielding will make the viscosity too high for proper coating. In order to reach EMI shielding levels; our group is developing an alternative approach, consisting of locating a CNF nanopaper on the mold wall prior to injection molding then in mold coating with the IMC resin without CB. Preliminary results of this alternative method show good potential for parts requiring EMI shielding [12], as also shown in Figure 5.5.
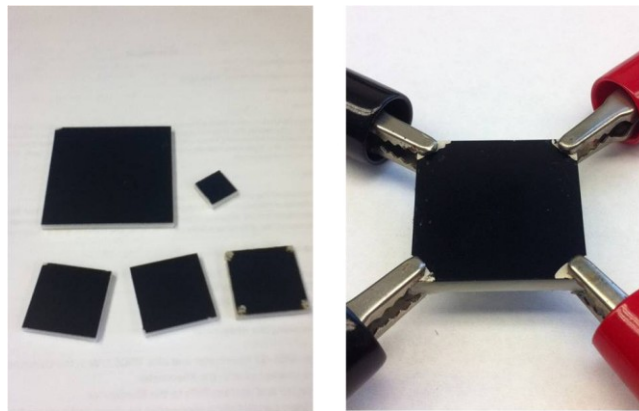
Figure 5. 4 Electrical conductivity measurement using Van der Pauw method for IMC coated thermoplastic parts.
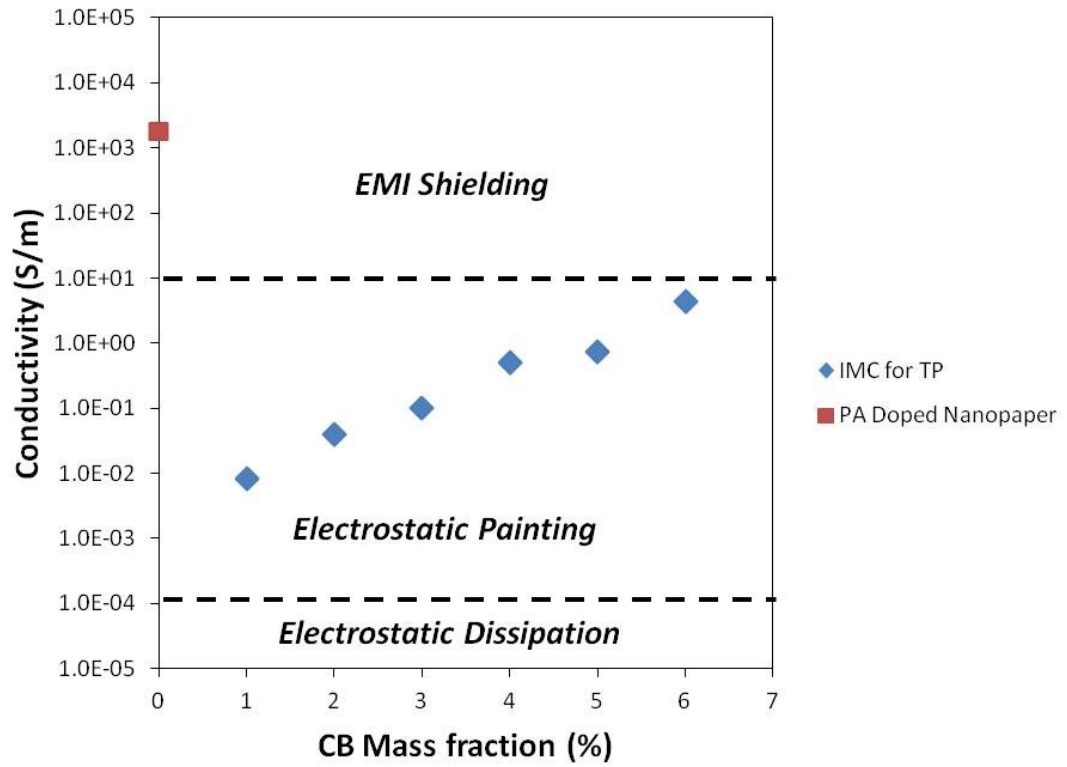
Figure 5. 5 Measured electrical conductivity versus carbon black weight fractions of 1 to 6% for specific applications

5.4 Viscosity Measurements

The IMC is formulated with enough inhibitor to prevent any reaction during filling [3]. The viscosity of IMC resin with and without carbon black was measured using an ARES-G2 Rheometer (TA instruments). The test was performed using 25 mm parallel plate geometry in shear rate sweeps mode at three different temperatures of 25°C, 50°C and 75°C without initiator. The shear rate range was from $0.1 s^{-1}$ to $100 s^{-1}$. Figure 5.6 shows the shear viscosity of the IMC resin with various CB contents at 25°C. The IMC resin without CB exhibited nearly Newtonian behavior. When adding CB into IMC, the IMC showed Non-Newtonian, shear shinning behavior due to the presence of CB. It was found that carbon black particles increased significantly the IMC resin viscosity, especially in the low shear rate region. The viscosity for typical IMC systems can be represented by the power law expression as shown in the figure 5.7 [3, 11]. Below we give the expressions for 2%, 4% and 6% CB:

$$\text{2\% CB IMC: } \eta = 0.0928 e^{\frac{1141}{T}} \dot{\gamma}^{-0.6904}$$

$$\text{4\% CB IMC: } \eta = 1.2253 e^{\frac{1052}{T}} \dot{\gamma}^{-0.8021} \tag{5.1}$$

$$\text{6\% CB IMC: } \eta = 1.8486 e^{\frac{1453}{T}} \dot{\gamma}^{-0.8154}$$

where η is the viscosity in $Pa \cdot s$, m and n are the power law constants, T is the temperature in $Kelvin$ and $\dot{\gamma}$ is the shear rate in sec^{-1}. The fitted power law models were used to predict injection pressure of IMC with varying CB contents.
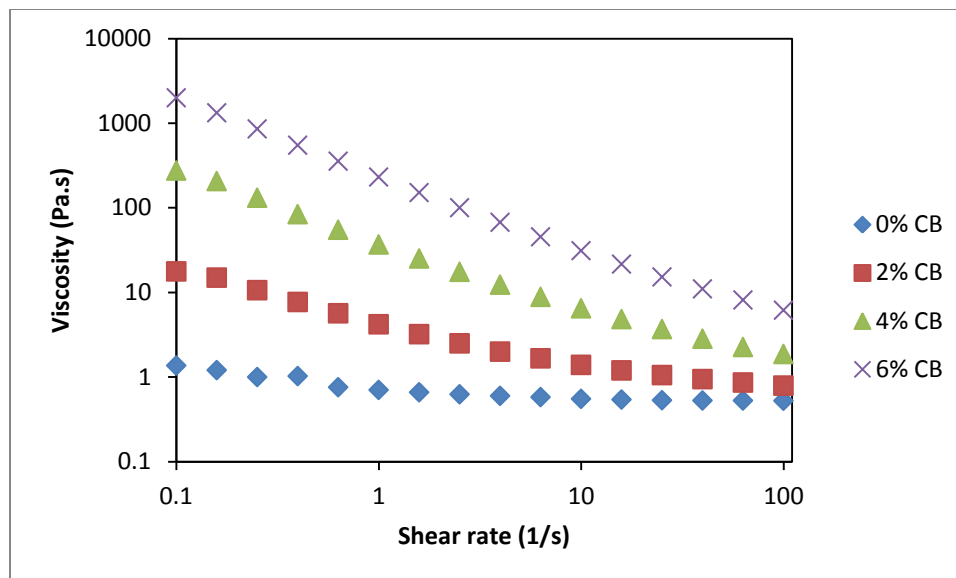
Figure 5. 6 Shear viscosity of IMC resins with various carbon black contents at 25 °C
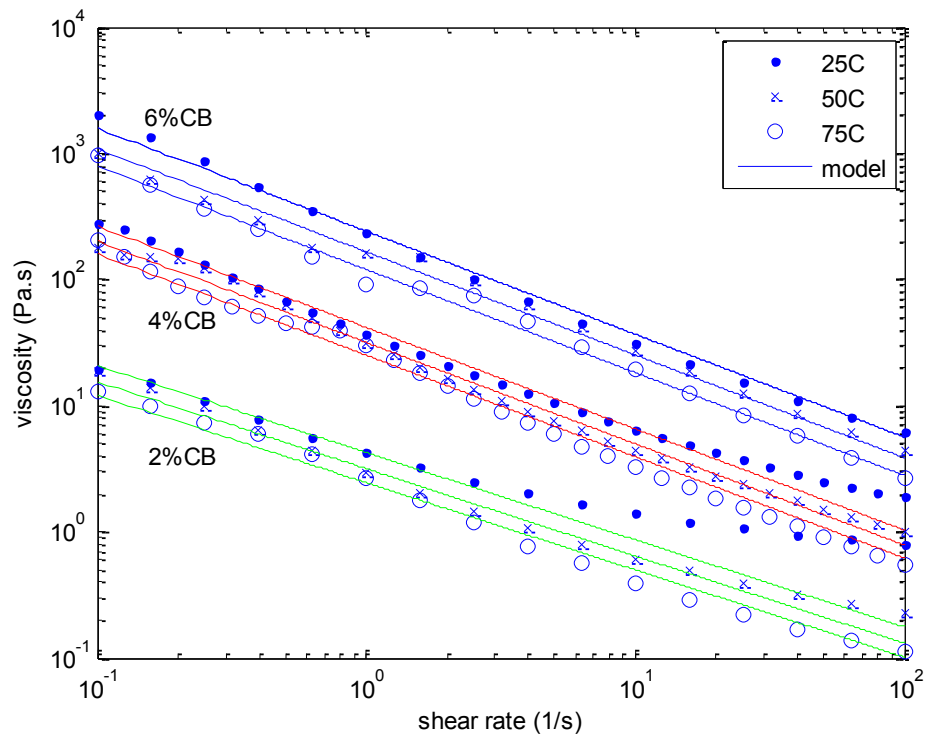
Figure 5. 7 Fitted power law model of IMC with 2%, 4% and 6% CB at different temperatures

5.5 Injection Pressure of IMC

Chen et al. [2, 5, and 11] developed a model to predict injection pressures needed for complete IMC coverage for a rectangular part. The coating flow from a line injection port can be approximated as a one-dimensional flow as shown schematically in Figure 5.1. In this model, the following assumptions were made: one dimensional flow, isothermal flow, quasi-steady state, and lubrication approximation. The relationship between the pressure gradient and the flow rate for any given location x is given by [6, 7]:

$$\frac{\partial p}{\partial x} = -\frac{\frac{Q}{w}}{\int_0^h \frac{z(z-h/2)}{\eta} dz} \qquad (5.2)$$

The gap available for IMC flow can be expressed as:

$$h = h_s(1 - \frac{V}{V_0}) \qquad (5.3)$$

where h_s is the thickness of the thermoplastic substrate, V is the specific volume of the thermoplastic substrate and is a function of the IMC pressure under the assumption of isothermal flow, V_0 is the specific volume of the thermoplastic substrate at the average (bulk) temperature just before the coating injection starts, and η, the viscosity of the coating at the given CB level. Thus to be able to predict the flow pressures we need to iterate as the gap depends of the pressure and the PVT relationship for the thermoplastic, and the pressures depend on the gap available for flow. For the more general case of flow in 2 directions, since the coating thickness is much smaller than the other two directions,

the generalized Hele-Shaw model can be applied as explained by Chen et al. [5] assuming power law model viscosity and Bhagavatula et al. [4] for the more general Carreau viscosity model. For the power law model, if a linear relation is assumed between the coating injection pressure and the thickness change of the substrate,

$$h = C_1(P - P_T)$$

(5.4)

Equation 5.1 and 5.4 can be integrated to obtain an analytical solution for the required IMC injection pressure at any point X as a function of the flow front position X_f. The relation between the pressure and the flow rate for any given location X is obtained as:

$$P = P_T + \left[\frac{q_x{}^n \left(\frac{1}{n} + 2\right)^n m(2^{1+2n})(2 + 2n)(X_f - X)}{2^n(C_1)^{1+2n}} \right]^{\frac{1}{2+2n}}$$

(5.5)

where C_1 is the thermoplastic compressibility, which can be obtained from the thermoplastic PVT relationship as indicated by Chen et al, P is the injection pressure, P_T is the packing pressure, q_x is the flow rate per unit width, X_f is the flow front position, and X is any point in the part where the pressure needs to be calculated. Chen et al. [5] and then Narayan et al. [4] have developed and experimentally tested more complete model for coating complicated parts that uses finite elements to solve the balance equations. Here for simplicity we limit ourselves to using the simpler analytical model. An example case to predict injection pressure for coating a rectangular part is discussed next. The injection molding process of the thermoplastic substrate is simulated by using

Moldex3D. The thermoplastic material used in the simulation was TPO (HifaxTYC735P, LyondellBasell). The plate had dimensions of 300×100×4 mm. The process parameters were melt temperature (200°C), mold temperature (40°C), filling time (1sec), packing time (20sec), cooling time (30sec), and packing pressure (42MPa). Figure 5.8 shows the temperature and pressure curves during filling, packing and cooling stages of thermoplastic part. The IMC must be injected at some point during the cooling stage [4]. Figure 5.9 shows the predicted injection pressures for IMC containing 2%, 4% and 6% CB injected 30 seconds after the thermoplastic was injected into the mold. At this point, the mold temperature was 75°C and the packing pressure was 2.5MPa (From Figure 5.8). From Figure 5.9 we can see that the predicted injection pressures of 6% CB IMC is about 23 MPa higher than 2%CB IMC. Figure 5.10 shows the predicted injection pressures of IMC at varying injection times. The later we inject the coating, the lower filling pressure but the lower the temperature which hinders proper curing of the coating. As a consequence, using more than 4%, will make coating unfeasible due to injection pressures being too high, to keep the mold fully closed and avoid coating leakage. This can be clearly seen in Figure 5.11, which shows the IMC filling pressure required for several values of electrical conductivity, with injection occurring at several times during the cooling stage.
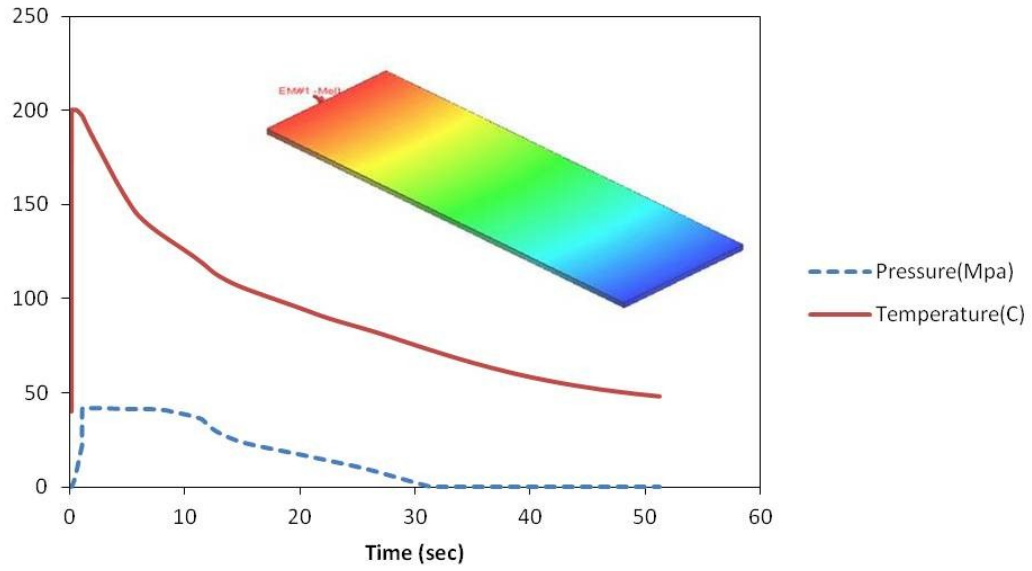
Figure 5. 8 Moldex3D IM simulation for rectangular part.
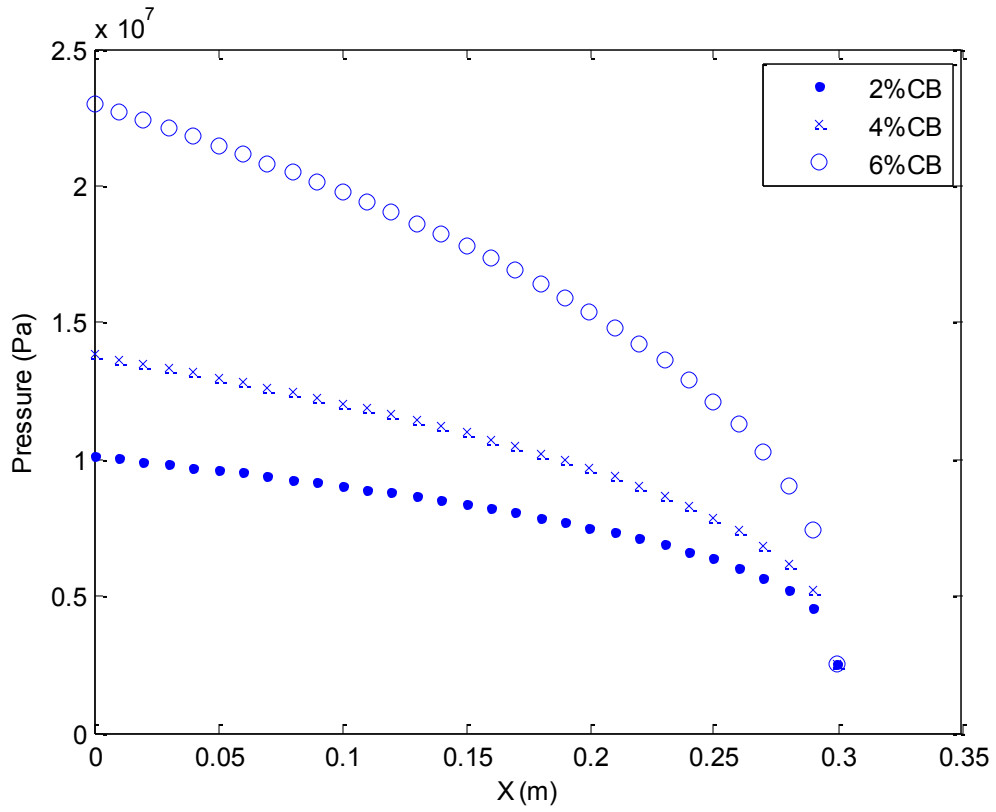
Figure 5. 9 Pressure at the end of IMC filling at 75°C for 2% CB, 4% and 6% CB IMC.
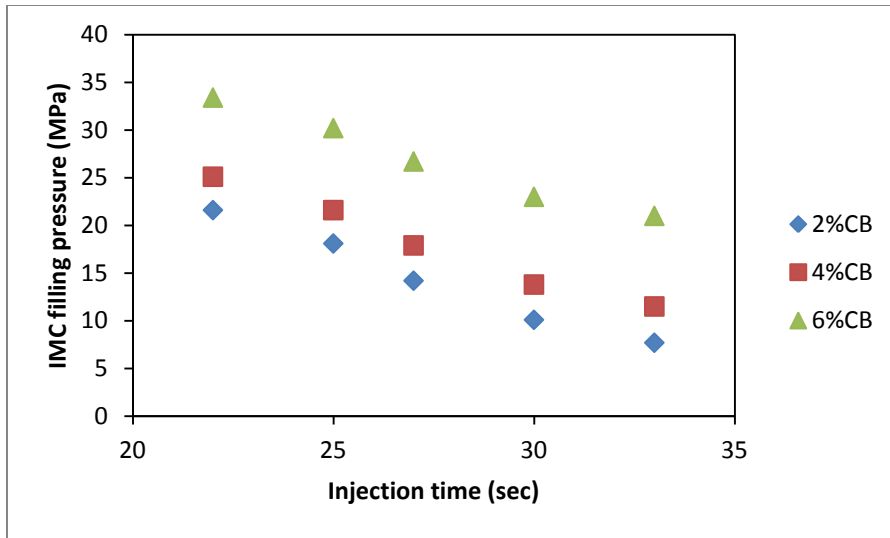
Figure 5. 10 IMC filling pressure at varying injection time.
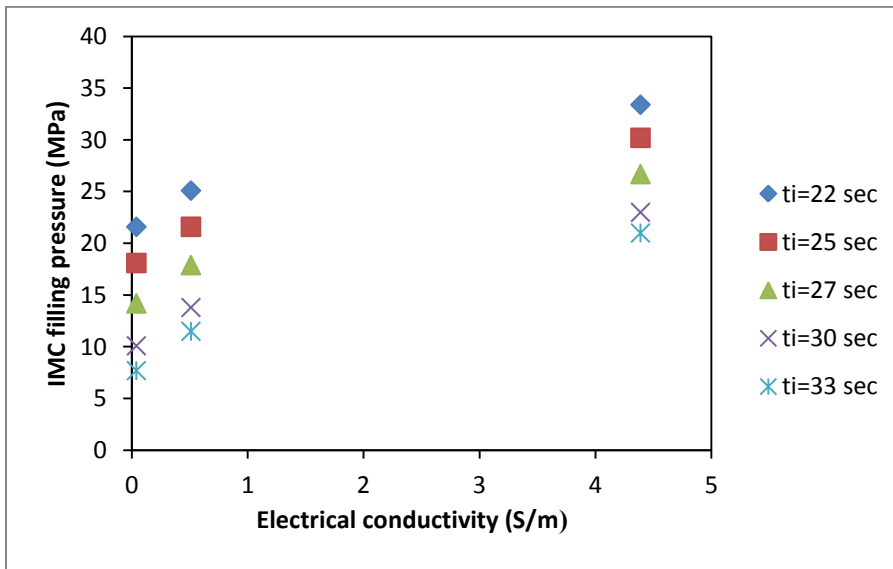
Figure 5. 11 Predicted filling pressures versus electrical conductivity for several values of time of injection

145

5.6 Conclusions

We studied the effect of carbon black on electrical conductivity and injection pressure of IMC for application to thermoplastic parts. Electrical conductivity of IMC coated thermoplastic parts was measured and rheological behavior of IMC in the presence of CB was investigated. The coating pressure to cover a typical part was estimated.

From the results obtained, we can see that by increasing the CB level we can increase the electrical conductivity and thus improve the paint transfer efficiency. However, preliminary results show that is probably not possible by simply adding CB or even CNF to reach the levels required for EMI shielding and be able to coat the part. A better approach for EMI shielding is as discussed earlier to locate a CNF nanopaper on the mold surface before thermoplastic injection then in-mold coating to fill the voids in the nanopaper [12].

A major challenge for IMC of thermoplastics is the relative low mold temperatures when compared to SMC molding. Thus future research will also be geared toward identifying catalyst systems with adequate shelf life but with a reasonable cycle time.

5.7 References

1. Moniruzzaman M, Winey KI. *Macromolecules* 2006, 39, 5194-5205.

2. Castro, JM, Griffith, RM. In *Sheet Molding Compounds: Science and Technology*, Kia, HG Eds., Hanser/Gardner Publications: Cincinnati, 1993, p 163.

3. Castro JM, Griffith RM. *Polymer Eng. Sci*. 1990, 30, 677-683.

4. Bhagavatula N, Castro JM. *Modelling Simul. Mater. Sci. Eng*. 2007, 15, 171-189.

5. Chen X, Bhagavatula N, Castro JM. *Modelling Simul. Mater. Sci. Eng*. 2004, 12, S267-S287.

6. Huang JC, *Adv. Polym. Tech*. 2002, 21, 299-313.

7. Gupta, RK, Kennel, E, Kim, KJ, Eds., *Polymer Nanocomposites Handbook*, CRC Press: Boca Raton, 2010.

8. Bauhofer W, Kovacs JZ. *Compos. Sci. Technol*. 2009, 69, 1486-1498.

9. Al-Saleh MH, Sundararaj U. *Carbon* 2009, 47, 2-22.

10. Van der Pauw LJ. Philips Res. Repts. 1958, 13, 1-9

11. Zuyev KS, Castro JM. J. Polym. Eng. 2002, 22, 233-260.

12. Cabrera ED, Ko S, Ouyang X, Straus E, Lee LJ, Castro JM. *SPE ANTEC* 2013.

Chapter 6: Conclusions and Future Work

6.1 Conclusions

In-mold coating is currently used successfully as an alternative to priming and in some limited cases of top coating, for compression molded sheet molding compound exterior automotive body panels. This success has attracted the interest of thermoplastic manufacturers to use IMC. In-mold coating is an attractive alternative for priming and or top coating since the coating resin is cured in the mold without opening the mold and releases no chemicals during the molding process. There are many controllable process variables and performance measure to be considered in the in-mold coating process. In this research, we focused on developing a method, to select the best compromises among flow time and mold opening time (cure time).

In chapter 2, the chemorheology of a commercial IMC material with and without carbon black was investigated using rheological measurements in both steady shear and dynamic oscillation mode. The rheological changes are correlated with the extent of reaction measured using DSC. . It was found that the IMC solidified (geled) at very low conversion values (0.01). This phenomenon is very different with the case of a standard epoxy resin system which has 0.75 of gel conversion. Our results indicate that the viscosity of IMC resin starts to increase as soon as the inhibitor is consumed therefore the maximum flow time should be the inhibition time. For actual manufacturing, we use as flow time, half the inhibition time as for typical molding cases, the temperature is

controlled within +/- 5 C. It was observed that the elastic modulus at a conversion of 0.9 reached a nearly constant plateau for all temperatures. Based on this and visual inspection as well as surface roughness measurements, from actual moldings, it was concluded that the mold opening time can be assumed to be that when the conversion is 0.9. In order to select the best compromises, we need to develop models to predict both the flow time and cure time. This is done in chapter 3. The effect of two initiators, as well as the effect of carbon black on the curing rate were studied.

In chapter 4, we used the multiple criteria optimization method developed by Villarreal to develop the best compromises among in-mold coating performance measures flow time and cure time for two cases: (1) inhibition and cure time for standard SMC conditions and (2) inhibition and cure time at low mold temperature condition. Mold temperature, initiator 1 and initiator 2 were considered as controllable variables to maximize inhibition time and minimize cure time. . The Pareto frontier was established for both cases. From the first case study we found that in order to maximize inhibition time and minimize cure time, we need to set the in-mold coating process variables at high mold temperature and contents of initiator 1 either low or middle range, depending on which performance measure is more important. It was fond that there was no effect of initiator 2 at high mold temperature. On the other hand at lower mold temperatures, we found that a small amount of initiator 2 can reduce the cure time in the range of desired inhibition time.

In chapter 5, we studied the effect of carbon black on electrical conductivity and injection pressure of IMC for application to injection molded thermoplastic parts. From

the results obtained, we observed that by increasing the CB level we can increase the electrical conductivity and thus improve the paint transfer efficiency. However, it showed that is not possible by simply adding CB to reach the levels required for EMI shielding and weight percent larger than 3% CB makes the coating unfeasible.

The chemorheology and curing analysis procedure in this research can be used to develop best compromises for other IMC coating systems. The minimum number of experiments needed when analyzing a new IMC would be three isothermal DSC experiments to fit the cure model and a DSC scan to verify the predictions and select the isothermal conditions. In this study it was found that the time available for flow is limited by the inhibition time and the mold opening time can be predicted from the time needed for the conversion to reach 90%. For a new system, it may be a good idea to do actual moldings at three different temperatures to verify these results.

6.2 Future Work

A major challenge for IMC of thermoplastics is the relative low mold temperatures when compared to SMC molding. Thus future research will be geared toward identifying catalyst systems with adequate shelf life and a reasonable cycle time. This may require the use of two component systems such as urethane systems used in reaction injection molding. A major challenge in this case would be to implement on-line mixing with injection under high pressure.

In this wok, the multiple criteria optimization method was applied for two performance measures which are inhibition time and cure time in the in-mold coating process. The multiple criteria optimization method can be applied to large number of controllable process variables and performance measures to select best compromises. In particular for IMC of injection molding thermoplastics, the part conductivity as well as the viscosity (or injection pressure) are critical performance measures.

Another potential area of growth is to use IMC as a substitute for the gel coats used for surface protection when manufacturing fiber reinforced polymeric composites (FRPC) made by vacuum assisted resin transfer molding (VARTM) in automotive and aerospace. This is also a low temperature process.

Appendix A: DSC Experiments

The reaction rate of neat IMC resin was measured using a DSC Q20 (TA instruments). The sample was prepared by adding the required quantity of initiator to the IMC resin and thoroughly mixed. About 10-15 mg of the sample was placed in a Tzero hermetic sample pan and sealed. Isothermal DSC experiments were conducted at 90, 100 and 110 °C followed by a dynamic DSC scan from 30 °C to 250 °C to measure the residual reaction heat. Non-isothermal DSC scans were performed with a heating rate 10 °C/min from 30 °C to 250 °C. The measured heat flow of a typical isothermal scan is shown in Figure A.1-3.
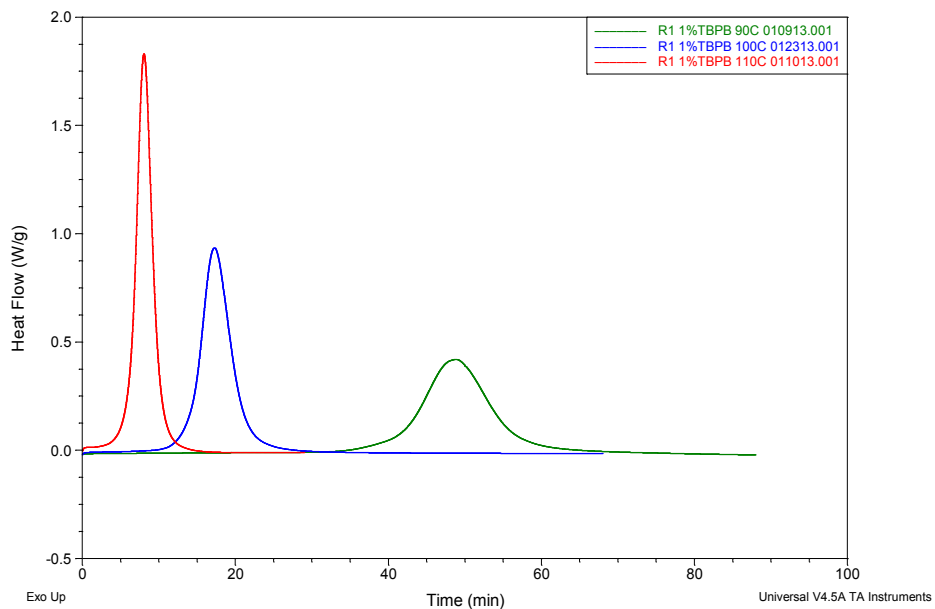
Figure A. 1 Isothermal scans. EC610 (0%CB). 1%TBPB
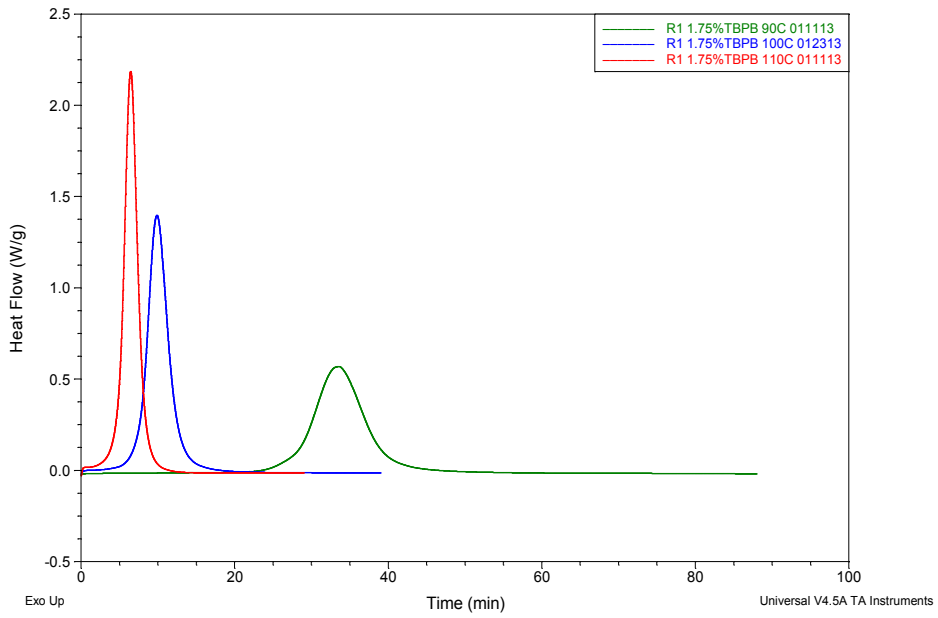
Figure A. 2 Isothermal scans. EC610 (0%CB). 1.75%TBPB
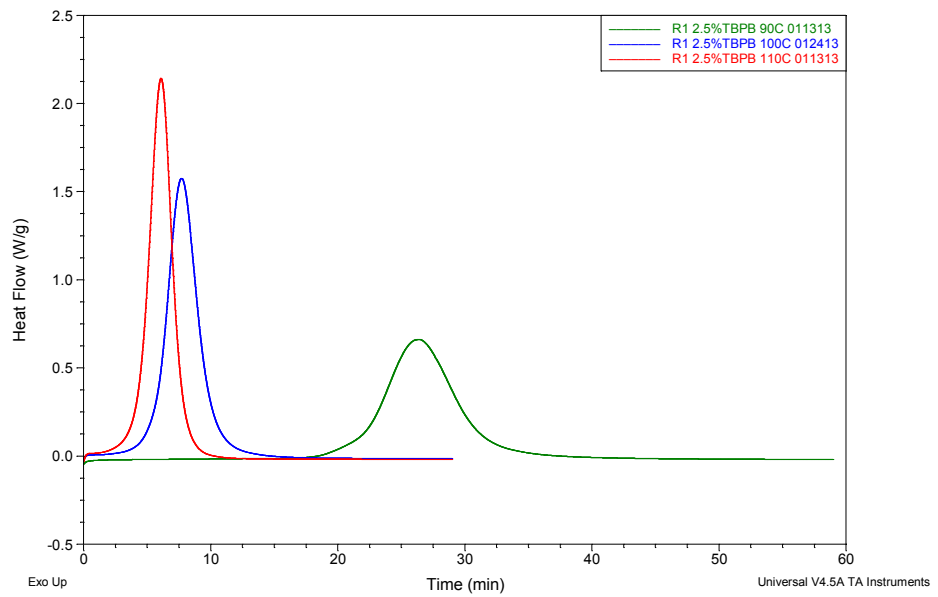
Figure A. 3 Isothermal scans. EC610 (0%CB). 2.5%TBPB

153

Appendix B: Determination of Autocatalytic Kinetic Parameters

To obtain kinetic parameters in the autocatalytic curing reaction, we used the analytical method proposed by Kenny. For autocatalytic curing reactions, an isothermal reaction rate is expressed as shown below:

$$\frac{d\alpha}{dt} = k_p \alpha^m (\alpha_{max} - \alpha)^n \qquad (B.1)$$

To determine the reaction order n, equation (B.1) can be modified in the following form:

$$\ln (d\alpha/dt) = \ln \left(k_p \alpha^m\right) + n\ln(\alpha_{max} - \alpha) \qquad (B.2)$$

The reaction order n is obtained from the slope of ln $(d\alpha/dt)$ vs. $\ln(\alpha_{max} - \alpha)$, Figure B.1 shows a plot of ln $(d\alpha/dt)$ vs. $\ln(\alpha_{max} - \alpha)$ for the isothermal experiment at 110°C for IMC with 1%TBPB.

154
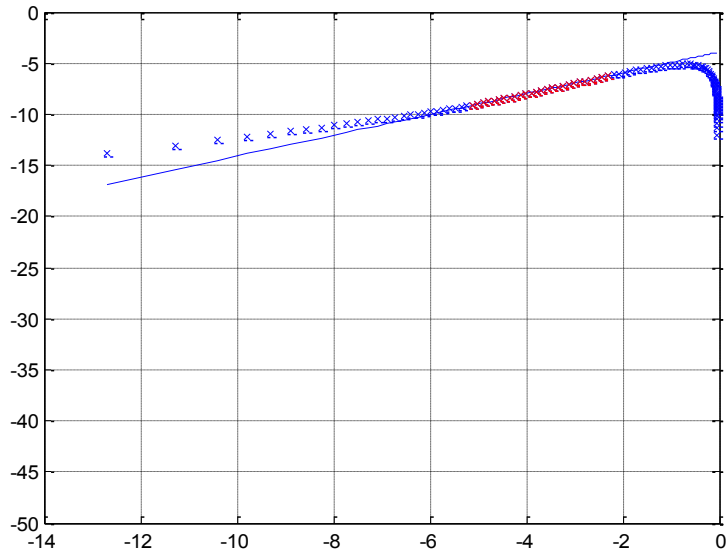
Figure B. 1 A plot of ln (dα/dt) vs. $ln(\alpha_{max} - \alpha)$

Equation B.1 can be also rearranged in a different form:

$$\ln[(d\alpha/dt)/(\alpha_{max} - \alpha)^n] = \ln k_p + m \ln\alpha \qquad (B.3)$$

Then, the reaction order of m and the constant k_p can be determined from the slope and intercept of a plot of n $[(d\alpha/dt)/(\alpha_{max} - \alpha)^n]$ vs. $\ln\alpha$ in Figure B.2. The kinetic parameters of the autocatalytic model for the case with x% TBPB are listed in Table B.1. This model successfully predicts the cure reaction with time. As an example, model and experimental data for the isothermal test at 110°C for IMC with 1%TBPB are well compared in Figure B.3 and B.4.

155
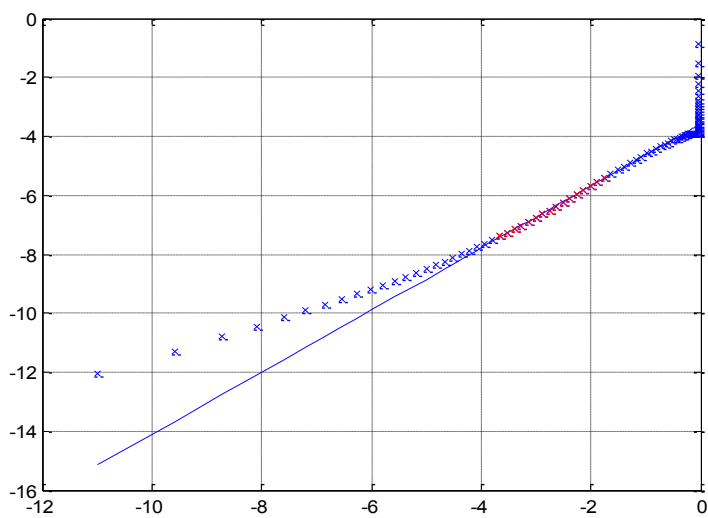
Figure B. 2 A plot of n $[(d\alpha/dt)/(\alpha_{max} - \alpha)^n]$ vs. $ln\alpha$

n	1.02
m	1.05
k_p	0.028

Table B. 1 Determined autocatalytic kinetic parameters

156
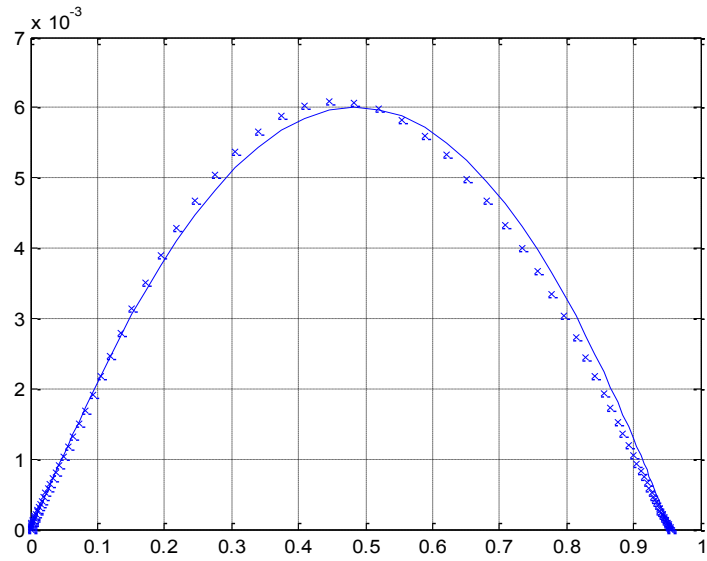
Figure B. 3 Reaction rate versus conversion between experimental result and kinetic model
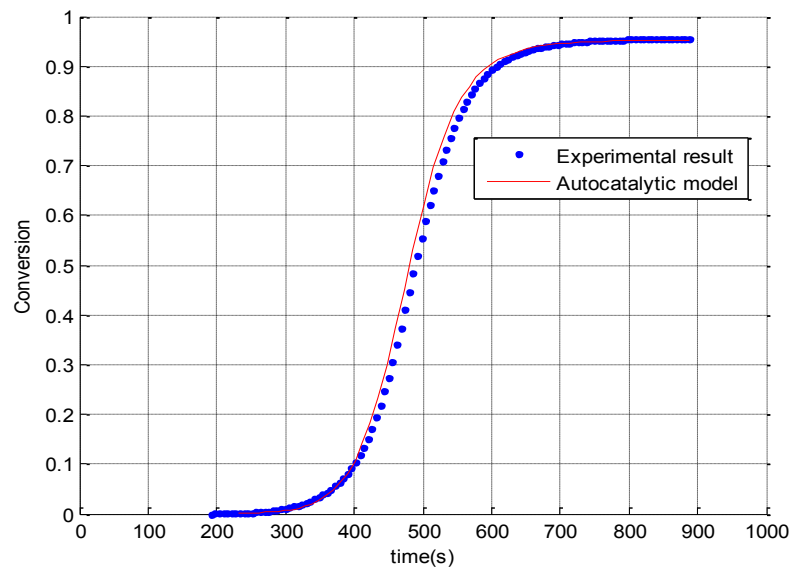
Figure B. 4 Conversion versus reaction time between experimental result and kinetic model

157

Appendix C. Determination of Proper Sample Size for DSC Tests

Typically, 5-20mg of sample size is used for DSC test. To determine proper sample size of IMC resins, several DSC tests were performed. Figure C.1 shows the isothermal scan for Genglaze EC2447 with 1.75%TBPB at 100°C for varying sample size. As increasing the sample size the heat flow curve moves to left side. The 5 mg of sample size shows slower reaction rate and 10-15mg of sample size shows similar reaction rate and a peak. We determined that the proper sample size for DSC tests of IMC is between 10 to 15mg because the measured heat flow is nearly independent of sample size.
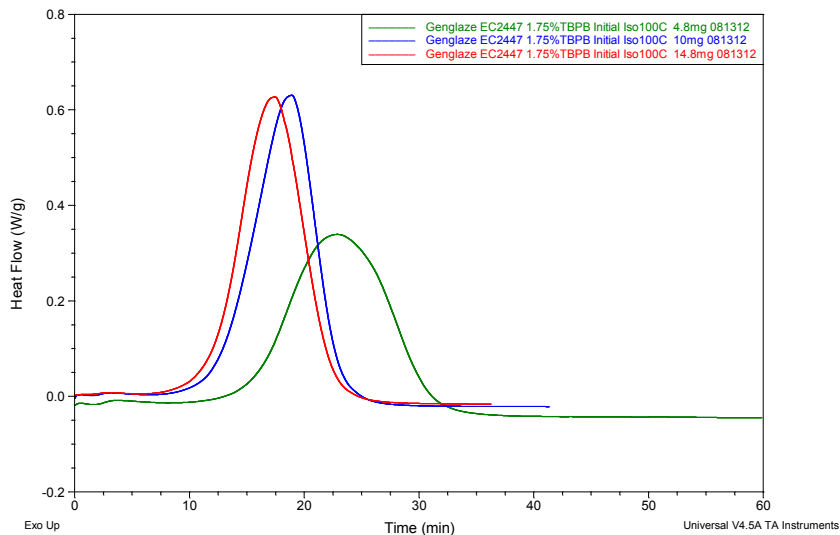
Figure C. 1 Isothermal scan for Genglaze EC2447 with 1.75%TBPB at 100C for different sample sizes

Bibliography

Chapter 1:

1. J. M. Castro and R. M. Griffith, "In-Mold Coating," in *Sheet Molding Compound: Science and Technology,* edited by Hamid G. Kia, Munich: Hanser, 1993, pp. 163-180.

2. William Rogers, Christoper Hoppins, Zoltan Gombos and John Summercales, "In-mould gel-coating of polymer composites: a review", Journal of clear production, 70, 282-291, 2014.

3. J. M. Castro and R. M. Griffith, "Mathematical modeling of the in-mold coating process", Polymer engineering and science, 30, 677, 1990.

4. Xu Chen, "Mathematical modeling of the in-mold coating process for injection molded thermoplastic parts", Ph. D. Dissertation, The Ohio State University, 2003.

5. Narayan L. Bhagavatula, "Modeling and experimental verification of pressure prediction in the in-mold coating process for thermoplastic substrates", Ph. D. Dissertation, The Ohio State University, 2006.

6. Konstantin S. Zuyev, "Processing studies in reactive in-mold coating for thermoplastic substrates", Ph. D. Dissertation, The Ohio State University, 2006.

7. Konstantin S. Zuyev, "Applications of chemo-rheology to develop process windows in reactive in-mold coating", Journal of polymer engineering, Vol. 22, No. 4, 2002.

8. Aramphongphun, C, "In-mold coating of thermoplastic and composite parts: microfludics and rheology", Ph. D. Dissertation, The Ohio State University, 2006.

9. Emily Cortright, "Microfludics and DNA suspensions", M.S. Thesis, The Ohio State University, 2009.

10. P. J. Halley and M. E. Mackay, "Chemo-rheology of thermoset: an overview", *Polym. Eng. Sci.* **36**, 593-609 (1996).

11. Maria G. Villareal-Mirroquin, "A metamodel based multiple criteria optimization vis simulation method for polymer processing", Ph.D. Thesis, The Ohio State University, (2012)

Chapter 2:

1. J. M. Castro and R. M. Griffith, "In-Mold Coating," in *Sheet Molding Compound: Science and Technology,* edited by Hamid G. Kia, Munich: Hanser, 1993, pp. 163-180.

2. J. M. Castro and R. M. Griffith, *Polym. Eng. Sci.* 30, 677-683 (1990).

3. H. H. Winter, *Mater. Res. Soc. Bull..* 16, 44-48 (1991).

4. P. J. Halley and M. E. Mackay, *Polym. Eng. Sci.* 36, 593-609 (1996).

5. J. Yang, J. Xiao, J. Zeng, C. Peng, X. Feng and B. Hou, *Appl. Compos. Mater*, 19, 573-582 (2012)

6. K. Raghu Raja Pandiyan and S. Neogi, *J. Appl. Polym. Sci.* 125, 1400-1408 (2012).

7. A. Terenzi, C. Vedova, G. Lelli, J. Mijovic, L. Torre, L. Valentini and J. M. Kenny, *Comp. Sci.Technol.* 68, 1862-1868 (2008).

8. H. Yari, M. Mohseni and Z. Ranjbar, *J. Appl. Polym. Sci.* 129, 1929-1938 (2013).

9. M. Abdalla, D. Dean, P. Robinson and E. Nyairo, *Polymer* 49, 3310-3317 (2008).

10. M. Monti, D. Puglia, M. Natali, L. Torre and J. M. Kenny, *Comp. Sci.Technol.* 71, 1507-1516 (2011).

11. Jose M. Castro, "Mold Filling and Curing Studies for the Polyurethane RIM Process", Ph.D. Thesis, University of Minnesota, 1980.

12. J. M. Castro and C. W. Macosko, *AIChE J.* 28, 250-260 (1982).

13. J. M. Kenny, *J. Appl. Polym. Sci.* 51, 761-764 (1994).

14. J. F. Stevenson, *Polym. Eng. Sci.* 28, 746 (1986).

15. L. J. Lee, *Polym. Eng. Sci.* 21, 483 (1981).

16. J. M. Castro and C. C. Lee, *Polym. Eng. Sci.* 27, 218 (1987).

17. K. S. Zuyev and J. M. Castro, *J. Polym. Eng.* 22, 233-260 (2002).

18. D. H. Chang and W. L. Kwok, *J. Appl. Polym. Sci.* 28, 3155-3183 (1983).

19. Xilian Ouyang, "Surface modified carbon nanoparticle papers and applications on polymer composites", Ph.D. Thesis, The Ohio State University, (2014).

20. Curtis R. Center, "Thermoplastic melt-mixed composition with epoxy-carboxylic acid compound heat stabilizer", Patent WO2013188488 A1, 2013.

Chapter 3:

1. A. Yousefi and P. G. Lafleur, Polymer Composites, Vol. 18, No. 2, 1997

2. S. Vyazovkin, A. K. Burnham, J. M. Criado, L. A. Perez-Maqueda, C. Popescu and N. Sbirrazzuoli, Thermochimica Acta, 520, 1-19, 2011

3. L. Zhao and X. Hu, Polymer, Vol. 51, 3814-3820, 2010

4. S. Park, M. Seo and J. Lee, Journal of Polymer Science, Vol. 38, 2945-2956, 2000

5. J. M. Kenny, Journal of Applied Polymer Science, Vol. 51, 761-764, 1994

6. 6.S. Sourour and M. R. Kamal, Thermochimica Acta, 14, 41-59, 1976

7. N. W. Manthey, F. Cardona and T. Aravinthan, Vol. 125, E511-E517, 2012

8. J. Y. Lee, H. K. Choi, M. J. Shim and S. W. Kim, Thermochimica Acta, 343, 111-117, 2000

9. K. Tao, S. Yang, J. C. Grunlan, Y. Kim, B. Dang, Y. Deng, R. L. Thomas, B. L. Wilson and X. Wei, Journal of Applied Polymer Science, Vol. 102, 5248-5254, 2006

10. P. Lei, Y. Yu and X. Yang, Journal of Applied Polymer Science, Vol. 109, 2539-2545, 2008

11. J. Bae, J. Jang and S. Hoon, Macromol. Chem. Phys, 203, 2196-2204, 2002

12. M. Monti, D. Puglia, M. Natlai, L. Torre and J. M. Kenny, Composites Science and Technology, 71, 1507-1516, 2011

13. X. Huang and B. Batham, , Journal of Applied Polymer Science, Vol. 127, 1959-1996, 2013

14. J. F. Stevenson, *Polym. Eng. Sci.* **28**, 746 (1986).

15. L. J. Lee, *Polym. Eng. Sci.* **21**, 483 (1981).

161

16. J. M. Castro and C. C. Lee, *Polym. Eng. Sci.* **27**, 218 (1987).

17. K. S. Zuyev and J. M. Castro, *J. Polym. Eng.* **22**, 233-260 (2002).

18. J. M. Castro and R. M. Griffith, "In-Mold Coating," in *Sheet Molding Compound: Science and Technology,* edited by Hamid G. Kia, Munich: Hanser, 1993, pp. 163-180.

19. J. M. Castro and R. M. Griffith, *Polym. Eng. Sci.* **30**, 677-683 (1990).

20. J. D. Fan, J. M. Marinelli and L. J. Lee, Polymer Composites, Vol. 7, No. 4, 1986

21. J. M. Barton, Advances in Polymer Science, Vol. 72, 1985.

22. A. Dutta and M. E. Ryan, Journal of Applied Polymer Science, Vol. 24, 635-649, 1979

23. Abdalla M, Dean D, Robinson P and Nyairo E, Polymer, 49, 3310-7, 2008

24. N. L. Ranikumar, K. K. Kar, S. Sarkar and D. Sathyamoorthy, Polymer Composites, 2010

25. Terenzi A, Vedova C, Lelli G et al., Compos. Sci. Technol., 68, 1862-8, 2008

26. Xu L and James Lee L, Polym. Eng. Sci.,45, 496-509, 2005

27. Movva, Journal of Composites Materials, 43, 611, 2009

28. Xie et al., Journal of Applied Polymer Science, 96, 329-335, 2005

29. Chou, Composite Science and Technology, 70, 1, 2009

30. J. Wu and D.D.L. Chung, Carbon, 42, 3003-3042, 2004

31. S.B.Susin, V. Pistor, S. C. Amico, L. A. F. Coelho et al., Journal of Applied Polymer Science, 2014

Chapter 4:

1. Rosen, S., Harmonsky, C. M. and Trand, M, "Optimization of systems with multiple performance measures via simulation: survey and recommendation", Computers and industrial engineering, 52(2), 327-339, 2008.

2. Sevenson, J. D., "Computer experiments: multiobjective optimization and sensitivity analysis", Ph. D. Thesis, The Ohio State University, 2011.

3. Evans, G., Stuckman, B. & Mollaghasemi, M., 1991. Multicriteria optimization of simulation models. *Proceedings of the 1991 Winter Simulation Conference,* pp. 894-900.

4. Dellino, G., Kleijnen, J. & Meloni, C., 2009. Robust Simuation-Optimization using metamodels. *Proceedings of the 2009 Winter Simulation Conference*, pp. 540-550.

5. Zakerifar, M., Biles, W. & Evens, G., 2009. Kriging Metamodeling in Multi-Objective Simulation Optimization. *Proceedings of the 2009 Winter Simulation Conference*, pp. 2115-2122.

6. Ryu, J.-H., Kim, S. & Wan, H., 2009. Pareto front approximation with adaptive weighted sum method in multiobjective simulation optimization. *Proceedings of the 2009 Winter Simulation Conference*, pp. 623-633.

7. Mauricio Cabrera Rios, "Multiple criteria optimization studies in reactive in-mold coating", Ph.D. Thesis, The Ohio State University, (2002)

8. Carlos E. Castro, " Optimization and analysis of variability in high precision injection molding", M.S. Thesis, The Ohio State University, (2005)

9. Maria G. Villareal-Mirroquin, "A metamodel based multiple criteria optimization vis simulation method for polymer processing", Ph.D. Thesis, The Ohio State University, (2012)

10. Montgomery, D. C., 2005. *Design and Analysis of Experiment.* 6th ed. s.l.:John Wiley & Sons, Inc..

11. Barton, R. R., 2009. Simulation optimization using metamodels. *Proceedings of the 2009 Winter Simulation Conferenc*e, pp. 230-238.

12. Simpson, T., Poplinski, J., Koch, P. N. & Allen, J., 2001b. Metamodels for computer-based engineering design: Survey and recommendations. *Engineering with Computers,* 14(2), pp. 129-150.

13. Konstantin S. Zuyev, "Processing studies in reactive in-mold coating for thermoplastic substrates", Ph. D. Dissertation, The Ohio State University, 2006.

Chapter 5:

1. Moniruzzaman M, Winey KI. *Macromolecules* 2006, 39, 5194-5205.

2. Castro, JM, Griffith, RM. In *Sheet Molding Compounds: Science and Technology*, Kia, HG Eds., Hanser/Gardner Publications: Cincinnati, 1993, p 163.

3. Castro JM, Griffith RM. *Polymer Eng. Sci*. 1990, 30, 677-683.

4. Bhagavatula N, Castro JM. *Modelling Simul. Mater. Sci. Eng*. 2007, 15, 171-189.

5. Chen X, Bhagavatula N, Castro JM. *Modelling Simul. Mater. Sci. Eng*. 2004, 12, S267-S287.

6. Huang JC, *Adv. Polym. Tech*. 2002, 21, 299-313.

7. Gupta, RK, Kennel, E, Kim, KJ, Eds., *Polymer Nanocomposites Handbook*, CRC Press: Boca Raton, 2010.

8. Bauhofer W, Kovacs JZ. *Compos. Sci. Technol*. 2009, 69, 1486-1498.

9. Al-Saleh MH, Sundararaj U. *Carbon* 2009, 47, 2-22.

10. Van der Pauw LJ. Philips Res. Repts. 1958, 13, 1-9

11. Zuyev KS, Castro JM. J. Polym. Eng. 2002, 22, 233-260.

12. Cabrera ED, Ko S, Ouyang X, Straus E, Lee LJ, Castro JM. *SPE ANTEC* 2013.